CHAPTERS 1 - 7

THE DEVELOPMENT OF NEW ANALYTICAL TECHNIQUES APPLICABLE TO THE POWDER FORGING PROCESS

by

T. J. GRIFFITHS, B.Eng.(Tech.), C.Eng.,
M.I.Mech.E., M.I.Prod.E.

A thesis submitted in pursuance of the requirements of the Council for National Academic Awards, for the degree of Doctor of Philosophy.

Department of Mechanical
& Production Engineering,
The Polytechnic of Wales.

June 1979

DECLARATION

This dissertation has not been nor is being currently submitted for the award of any other degree or similar qualification.

T. J. Griffiths

CONTENTS

PREFACE

During the period of time that the writer has been enagaged on this programme of research he has produced five publications, two of which have been presented at Powder Metallurgy Conferences organized by The Metals Society. He has also undertaken a 3 month study tour of Powder Metallurgy in Europe, with the aid of a Goldsmiths' Travelling Fellowship.

Furthermore, he has supervised at least half a dozen undergraduate students who have chosen powder metallurgy projects during the final year of their studies for a C.N.A.A. degree in Mechanical Engineering. Thus in this way it can be seen how the research being undertaken within the Department of Mechanical and Production Engineering, has been reflected in the teaching programme.

The actual research programme is principally involved with devising new analytical techniques applicable to the powder forging process. However, since powder forging is essentially a post-sintering operation, it has been necessary to examine all the various operations involved in conventional powder metallurgy processing. This exercise has served to reveal that most of the work carried out in this field tends to be either empirical or philosophical in nature, rather than based upon rigorous scientific analysis, see Chapter 3. Hence it has been necessary to approach the research programme on a broader front than was originally envisaged, in order to include some analytical work relating to the preform material i.e. conventional sintered material.

ACKNOWLEDGEMENTS

The writer wishes to acknowledge grateful thanks to Dr. M.B. Bassett of The Polytechnic of Wales and Dr. R. Davies of the University of Birmingham for encouragement and helpful advice given throughout this entire research programme.

He also wishes to express his gratitude to a number of colleagues within the Department of Mechanical and Production Engineering at the Polytechnic, for assistance and stimulating discussion on a variety of topics related to the project.

Furthermore, grateful appreciation is extended to virtually all of the Department's technician staff for manufacturing and modifying tools and other equipment, and in particular to draughtsman Tony Evans for his painstaking work in preparing the excellent illustrations which appear in this thesis.

A special debt of gratitude is due to a number of outside bodies and organisations who have provided invaluable assistance in various ways. These include the Goldsmith's Company of London for their confidence and generosity in awarding a Travelling Fellowship to enable the writer to undertake a 3 month study tour of powder metallurgy in Europe. Regarding the various commercial organisations, thanks are due to The South Wales Forgemasters Ltd., and Firth Cleveland Sintered Products Ltd., both of whose contributions are acknowledged in the relevant sections of the thesis, and also to Hoganas AB, for kindly donating all of the AHC 100.29 iron powder used throughout the project.

SYNOPSIS

THE DEVELOPMENT OF NEW ANALYTICAL TECHNIQUES APPLICABLE TO THE POWDER FORGING PROCESS

T. J. GRIFFITHS

Five publications[6, 18, 28, 68, 110] were produced and a 3 month study tour of powder metallurgy in Europe[6] was undertaken.

Elemental iron powder/graphite mixes of "as supplied" and "coarse fraction" powders were used throughout, and these were characterized in the normal manner.

Test specimen and preforms were produced by mechanical compaction, and generally sintered in accordance with standard industrial practice, followed by micro-examination of selected specimen.

Specimen were subjected to hot torsion, hot tensile and dilatometer tests. Room temperature tests were performed to measure the lateral and longitudinal strain components arising from uniaxial tensile stress.

A mathematical model[110] was devised to represent a porous material subjected to tensile testing to destruction. Tensile tests were conducted at room temperature, to characterize the preform material, and check the findings of the micro-examinations.

A pilot study of preform design[28] was undertaken to provide first-hand experience of some of the problems involved in powder forging. A mathematical technique[68] was devised to assist in the design of new preforms, and to analyse successful preform shapes obtained by trial and error methods.

Some preliminary fatigue tests were performed on partly forged components.

Use was made of the mathematical model [110], to help explain the consolidation process. The concept of a "coefficient of consolidation" was introduced and verified experimentally by a series of cold axisymmetric upset tests. The dependence of the apparent plastic Poisson's ratio on the initial density of the preform was demonstrated, and information provided regarding the plastic flow stress requirements for cold axisymmetric upsetting.

Hot axisymmetric upset and closed die tests were performed on cylindrical preforms, and the densification rates obtained were compared with the theoretically predicted values[18]. Apparent plastic Poisson's ratios were measured at various sections along the partly forged preforms. Finally, a general appreciation of the forging load requirements was ascertained.

CHAPTER 1

CHAPTER 2

CHAPTER 3

CHAPTER 4

Powder Characterization and Preparation

CHAPTER 5

Powder Compaction

CHAPTER 6

CHAPTER 7

CHAPTER 8

CHAPTER 9

Analysis of Consolidation During the Upsetting Stage of the Powder Forging Process

CHAPTER 10

Hot Forging of Cylindrical Preforms

CHAPTER 11

LIST OF ILLUSTRATIONS

NOMENCLATURE

M	=	degree of mixedness
F, H	=	empirical constants describing the powder compaction process
Φ	=	compaction pressure MN/m^2
ρ_s	=	density of solid metal
ρ	=	density of preform material
ρ_*	=	density of porous material relative to solid density
P	=	$(1 - \rho_*)$ = porosity
R_c	=	Rockwell hardness number - Scale C
ν	=	Poisson's ratio for a perfectly plastic solid metal, assuming volume constancy
ν_e	=	elastic Poisson's ratio
ν_{ap}	=	apparent plastic Poisson's ratio
A_a	=	apparent cross sectional area
A_b	=	load bearing area
b, f	=	geometrical constants describing distribution of cavities
c, g	=	geometrical constants describing the morphology of the cavities
k	=	$\frac{g}{f}\left[\frac{b}{c}\right]^{\frac{2}{3}}$
p	=	minimum pore pitch
d	=	pore diameter
σ	=	tensile strength of porous material
σ_o	=	tensile strength of pore free matrix material
σ_t	=	"true" stress
σ_r	=	radial stress
σ_θ	=	circumferential stress

W = $\frac{\text{distance between layers of pores}}{P}$

K_t = geometric elastic stress concentration factor

K = tensile strength reduction factor

λ = empirical constant

x = $\frac{\text{major diameter of oblate ellipsoid}}{\text{diameter of sphere of equilalent volume}}$

y = $\frac{\text{minor diameter of oblate ellipsoid}}{\text{diameter of sphere of equivalent volume}}$

n = number of pairs of data points

R = correlation coefficient

m = slope of graph

E = true Young's modulus of elasticity MN/m^2

E_{ap} = apparent Young's modulus of elasticity MN/m^2

r = radius

t = thickness

D = diameter of PM preform

h = height of PM preform

V_s = volume of solid metal

V = total volume of preform

V_c = volume occupied by cavities

C = coefficient of consolidation

ε_z = principal natural strain in longitudinal direction

ε_r = principal natural strain in radial direction

ε_θ = circumferential strain

By definition:-

$d\varepsilon_z = \frac{dh}{h}$ and $d\varepsilon_r = \frac{dD}{D}$

η = work hardening exponent

β = strength coefficient

u_i = radial displacement of die insert

u_o = radial displacement of shroud

A, B, C, N } constants, see Appendix F

Suffices:

"1" and "2" used to denote initial and final conditions respectively

"X" and "Y" used to denote sections X and Y respectively, Fig. 9.5

"i" and "s" used to denote die insert and shroud respectively

CHAPTER 1

Brief Review of Powder Metallurgy Activity

1.1 Definition and Origins

Powder metallurgy (PM) has been defined[1] as the art and science of producing metal powders, and their subsequent transformation into useful objects.

Although it is regarded as a fairly recent technique, its origins can be traced back approximately 5000 years to the Egyptians[2], who, because they lacked the technology to build furnaces capable of attaining the temperature of 1535°C required to melt iron, were obliged to reduce iron oxide in a blown charcoal fire. This process lowered the melting temperature to about 1130°C as a result of the diffusion of approximately 4.3% carbon into the metal, see Fig. 1.1, the chemical reaction being,

$$3Fe_2O_3 + 11C = 2Fe_3C + 9CO$$

The resulting mass of spongy metallic iron was then hammered and forged into various shapes, thus demonstrating their awareness of the use of pressure welding for the dual purpose of (i) producing massive metal and (ii) the consolidation of porous metal.

Further PM activity occurred approximately 1000 years later, when the Peruvian Incas of South America used such techniques to produce platinum, from which they made ornaments.

More recently, the famous Delhi column, a $6\frac{1}{2}$ ton iron pillar dating from A.D. 300, was produced by hammering hot granules of reduced iron oxide, into a substantially solid shape.

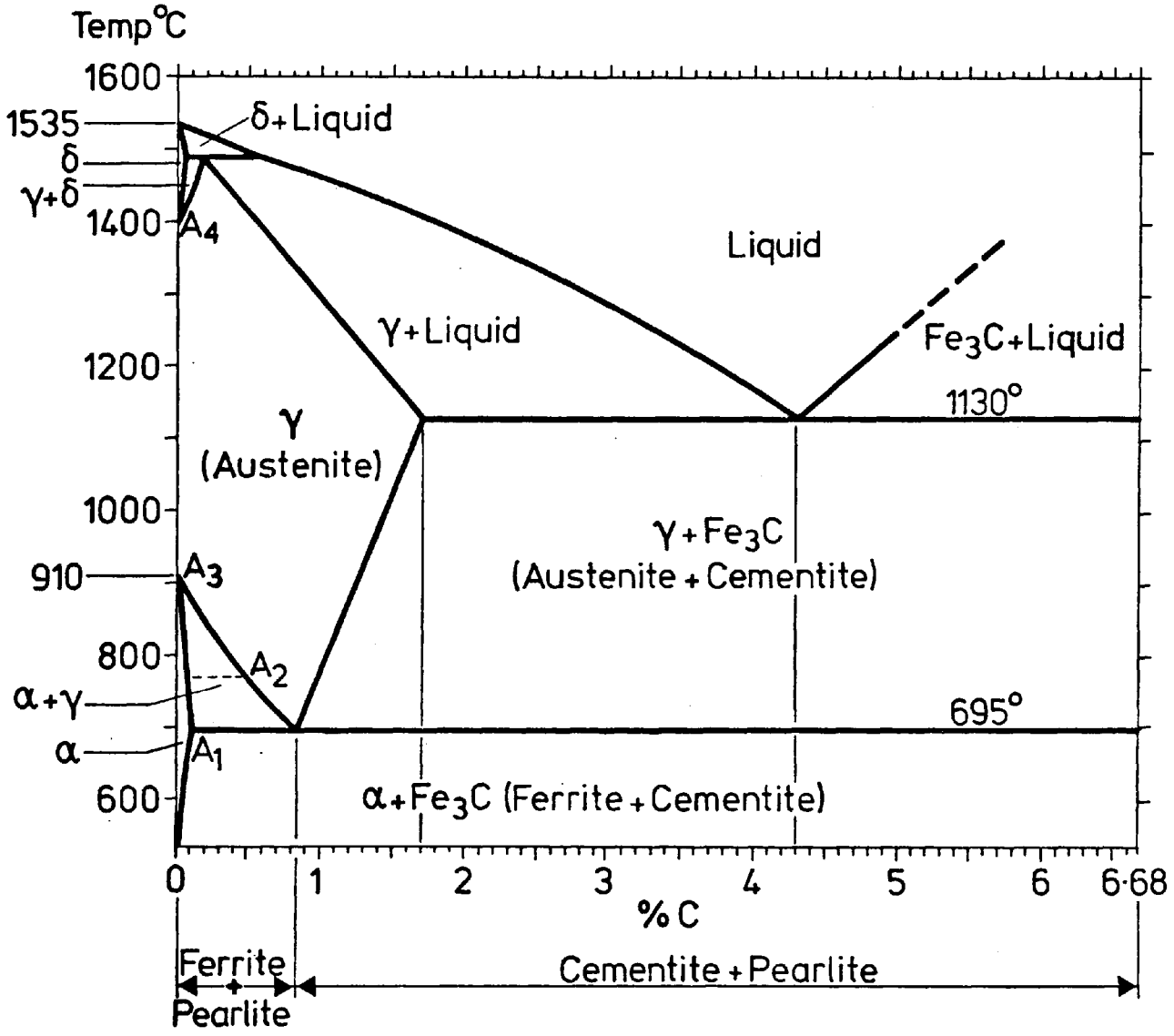

FIG. 1.1 IRON-IRON CARBIDE THERMAL EQUILIBRIUM DIAGRAM

1.2 Birth of the Modern Powder Metallurgy Industry

In the early 1800's a method of making platinum ingots was conceived by Wollaston[3], and this together with Bessemer's[4] work on the manufacture of brass powder, in the mid 1800's, established most of the basic techniques employed in the modern powder metallurgy industry.

Wollaston's process entailed heating ammonium platinum chloride to produce a sponge powder which was ground, washed, graded, compacted and heated in a coke fired furnace with forced draught. Consolidation of the material was then carried out by hot hammering, the underlying principle being similar to that of the modern powder forging process.

In the early 1900's Coolidge[3] introduced a method for producing ductile tungsten wire, to cater for the needs of the electric lamp filament industry. Bars of tungsten were produced by compacting tungsten powder, followed by sintering in a reducing atmosphere, using an electrical resistance furnace. The cross sections of these bars were then reduced to that of thin rods by hot swaging, and the ductile filament wire drawn from these rods.

1.3 Twentieth Century Growth

It was just after the First World War that the need arose for a hard die material for drawing tungsten rods into filament wire. This resulted in the development, by the German firm of Krupp's, of cobalt cemented tungsten carbide, which marked the beginning of the modern hard metal industry.

About the same time, self-lubricating porous bearings were produced for automobiles, fractional horse-power electric motors and similar machines. Porous metal filters were also being produced for gas and fluid filtration. During the Second World War these led to the development of aircraft de-icing equipment[5], in the form of porous leading

edges on aircraft wings, through which de-icing fluid could be pumped.

Just prior to the Second World War it became evident that ferrous based structural components could be produced at prices competitive with those of conventional manufacturing methods. This led to a tremendous development in iron powder metallurgy, especially in America and Germany.

It was during the post war era that the powder metallurgy industry in Great Britain began to expand and produce sintered magnet materials, frictional materials, steel backed bearings and eventually the wide range of diverse components in current production. More recently attention has been focussed on powder forging and considerable success has been achieved with this relatively new process.

1.4 The Modern PM Industry in Europe

A first-hand insight into modern PM activity in Europe was obtained by undertaking a three month study tour from approximately mid-April to mid-July 1975, with the aid of a Goldsmith's Travelling Fellowship. Details of the impressions gained as a result of the tour have been previously published[6], and appear in Appendix A.

CHAPTER 2

General Review of the Powder Forging Process

2.1 Introduction

Powder forging is an emerging technology[7, 8], which originated less than forty years ago[9, 10, 11]. It was introduced commercially[12] in 1972 and, at present, about fifty parts are in high volume production throughout the world.[13]

As its name suggests, it is a hybrid process[14, 15, 16], combining conventional PM techniques with those of closed die forging. The method was developed in order to extend the use of powdered metals into the realms of high performance applications[17]. This was achieved by eliminating the porosity inherent in PM parts, by closed die hot forging, see Fig. 2.1, as opposed to liquid phase sintering and infiltration techniques. Briefly, the process involves the production of a PM preform, which is closed die forged to simultaneously consolidate the material, and impart the desired shape on to the component.

The harmful effects of porosity in conventional PM structural material is to reduce the tensile strength, elongation, and impact strength, together with the virtual elimination of the yield point[19, 20, 21]. The closure of this porosity enhances the mechanical properties of the material so that it can bridge the gap between conventional PM parts and high integrity forgings[8], although the latter are likely to exhibit marked anisotropy, whereas the powder forged material is extremely isotropic[22, 23] in nature.

2.2 Terminology

Although the name "powder forging[9]" now seems to be well established,

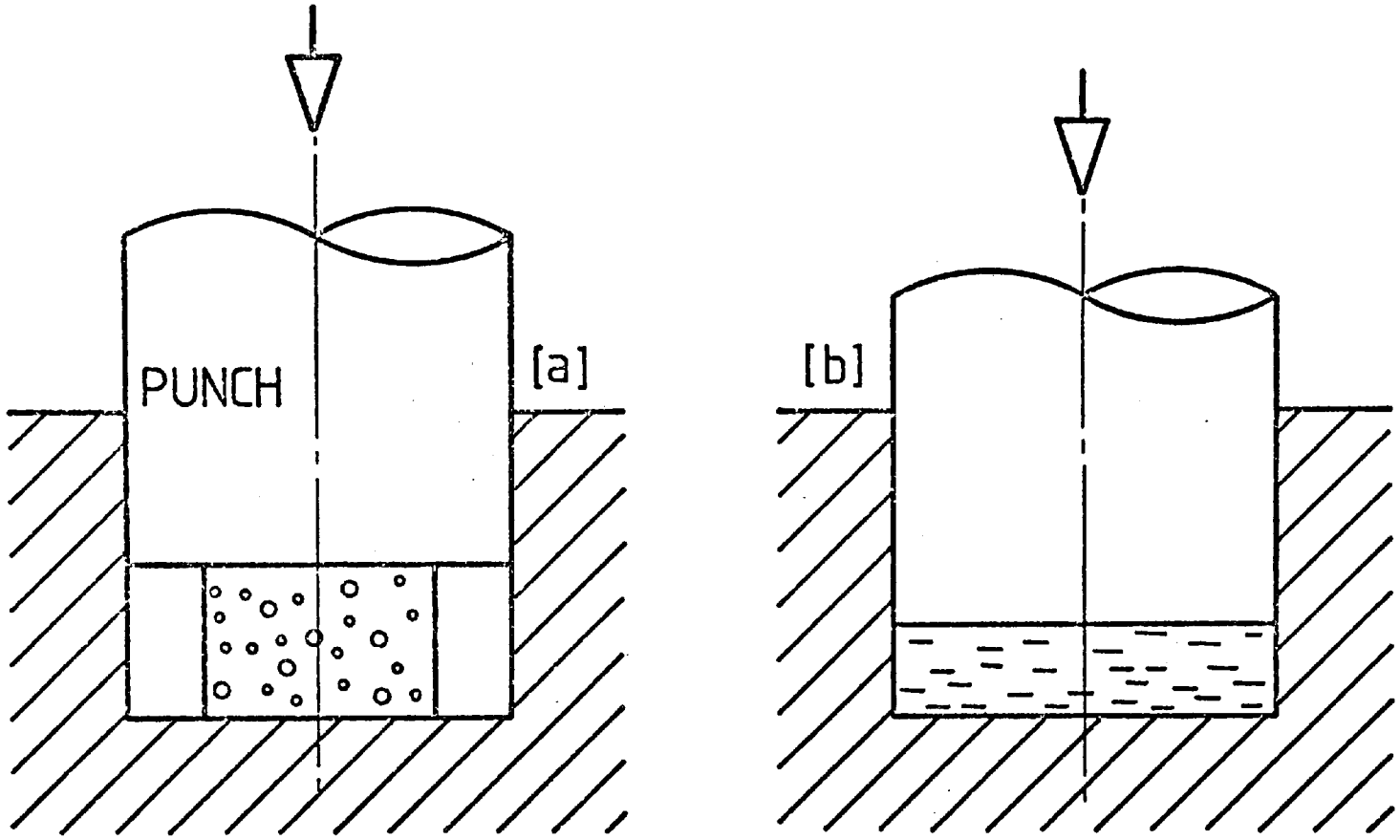

FIGURE 2.1 Deformation of cylindrical preform during closed-die forging:

(a) porous preform at beginning of upsetting stage;

(b) fully consolidated forging at end of re-pressing stage.

(Ref. 28)

and is defined by the International Standards Organisation as, "Hot densification by forging of an unsintered, presintered or sintered preform, made from powder, with accompanying significant change of shape", other names were used during the development stages of the process. These included "P/M forging[24]", "HD: P/M" i.e. high density parts via P/M techniques[25], "powder forming[26]", "sinter forming[26]" and "sinter forging[22, 26]", from which the name "Sinta Forge[27]" was adopted by Federal Mogul, to describe their particular process. The variety of names came into being as a result of variations in the heating cycle, plus the fact that, occasionally, the process is virtually that of hot repressing[25]. However, in the majority of cases the consolidation is accompanied by some bulk metal plastic flow[28].

2.3 Early Development

Most of the early development work in powder forging was undertaken by commercial organizations. These included Chevrolet[10], in 1941, although the starting material appears to be swarf rather than powdered metal, and Engineering Sinterings and Plastics Incorporated[8] in the late 1960's. Other American firms include Cincinnati[29], the Federal Mogul Corporation[27, 29] and the Burgess Norton Manufacturing Co.[11] European firms include G.K.N. Ltd.[29], and the British Steel Corporation[30] in Britain, Hoganas [31] in Sweden and Mannesmann - Pulvermetall GmBh[32] in West Germany.

Many other firms also showed interest in this new process. This is indicated in a report[33] of November 1971 in which a three year research programme was proposed; this programme was to be undertaken at the Columbus, Ohio Laboratories of Battelle, and supported by nine companies, including the Caterpillar Tractor Company, the Timken Company and the Toyoto Motor Company.

In addition to these commercial interests, the potential of powder forging, as an economical means of producing precision engineering parts was quickly recognized by the United States Army and Department of Defence. This resulted in the award of major grants, under project "Themis[17, 34]", which was aimed at developing and applying analytical techniques to a broad range of problems existing in powder metallurgy processing.

Hence powder forging gradually developed from laboratory experiments in the late sixties to pilot plants in the early seventies and ultimately to the present day full commercial production[35]. Unfortunately, however, over zealous claims were made in the early stages which resulted in the over selling of the process before it had been properly investigated[35, 36]. The outcome of this was that many of the smaller potential users lost interest when faced with the costly development needed to solve a whole range of problems associated with this new process. Nevertheless, many of the larger firms successfully managed to overcome the main difficulties, and so developed powder forging into the technically feasible, and economically viable process it is today.

2.4 General Appreciation of the Forging Operation

The actual powder forging process involves the forging of a well defined preform, which has been produced using the conventional PM techniques of powder blending, compaction and sintering, see Fig. 2.2. In point of fact the sintering may be incorporated in the forging operation[26], or even occur after it[37]. For present purposes, however, it will be assumed that the preform is sintered immediately after compaction, in accordance with normal PM practice. Furthermore, only ferrous based powders will be considered, although the process can be

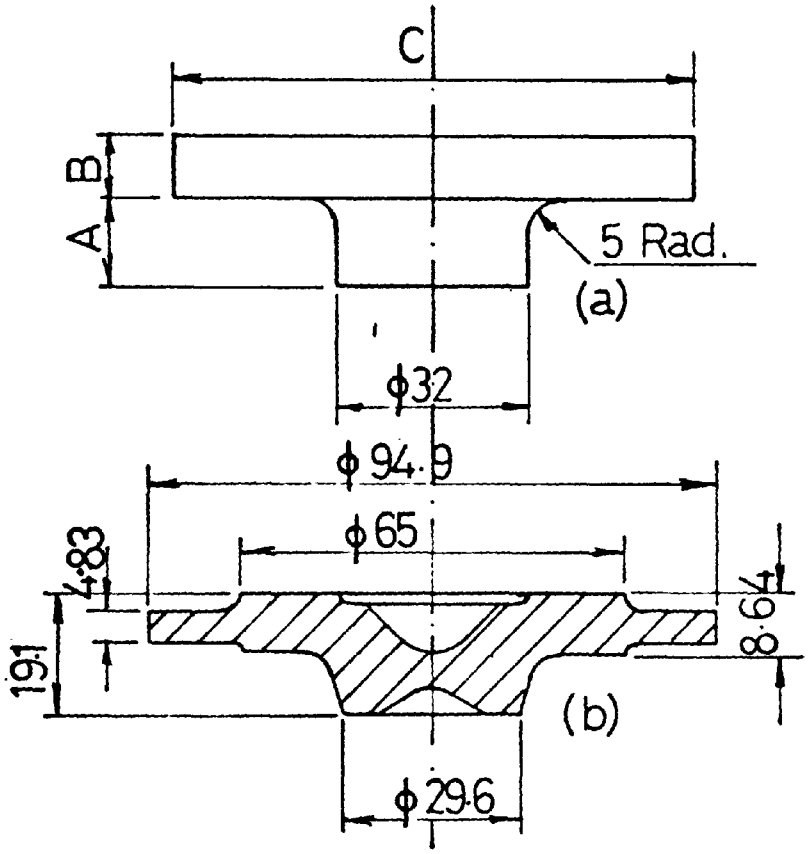

FIG. 2.2 (*a*) Preform shape. Boss dia. 32 mm for location; dimension A depends upon preform density. (*b*) Section through component. (Ref. 28)

applied equally well to aluminium, titanium and superalloy powder parts[10, 38, 39].

After sintering, the preforms may be either cooled, stored and then reheated before forging, or else transferred directly from the sintering furnace to the forging press[18]. Since the PM preform material displays a much smaller degree of plasticity at elevated temperatures than that of wrought material of comparable composition[28], it is necessary to carefully distribute the metal in the preform to minimize unsupported lateral flow, and the accompanying risk of cracking during the forging operation, see Figs 2.3, 2.4 and 2.5.

One of the many advantages of the process is that the well defined preform obviates the need for multi-impression dies[24], and enables the component to be produced in a single blow, thereby overcoming the need for skilled hammer-men. Despite the fact that the process is termed "closed-die forging", during the early stages it is essentially one of open-die forging. This results in the upsetting of the blank until lateral flow of the preform is checked by the material making intimate contact with the die walls. Since most of this lateral flow takes place with the material in its most porous state, it means that the initial forging loads are quite low. This reduces the frictional forces which tend to impede relative movement of preform material across the die faces; this, in turn, helps to reduce tool wear[40]. Furthermore, the final forging loads are less than those encountered in conventional forging due to the fact that it is a flashless process, and hence does not require the high loads necessary to extrude the surplus metal through small flash apertures[24, 40].

The three principal modes of deformation encountered during powder forging are (i) axisymmetric compression, Fig. 2.6 (ii) plane strain compression, Fig. 2.7 and (iii) repressing, Fig. 2.1(b). These may occur

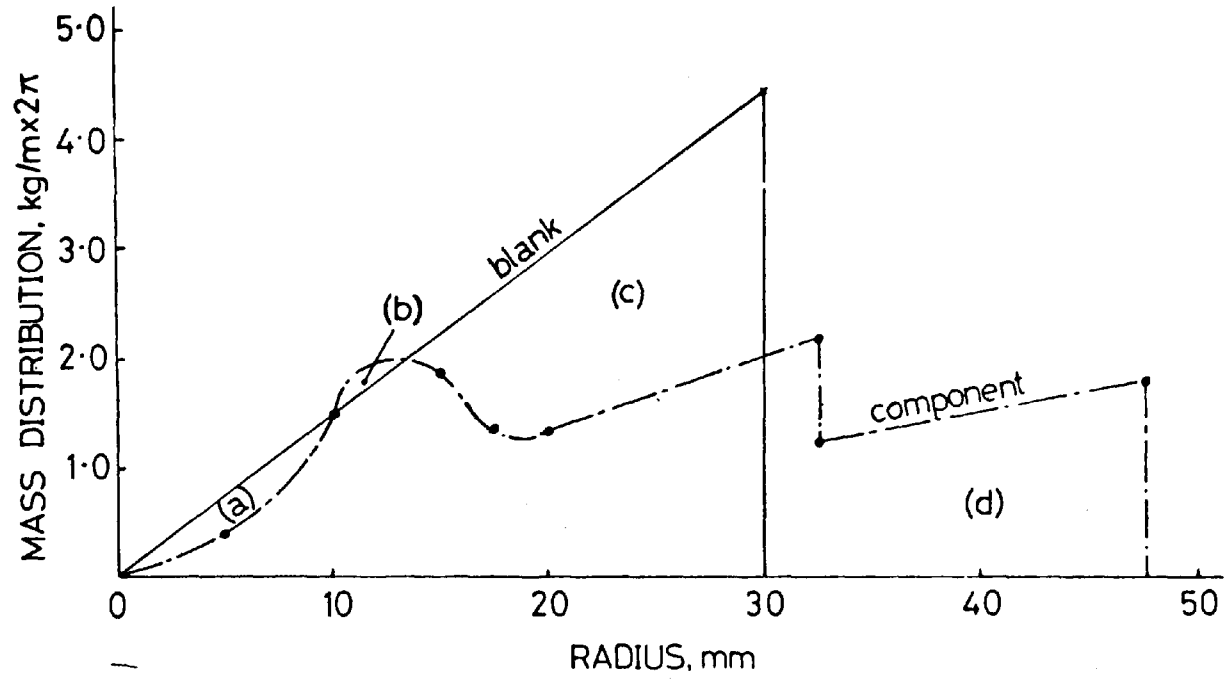

FIG. 2.3 Comparison of mass distribution of solid cylindrical blank with that of finished component. Metal displaced from region (a) makes up the deficiency at (b), the surplus spreading into (c), which is then displaced to make up the deficiency in region (d). (Ref. 28)

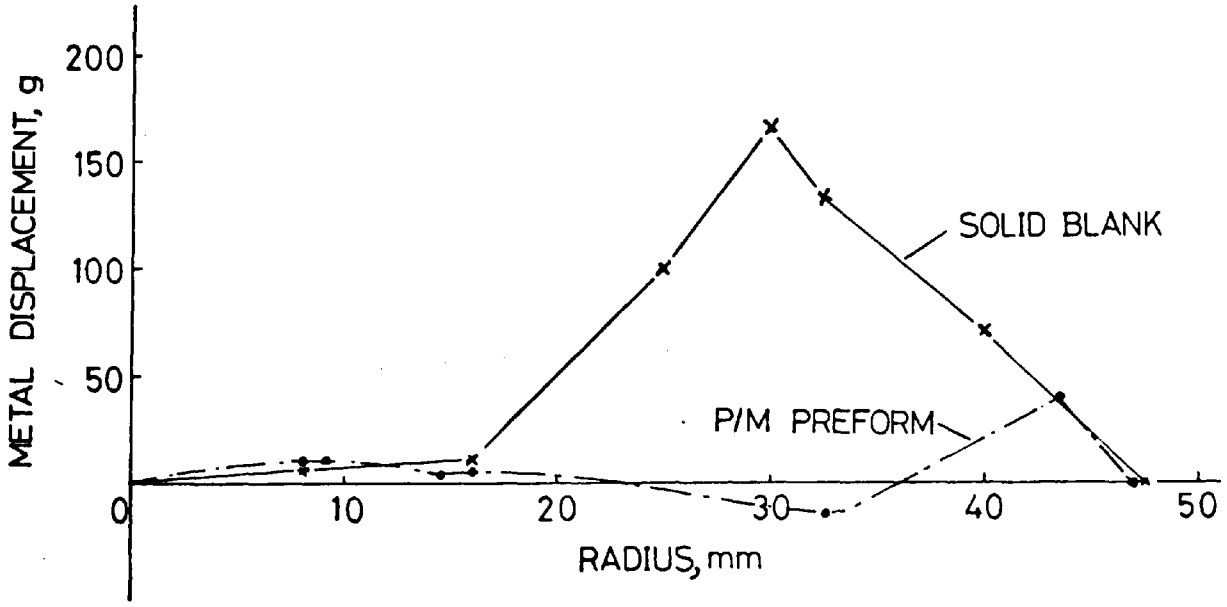

FIG. 2.4 Comparison of metal displacement resulting from conventional forging of solid material with that of the same component, sinter forged. (Ref. 28)

Fig. 2.5 TYPICAL PERIPHERAL AND CIRCULAR CRACKS IN POWDER FORGED TURBINE HUB

(See Section 8.4 and Ref. 28)

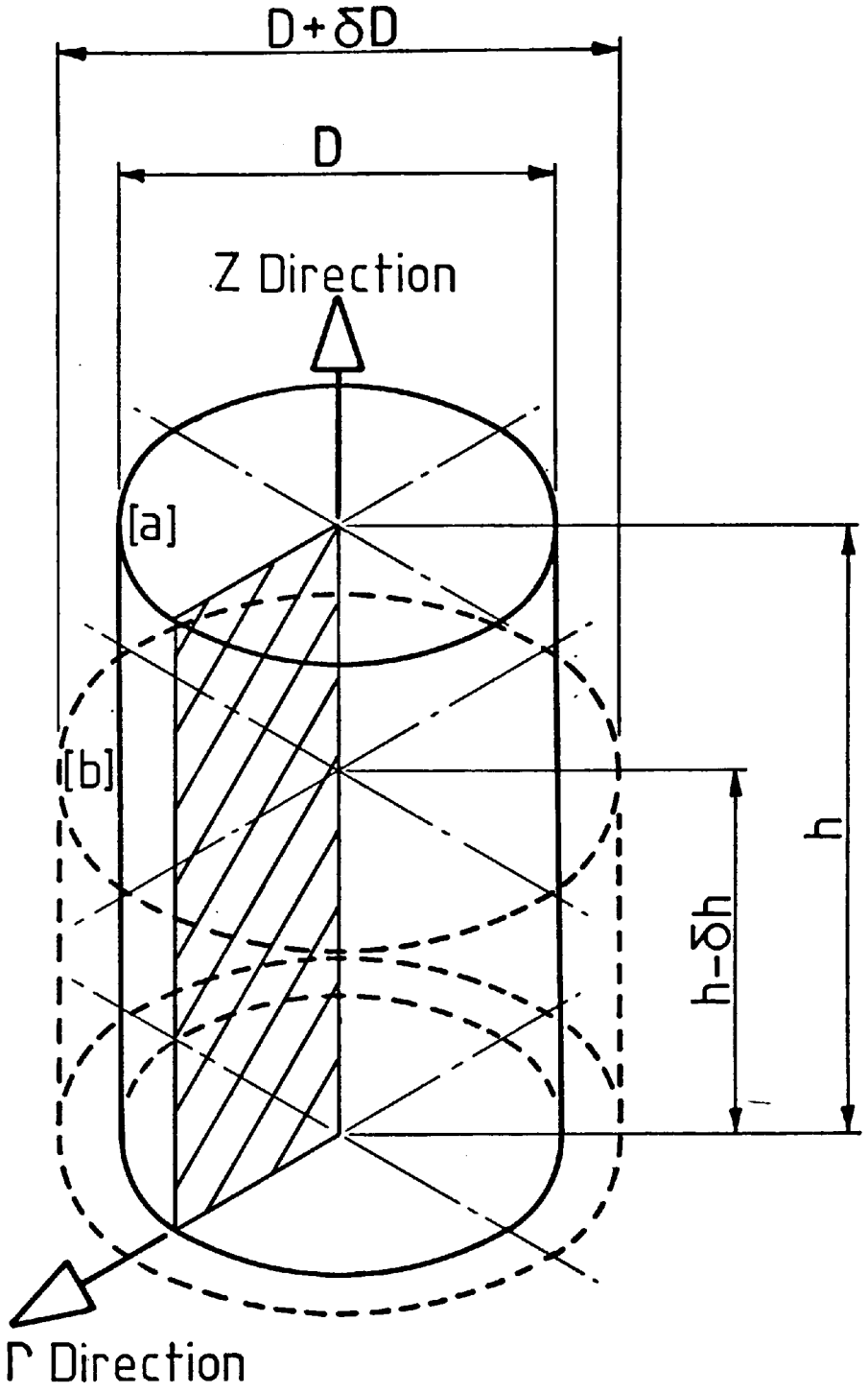

FIG. 2.6 FRICTIONLESS UPSETTING OF CYLINDRICAL PREFORM:

(a) preform of initial density ρ ;

(b) preform after frictionless upsetting to new density ($\rho + \delta\rho$). (Ref. 18)

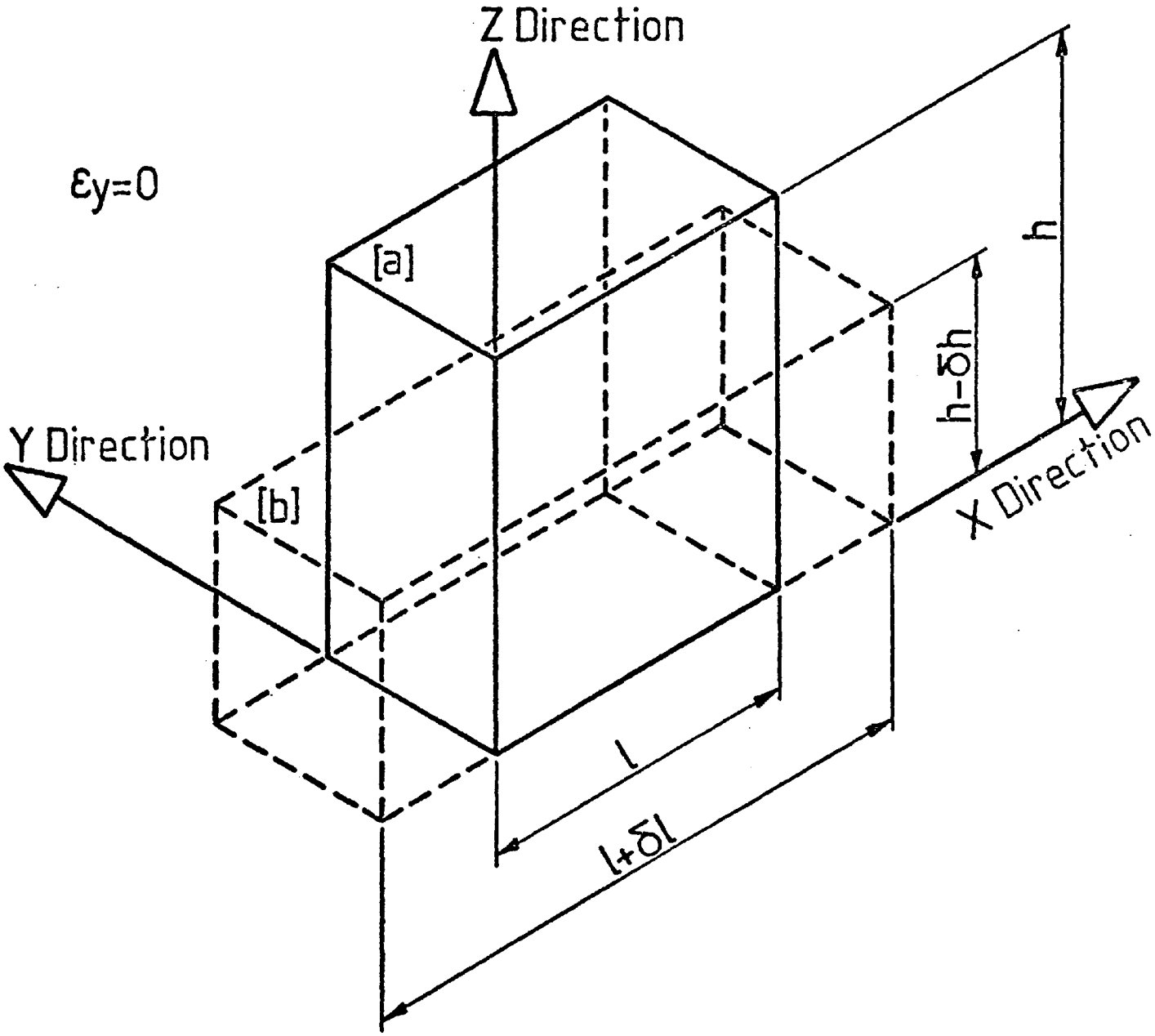

FIGURE 2.7 Plane-strain compression:
(a) preform before deformation;
(b) partly forged preform.
(Ref. 18)

individually or simultaneously, either with or without friction, depending upon the final shape of the component, design of preform, and effectiveness of lubricants.

Axisymmetric compression involves triaxial strain with the predominant reduction in pore dimensions taking place in the direction of compression. However, this consolidation is accompanied by lateral spreading of the pores with two degrees of freedom, thereby producing a relatively low rate of densification. In the case of plane-strain compression, i.e. biaxial strain, the predominant reduction in pore dimensions will again occur in the direction of compression, but lateral spreading can now take place with only one degree of freedom. This partial restriction in lateral spread brings about an enhanced rate of consolidation, or densification, as compared with the axisymmetric case[18]. With re-pressing, i.e. uniaxial strain, there is very little lateral spread, due to constraint caused by the die walls. However, until such times as there is absolutely no lateral spread, the dimensions of the pores will decrease in the direction of compression while their lateral dimensions remain constant, resulting in relatively rapid rates of densification. When a state of pure hydrostatic stress[36] exists due to complete lateral restraint, the pores will diminish in size, but not in shape, and in theory, will require an infinite stress to effect complete densification[41, 42].

In a real situation, a cylinder subjected to axisymmetric upsetting will barrel due to friction so that the middle portion of the preform makes contact with the die walls before the ends. It is possible that, during this transition period from axisymmetric to the re-pressing stage, the central portion of material in contact with the die wall will tend to behave as if it were subjected to plane strain

conditions[43].

From the foregoing it can be concluded that frictionless axisymmetric and unlubricated plane strain compressions produce the least and greatest rates of densification, respectively, during the upsetting stage of the powder forging process, as shown in Fig. 2.8. The actual conditions encountered in practice will lie somewhere between these two extremes.

2.5 Selection of Powders for Forging Applications

A considerable amount of attention has been focussed on the selection of the right type of powder for forging applications. Just as porosity is a limiting factor in conventional PM parts, so do the non-metallic inclusions have a similar effect on powder forged components[20, 22, 32]. Sponge iron powders are therefore avoided owing to the difficulty experienced in completely removing all the silica and alumina contained in the original ore, and water atomized or electrolytically reduced powders are favoured[16, 22, 44]. The advantage of high compressibility offered by sponge iron powders is no longer important, since preform densities within the range $\rho_* = 0.72 - 0.83$ are normally required[21], and these can easily be obtained with the other types of powders at moderate compaction pressures.

Water atomization is preferred to gas atomization, since it produces an irregular powder particle shape which is necessary for good mechanical interlocking during compaction[22], and hence ensures that the preform has good green strength. Powders produced in this way are annealed in a reducing atmosphere which helps to reduce some of the oxide film formed as a result of the atomizing water.

This oxide film can be further reduced during sintering by

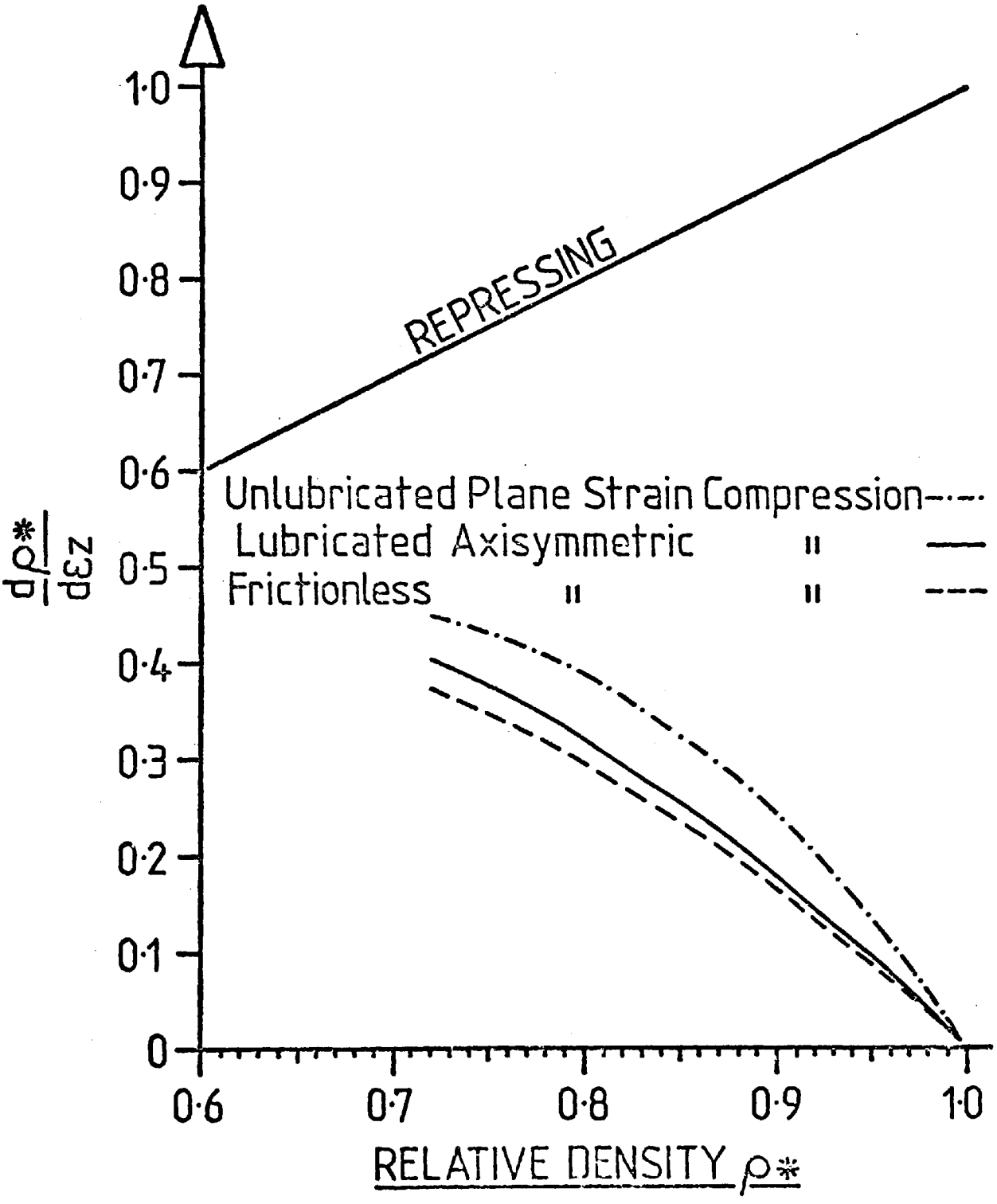

FIGURE 2.8 Comparison of "densification rates". (Ref. 18)

reacting with some of the admixed graphite[45] deliberately blended into the powder to adjust the carbon content of the final product. Additionally, it is considered that the use of coarser powder particles, apart from being economically attractive, may also help to overcome some of the problems of oxidation[10, 16].

2.6 Elemental Iron Powder Mixes

Mixes of iron powder, graphite and zinc stearate (see Section 2.8), represent the simplest possible material suitable for powder forging[46]. However, apart from limiting the range of mechanical properties available, such combinations can also result in a considerable degree of inhomogeneity in the microstructure. This is because the economically desirable sintering times[22, 47] normally employed in practice are too short to permit complete diffusion to occur throughout the material.

The actual changes which take place in the microstructure can be described as follows. Assuming that the graphite particles are small, uniformly distributed, and in intimate contact with the surrounding powdered metal, then, at the normal sintering temperature of 1130°C, all the carbon will go into solution in approximately four minutes[48]. However, if recourse is made to Fig. 1.1, it can be seen that at 1130°C it is possible for γ iron to contain a maximum of 1.7%C, although this will now occur in highly localised regions adjacent to where the graphite particles had originally been. As sintering, and hence diffusion proceeds, it is reasonable to suppose that a carbon gradient will gradually radiate outwards from these points. However, economic factors dictate that this process must cease before the homogenization is complete; this results in a final microstructure containing ferrite, pearlite, free cementite, porosity, and possibly some free graphite. After forging and quenching, such a microstructure

will probably contain ferrite, cementite, martensite and retained austenite[22].

2.7 Prealloyed Powders

Improved mechanical properties can be obtained by using low-alloy steel powders[24, 49, 50, 51], which also help to overcome many of the problems of inhomogeneity. However, since the cost of such powders increases sharply in proportion to the amount of alloying elements added, it is important to select the cheapest material possible to satisfy the functional requirements of the component[50]. With regard to carbon content, the standard practice seems to be to blend the requisite amount of carbon with the prealloyed powder, since prealloyed carbon reduces compressibility and therefore increases compaction pressure and tool wear[10, 16]. The optimum mechanical properties required to satisfy the component function are then obtained by suitable heat treatment, and the choice of prealloyed powder will depend upon the depth of hardness required in relation to the size of the part[50].

There is a marked tendency to avoid alloys containing chromium and manganese [10, 22] on account of premature failure of forgings made from these steels, because of such inclusions[32, 52] as Spessartite ($3\ MnO,\ Al_2O_3,\ SiO_2$), chromite spinell ($FeO,\ Cr_2O_3$) and escolite (Cr_2O_3). For these reasons powders such as the A.I.S.I. 4600 Ni.Mo. prealloyed powder, manufactured by A.O. Smith-Inland Inc., Milwaukee, have received much acclaim for powder forging applications[49]. However, in instances when hardenability is more important than mechanical strength, it may be possible to select a suitable alloy powder in which much of the expensive nickel has been replaced by cheaper chromium[50].

2.8 Mechanical and Isostatic Compaction of Powders

Although the precise geometry of preforms is neither as critical nor as complicated as it is with conventional PM parts[53], nevertheless the total mass[27] together with its careful distribution are important[28], and the success, or measure of success, of the final forging is very dependent upon good preform design[13, 16]. As with conventional PM practice, mechanical compaction tools for the production of preforms consist of two end punches, a die and possibly a core rod. In addition to its main purpose of helping to apply the compaction pressure, the lower punch may also be used for ejection. The tools are usually made from hardened and tempered alloy steels, although it is not uncommon for dies to be made from tungsten carbide. The degree of skill and quality of workmanship involved in the design and manufacture of the tools are of the highest order[6]. The lubricant used to reduce die wall friction generally takes the form of zinc stearate which is admixed with the powder in quantities not exceeding 1% by weight[54]. The compacting presses used are invariably of the double acting type and may be either mechanical or hydraulic[53], depending upon the size of the component, the quantity, and rate of production required.

Isostatic compaction does not require the use of admixed lubricants, since the powder is meteredout into an elastomeric mould, sealed, and placed in a pressure chamber where it is subjected to uniform fluid pressure in all directions[55]. The process may be either wet-bag or dry-bag. Whilst the former is useful for experimental work and the production of prototypes, the latter is favoured for mass production purposes. The poor dimensional accuracy associated with isostatic compaction is of little consequence in the manufacture of powder

forging preforms[16].

2.9 The Loose-Pack Method[56]

The Loose-Pack method is one whereby preforms can be produced without compaction. It involves pouring "as atomized" powders, mixed together with sucrose, which acts as a binder, into a disposable, consumable mould made from paper pulp. The filled mould is then vibrated at room temperature to densify the preforms prior to sintering and forging. The purpose of the binder is to hold the preform together after the mould has been consumed during sintering, to reduce the oxide layer on the powder particles, and to provide a source of carbon for alloying. Apart from capital saving costs on compaction tools and presses, other apparent advantages of the process include the use of cheaper "as atomized" powders, since annealing and grinding are no longer required, and overcoming the preform size limitation of 5lb (2.27 kg), imposed by conventional pressing techniques. Despite all these advantages, it appears that at the present time the Loose-Pack method is dormant in terms of commercial application[57].

2.10 Sintering

The purpose of sintering is to replace the weak mechanical bonds formed during compaction with very much stronger metallurgical bonds resulting from diffusion, recrystallization and grain growth. In general, sintering is carried out in a protective atmosphere at temperatures of between 60% to 90% of the melting point of the main constituent. In the case of ferrous based compacts, endothermic atmospheres capable of a range of controllable carbon potentials[58] are usually used in conjunction with sintering temperatures and times of approximately 1130°C and 30 minutes respectively. Although it has

been suggested that sintering in nitrogen rich atmospheres could lead to the possibility of nitriding[37] the surface of the preform, it has recently been reported[59] that the use of cryogenic nitrogen with controlled small additions of endogas has proved to be satisfactory.

Commercial sintering furnaces[58] may be of the mesh belt conveyor, roller hearth, pusher, or walking beam type, heated by either electricity or gas. Electrical heating at temperatures of 1130°C is achieved by the use of silicon carbide rods. Most sintering furnaces consist of three distinct sections[60], viz. lubricant removal, sintering, and cooling. The purpose of the first section is to dewax and preheat the component prior to sintering. This results in the volatilization of the lubricant, so that care must be taken not to contaminate the sintering region. Although the component may attain a temperature of 680°C during the process, the lubricant can be removed in air at 400°C. The cooling section is normally water jacketed to reduce the temperature of the component sufficiently to prevent it oxidising on removal from the furnace.

On entering the sintering region the component soon acquires its full sintering temperature, thus increasing the mobility of the atoms and allowing the sintering to proceed. The main driving force[58] is derived from the free surface energy associated with the cavities, so that as the process continues the irregular cavity shape resulting from compaction tends towards a spherical form, in keeping with the gradual reduction in surface energy. Meanwhile, the mechanical boundaries are transformed to grain boundaries and then disappear as a result of recrystallization[11]; this results in the original particles completely losing their individuality, and thus forming a coherent mass.

In the case of iron/graphite mixes, the oxide films on the iron powder particles must be reduced by the graphite and the sintering atmosphere before the iron and the graphite can effectively combine. Natural graphites are preferred to the synthetic variety[61], and the quantity added should be slightly greater then the amount of combined carbon required in the final microstructure. The diffusion of the carbon into the iron is described in Section 2.6.

Careful control of the carbon potential of the sintering atmosphere is necessary to prevent either excessive carburization or decarburization. In this latter connection it is necessary to keep the CO_2 content low by maintaining a low dew point, i.e. H_2O content, otherwise the following reaction will occur: $H_2O + CO = CO_2 + H_2$. This will increase the ratio of CO_2 to CO which results in a lowering of the amount of combined carbon formed during sintering. The amount of combined carbon is also influenced by the ratio of CH_4 to H_2, so that the carburizing tendency is increased by the presence of quite small amounts of CH_4. The extent to which the sintering atmosphere tends to be either oxidizing or reducing depends upon the ratios of CO_2 to CO and H_2O to H_2.

The effect of sintering temperature and time on the amount of combined carbon formed is illustrated in Fig. 2.9 , which shows the results for a series of bars made from iron plus 1.25% graphite. Sintering at temperatures below approximately 1000°C results in virtually no combined carbon occurring in the microstructure; whereas sintering at 1040°C results in the maximum amount of combined carbon. Higher temperatures and longer sintering times will, initially, allow the matrix material to develop its full mechanical strength by forming strong metallurgical bonds in the manner described earlier. Any

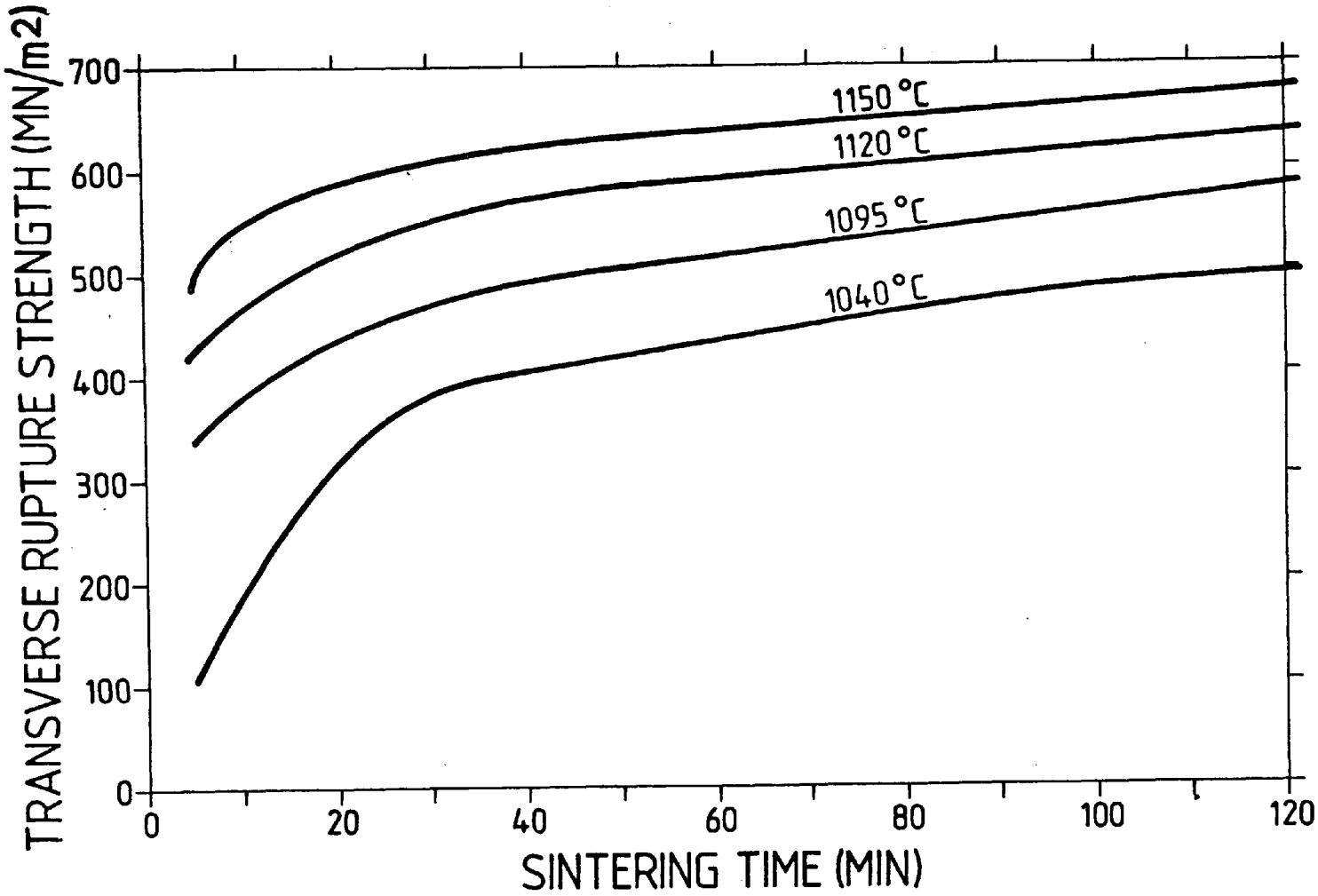

FIG. 2.9 CURVES SHOWING THE EFFECTS OF DIFFERENT SINTERING TIMES AND TEMPERATURES ON THE TRANSVERSE RUPTURE STRENGTH OF SPECIMEN MANUFACTURED FROM IRON/GRAPHITE MIXES

(Ref. No. 61)

further increase in the strength of the component must then be attributed to improved pore morphology resulting from spheroidization of the cavities. However, as far as the manufacture of powder forging preforms is concerned, this spheroidization does not offer any particular advantages, so that costly, prolonged sintering is quite unnecessary.

2.11 Sintering/Forging Heating Cycles

As stated in Section 2.4, preforms can be sintered in the normal manner, cooled for storing, and then reheated immediately prior to forging. Much attention has been focussed on induction[10, 12, 29, 37, 53, 62, 63] heating for this latter purpose, whilst Fig. 2.10 provides evidence to suggest that the optimum temperature for forging is approximately 800°C. Nowadays, it appears to be standard practice to coat the preforms with graphite suspended in water[63] in order to prevent oxidation and decarburization on exposure to the air whilst being transferred from the heating coil to the forging die. The same water-graphite dispersions[10] are also used to lubricate the dies, which ideally should be preheated to prevent chilling; this results in surface porosity as shown in Fig. 2.11. Earlier work on powder forging adopted the use of impervious anti-scaling compounds[24], e.g. Biratekt[28], to protect the hot preforms in the absence of protective atmospheres, whilst copper based lubricants were sprayed on to the dies to reduce friction, and hence the forging loads and associated tool wear.

An economically attractive alternative to the heating cycle just considered, is that of forging the hot preform immediately after sintering[37, 53], i.e. either at 1100°C, allowing for some heat loss during transfer, or by cooling to approximately 800°C. This procedure would necessitate the sintering furnace being modified[16] to

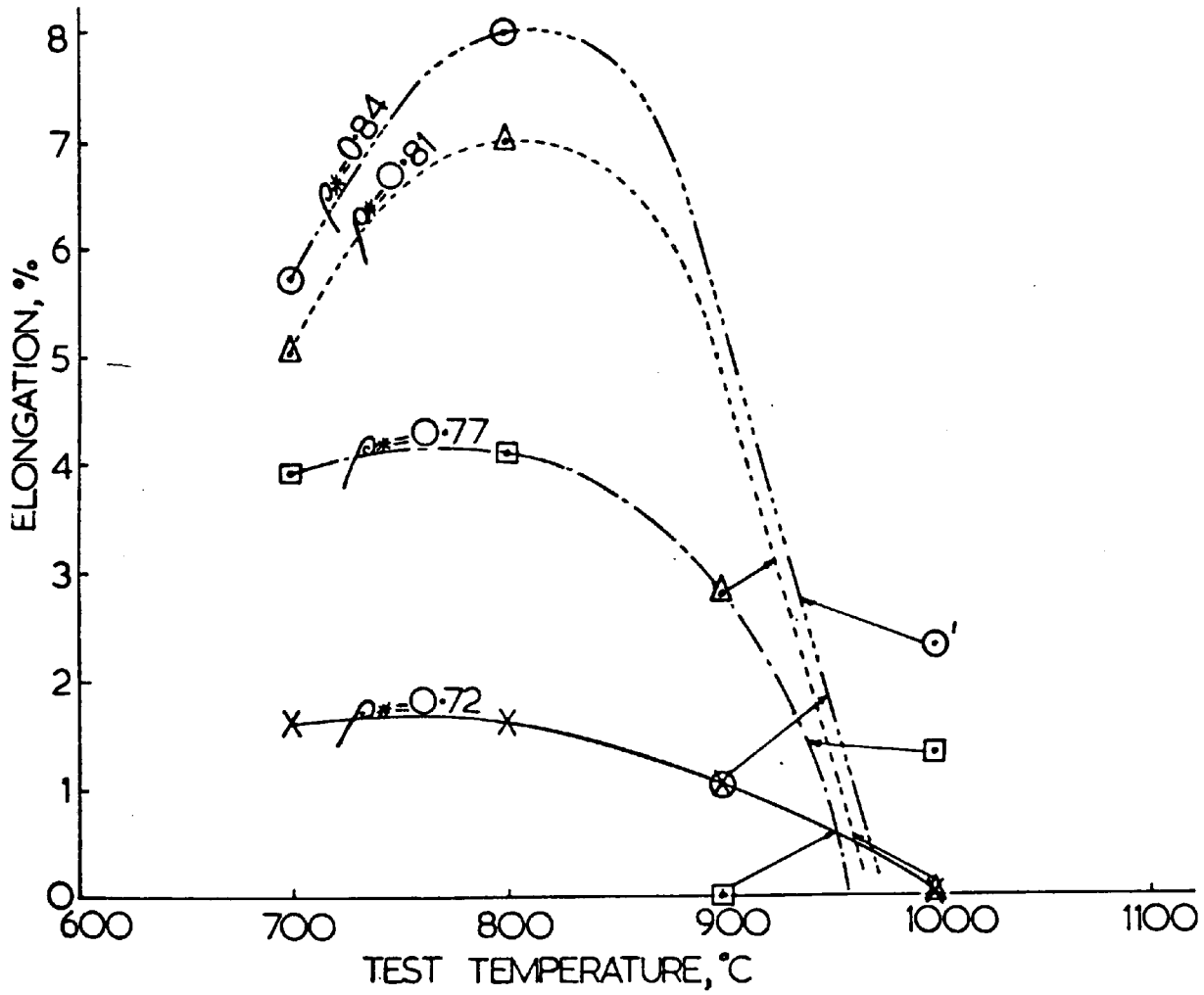

FIG. 2.10 Curves showing variation of percent. elongation with test temperature. (Ref. 28)

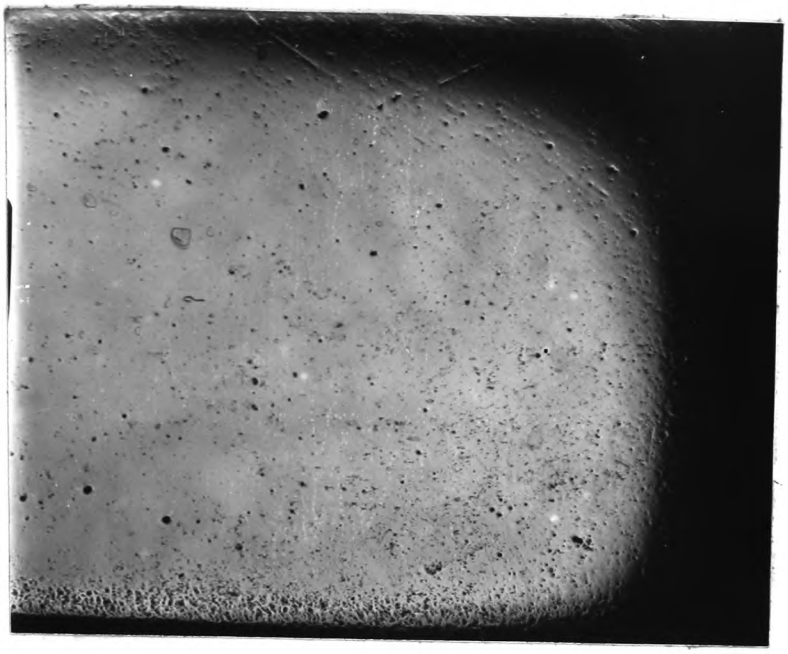

Fig. 2.11 PERIPHERAL POROSITY IN POWDER FORGED TURBINE HUB

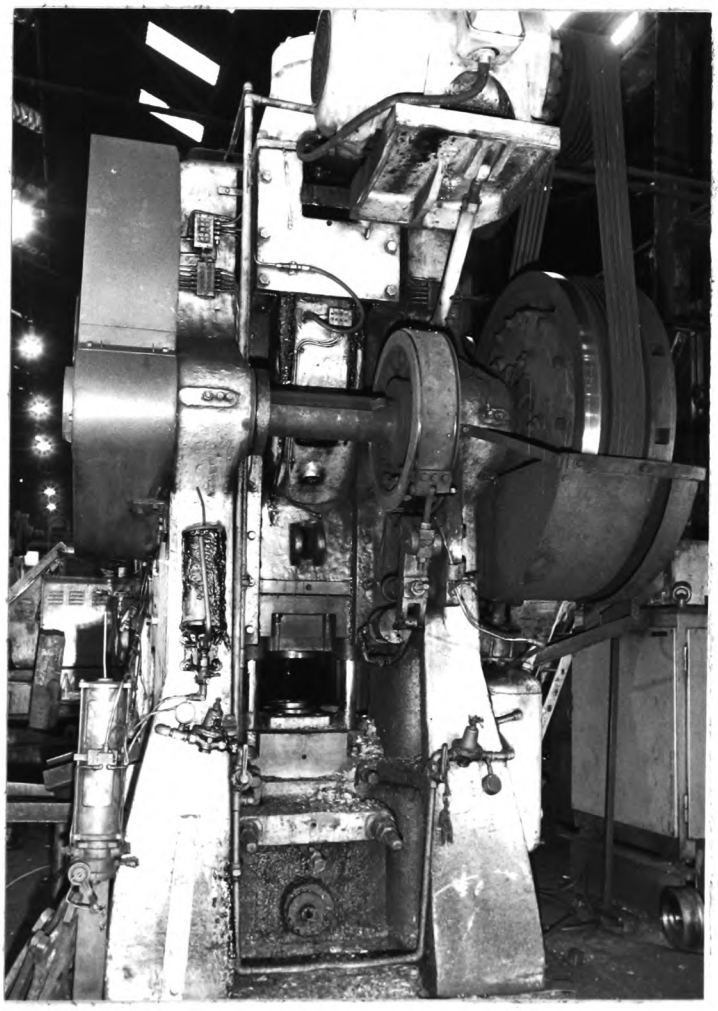

Fig. 2.12 "AJAX" 750 tonf (7.5 MN) FORGING PRESS
(South Wales Forgemasters Ltd., Cardiff, see Chapter 8)

either eliminate or reduce the size of the cooling region. Furthermore, in the event of the preforms being produced by isostatic compaction, and therefore not containing admixed lubricants, the preheat region could also be modified accordingly. Such modified furnaces would have to be located near the forging presses, and the respective production rates of both operations would have to be suitably matched. The problem of oxidation and decarburization during the $\sim$ 4s transfer[63] from the furnace to the forging equipment is likely to be offset by the fact that some of the protective atmosphere of the furnace will have permeated into the surface pores of the preform, thus affording protection from oxygen penetration.

Another heating cycle which combines the sintering with the heating for forging, is that of sintering by induction[35, 37] in a protective atmosphere. However, care must be taken to ensure that the rate of heating is not too rapid otherwise thermal gradients will be set up from the outer layers to the core of the preforms. These in turn will result in thermal stresses which, if excessive, will cause the preforms to crack. Furthermore, internal cracking may occur due to the rate at which the admixed lubricants tend to volatilize within the preform, compared with the rate at which they can escape from its surface. It therefore follows that dewaxing and preheating may prove to be a prerequisite to induction sintering.

2.12 Forging Presses

Since the aim of powder forging is to produce precision parts, the forging presses must have good rigidity and good ram guidance. Mechanical forging presses[10, 37] employing cranks (see Fig. 2.12), or eccentrics, seem well suited to the task, especially when fitted with ejection mechanisms. Screw presses can also be used, but

hydraulic presses are unsuitable for production purposes because their relatively slow speed of operation and long contact times with the preform result in chilling. High energy rate forming (HERF), in the form of the Petro-Forge[64], has also been used to produce powder forgings; the advantages offered are those of reducing both the physical size of the equipment, and the capital cost.

2.13 Forging Tools

As with conventional PM components, the number of parts required is an extremely important criteria in deciding whether to produce the parts by powder forging, as opposed to some alternative manufacturing route. In this connection, it appears that quantities of less than 10 000 components[13] per annum are not economically attractive, whilst in some cases minimum orders totalling 50 000 have been quoted[65].

In view of this, it follows that tool life is a very important consideration, and it has been suggested that easily replaceable parts of the tooling should have a life expectancy of 5000 to 10 000 components, whilst the rest of the tool should have a life of 10 000 to 20 000 components[10]. Such tooling will be required to operate at forging pressures of between 800 to 1 200 MN/m^2. (Based on data provided in Ref. No. 49.) Owing to lack of long-term experience with this process there is not a great deal of information available regarding tool wear. However, this is obviously influenced by the choice of tool material, heat treatment, complexity of tooling, geometry of preform, lubrication, and forging temperature. Tool life is enhanced by the absence of scaling on preform surfaces, reduced lateral flow, lower forging loads resulting from porosity during the initial stages of forging, and the absence of flash at the end of the forging operation (see Section 2.4). Tight tolerances on finshed

parts will limit tool life. Realistic tolerances are given in Table 2.1.

Table 2.1 (Based on data provided in Ref. No. 12)

Part Feature	Tolerance
Outside diameter or profile	± 100 μm
Length parallel to press axis	± 380 μm
Cored hole diameter	± 80 μm
True position of cored holes	± 130 μm*
Surface roughness (RMS)	30 μm (Ref. No. 10)

The ability to hold these tolerances will depend upon accurate control of preform temperature since this controls the amount of thermal contraction of the component on ejection from the die. Preliminary work undertaken by Griffiths et. al.[28] show that the thermal expansion of porous, ferrous materials is almost identical to that of wrought ferrous materials. This led to the conclusion that the 1 in 60 contraction allowance commonly employed throughout the forging industry could, in the first instance, be applied to the design of tools for powder forging. However, in addition to the preform temperature, the precise amount of contraction of the powder forging will also depend upon the thermal expansion properties and amount of preheating of the die, together with the elastic properties of both the die and the PM material.

2.14 Control of the Process

The success of the powder forging process is very dependent upon the amount of control[10, 29] governing each of the stages involved. It

is therefore important that the process be as automated as possible. In this connection, Unimate industrial robots[66] have been successfully used to load green compacts into rotary hearth sintering furnaces and then transfer heated preforms from the furnace to the forging presses. Control of the sintering furnace atmosphere is also important; here the methods are quite well established[58], e.g. the use of the lithium chloride dew cell and infrared CO_2 analysis.

For the control of forging temperature use has been made of both radiation[63] and optical pyrometers[27]. Not only will these instruments sense and control the temperature, but they are also arranged to actuate mechanisms to reject those parts which do not conform to the stipulated requirements.

The mass of the preform is critical, since it dictates the final properties of the forging. Such properties will be sub-standard because of incomplete densification[20] in the case of preforms that are underweight, whereas overweight preforms may damage the tooling and presses. Hence it is not uncommon for green compacts to be individually weighed[27, 29] before sintering.

Since it is obviously important to monitor and control various operations from start to finish, it is likely that specialized control equipment will be developed to suit the needs of the process. Although this will inevitably lead to an increase in the amount of capital expenditure required to install new production lines, it should reduce the size of the work force needed, there by making the overall process more economical.

2.15 Powder Forging Successes and Future Market Potential

In the early 1970's it was anticipated that the automotive industry [29, 31] would provide the greatest potential market for powder

forged parts, most of which resembled solids of revolution, the connecting rod being a notable exception. At the same time it was considered that the first actual use of powder forgings would be in superalloy turbine discs for military aircraft[38]. In fact, a selection of components[12, 35] which have been successfully produced by powder forging include overrunning clutch races, differential gears[63], spur gears, bevel gears, outboard motor drive gears, rotors for high pressure hydraulic motors, ratchet heads, roller bearings, and connecting rods[62] for automotive, chain saw, and outboard motor applications. Hence it can be seen that in addition to the automotive and military applications originally envisaged, powder forging has also made in-roads into those industries involved with agricultural and lumber equipment, hydraulic and marine equipment, and the manufacture of industrial hand tools. The success of the process can be attributed to its competitiveness arising from good material utilization, reduced machining costs and the elimination of weight balancing of moving parts such as the connecting rod[23].

It has been reported[59] that in 1977 the production of powder forged parts in the U.S.A. was approximately 10 000 tonnes as compared with 200 to 300 tonnes in Europe. However, Brown[67] suggests that in 1975, the United Kingdom production of powder forged parts alone was nearer 1 000 tonnes per annum, and it has been estimated[35, 67] that the potential output could be in excess of 50 000 tonnes per annum before the end of the 1980's.

CHAPTER 3

Aims and Approach to Project

3.1 Development of Analytical Techniques

Owing to the lack of the specialized equipment needed to exercise careful control over the heating operations involved in the powder forging process, it was regarded as futile to attempt to embark on a programme aimed at the optimization of mechanical properties. Furthermore, to do so would only involve a duplication of the extensive amount of work which has already been carried out in this area, in order to prove the process.

It was therefore decided to concentrate on work of a more fundamental nature, aimed at devising new analytical techniques to help understand and explain some of the phenomena associated with the various operations involved in the entire powder forging process. This meant that in addition to devising analytical techniques having a direct bearing on the forging process[18], techniques were also developed to analyse the behaviour of the preform material, and also to quantify the material flow which takes place during forging[68]. The purpose of this latter technique was to analyse successful preform designs arrived at by trial and error methods, to provide information that could be useful in the design of preforms for similar future components.

The success of the powder forging process to date, can be directly attributed to the amount of analytical work which has already been undertaken[13]. It was in recognition of the need for such an approach that the United States Department of Defence implemented project "Themis".

3.2 Implications of Alternative Methods of Preform Manufacture

Evan at this early stage in its development there is evidence to suggest that ultimately the process may not involve conventional powdered metals, since porous preforms may be produced from swarf[69], or alternatively by the "Osprey" process[70] i.e. spray forging. Since this implies that the method of producing the porous preforms may be of little consequence, as the mechanical properties of the finished component are developed during the final forging operation, then it may be possible to produce satisfactory preforms from coarser sized powder fractions[10, 16] than those normally employed in conventional PM. Such an approach would represent a considerable saving in powder cost, since added expense is generally involved in removing or minimizing these coarser fractions. It seems that the practice to date has been to manufacture preforms from commercially available powders conforming to specifications that have been evolved with a view to optimizing the mechanical properties of conventional PM parts. It therefore follows that such powders may be unnecessarily expensive for powder forging applications, and for this reason it was decided to examine the possibility of using coarser grained powder, by sieving out the coarse powder fraction, and using this in addition to the "as supplied" powder.

3.3 Effects of Residual Porosity

It is a well acknowledged fact that the vast majority of service failures occur as a result of fatigue fracture[71]. Since it is also recognised that it is not always possible to completely close up all the porosity in a powder forged component[67], the next best thing is to ensure that any residual porosity is strategically arranged to occur in low stressed regions. Nevertheless, for high performance components operating under conditions of fluctuating or alternating stress, even these small pockets of porosity may lead to premature failure. The

reason is that although they may only represent a few percent in terms of the whole component, the localised concentration may represent an equivalent porosity of 10-20%. Walker[72] cites an example of a cast steel with an overall porosity of only $\sim$ 3%, resulting in a reduction in tensile strength of $\sim$ 85%, due to the fact that it was all concentrated into one region.

The foregoing serves to indicate that there is a need to examine the mechanical properties of partly forged powder preforms, in an attempt to simulate the conditions likely to be encountered in these localised regions.

3.4 Inductive Approach

It appears that the process of induction is the most common technique employed in the scientific study of the various aspects of powder metallurgy. This is understandable in view of the vast number of variables which occur in PM processes. Induction is the procedure whereby knowledge is acquired by observation and analysis. It involves collecting and classifying facts, and where possible, devising empirical laws to connect variables, without however, being able to justify why such laws should exist. These laws can therefore only apply over the limited range of experimental observation, and despite their convenience, they unfortunately contribute very little to a complete understanding of the processes involved. Furthermore, they may constitute a danger in as much as they could be used out of context, due to lack of appreciation of their origins, limitations, and the significance of the empirical constants involved. Such constants may be the result of the interaction of a number of variables producing both individual and combined effects. Although it is appreciated that it may be virtually impossible to quantify some of these variables, at least some attempt

should be made to interpret the significance of the empirical constants, until such time as the body of knowledge related to the particular topic has grown into an advanced and deductive science.

3.5 Deductive Approach

Deduction is the process whereby knowledge acquired by induction is used to make predictions of effects before they have actually been observed. Before such predictions can be regarded as valid they must, of course, be verified experimentally. In order to make these predictions it is necessary to form an hypothesis, based on the available information. By this method it is possible to plan meaningful experimental programmes rather than record facts without any distinct purpose. However, in conducting such experiments the investigator must be unbiased and prepared to abandon opinions as soon as the facts obtained prove them to be erroneous.

The deductive method may therefore be summarised as, (i) direct induction to provide an insight into the laws which operate, (ii) application of deductive reasoning to (i) to predict effects other than those already observed, and (iii) experimental verification of the predictions made in (ii).

3.6 Inter-relationship Between Natural Laws

There are three distinct ways in which one natural law may be explained in terms of others[73].

(i) Homogeneous inter-mixture of effects

i.e. where there are two or more separate causes in action, the results of which may be added or combined homogeneously.

(ii) Intermediate effect of a cause

i.e. A causes B, and B causes C instead of A causing C directly, so that B constitutes an intermediate link.

(iii) A case of a more general law

Many partial laws and facts which at first are seemingly disconnected, eventually prove to be special examples of a more general all embracing law.

CHAPTER 4

Powder Characterization and Preparation

4.1 PM Starting Material

In view of the comments made in Section 3.1 regarding the lack of equipment necessary to develop optimum mechanical properties, it was not considered that any useful purpose would be served by using anything but the simplest materials for the purpose of the present study. To this end water atomised[74, 75] elemental iron powders were used, see Section 2.5.

Early work was carried out with MP32 iron powder manufactured by Round Oak Steel Powders Ltd., (Rospol), Brierly Hill, Staffordshire. Unfortunately, however, manufacturing operations ceased[76] at this plant in the summer of 1977, making it necessary to continue experiments with the alternative Hoganas AHC 100.29 iron powder. Fig. 4.1 shows a flow sheet illustrating the Rospol process, and a visit was made to the plant[6] in April 1975 to gain a first-hand appreciation of the manufacturing process.

MP32 possessed good compressibility and excellent green strength. Tables 4.1 and 4.2 provide lists of typical properties as quoted in the Rospol brochure[77].

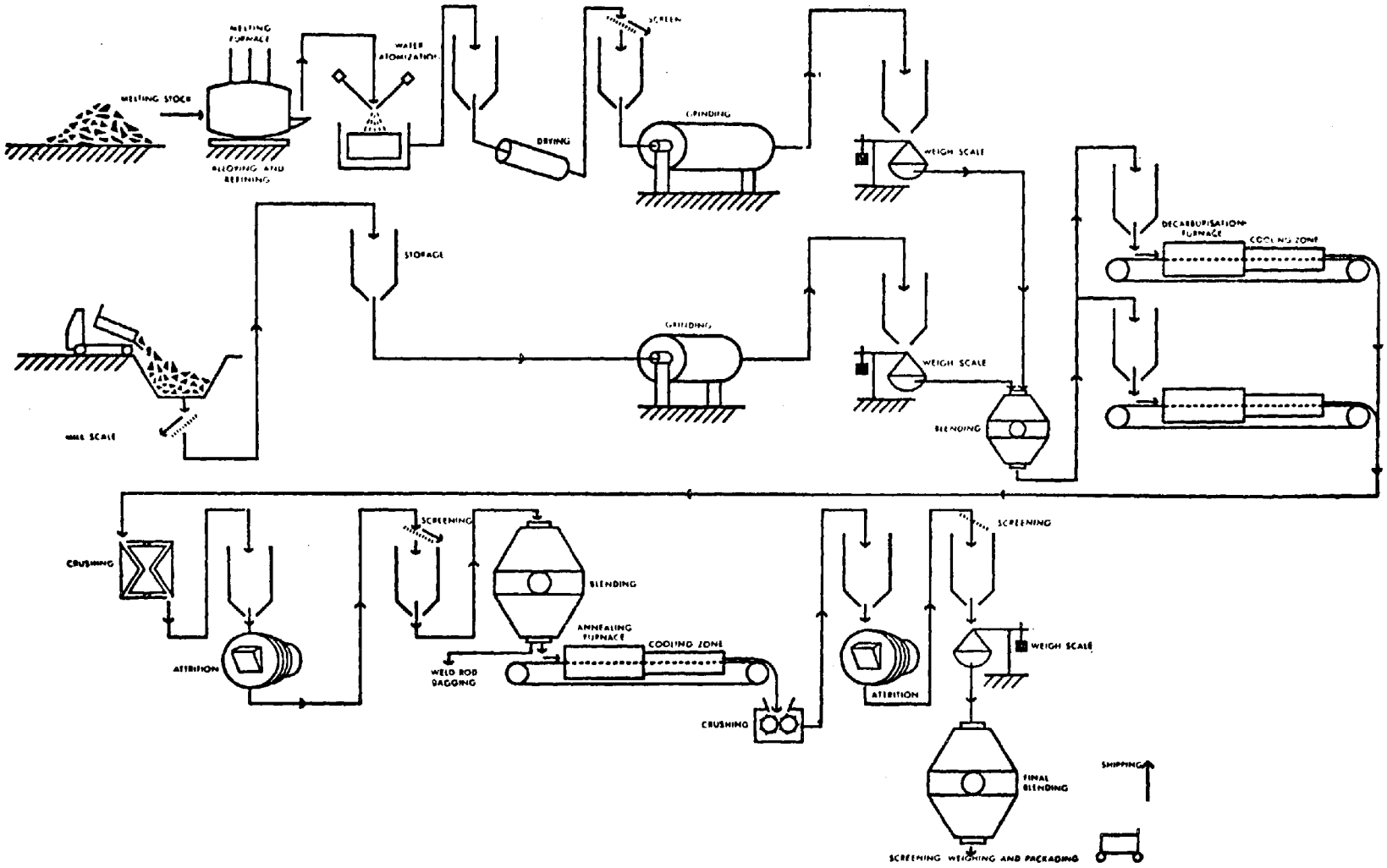

FIG. 4.1 FLOW SHEET ILLUSTRATING THE ROSPOL PROCESS

(Ref. 77)

TABLE 4.1

Screen Analysis of MP32 (% by weight)

ASTM Mesh. Spec. E 11		
+ 100 mesh	(150 μm)	2%
+ 140 mesh	(106 μm)	19%
+ 200 mesh	(75 μm)	26%
+ 325 mesh	(44 μm)	28%
- 325 mesh	(44 μm)	25%

TABLE 4.2

Chemical Analysis of MP32 (% by weight)

Carbon	0.02%
Sulphur	0.02%
Phosphorus	0.02%
Manganese	0.2%
Silicon	0.13%
Hydrogen loss	0.25%
Total iron	Balance

Apparent density (Hall) = 2.5 g/cm^3 *

Flow (Hall) = 30 s

* This is a non-SI metric unit[78].

Hoganas AHC 100.29 water atomised elemental iron powder[79] possesses high purity and high compressibility. The chemical analysis as supplied by the manufacturer is given in Table 4.3.

TABLE 4.3

Chemical Analysis of AHC 100.29 (% by weight)

Carbon	0.01%
Sulphur	0.01%
Phosphorus	0.01%
Manganese	0.05%
Silicon	0.02%
Hydrogen loss	0.1%
Total iron	Balance

Where relevant, all subsequent experimental graphs will indicate in the titles, whether MP32 or AHC100.29 iron powder was used for the tests.

4.2 Flow, Apparent Density and Tap Density of AHC 100.29 Iron Powder

Throughout these tests the powder was used in the unmixed, "as supplied" state, and the samples were selected at random from the bulk powder without any special precautions being taken to ensure that the samples were necessarily representative of the total mass.

All weighings were performed on a Sartorius top loading torsion balance, which overcame the problem of powder particles either damaging or interfering with knife-edges. Additionally the balance had a built-in optical taring system, which enabled the effects of the weights of containers and vessels to be completely eliminated, so that their contents could be weighed directly.

The rate of flow[80] and the apparent density[81] was determined with the aid of a standard Hall Flowmeter. The current standards for flow rate are ASTM B-213-48 and MPIF Standard 3-45, and those for apparent density are ASTM B-212-48 and MPIF 4-48.

The procedure to determine flow rate was to cover up the orifice at the bottom of the Hall Flowmeter, and introduce 50 g of powder into the funnel. The orifice was then uncovered and the time taken for the 50 g to flow out of the funnel was measured with a stop-watch. This time in seconds was recorded as the flow rate, and the average value obtained from a number of such tests is shown in Table 4.4, where it is compared with the value quoted by Hoganas AB.

The apparent density was determined by pouring approximately 35 cm^3 of powder into the Hall funnel, and then allowing this to flow freely into a 25 cm^3 density cup. When all the powder had flowed out of the funnel, it was levelled off the top of the cup with a straight-edge. The filled cup was weighed to determine the weight of the powder which was then multiplied by 0.04 to give the apparent density in g/cm^3 or Mg/m^3. The average value obtained from a number of these tests is shown in Table 4.4, together with the value quoted by Hoganas AB.

As an alternative means of measuring flow rate, the time for the set volume of 25 cm^3 contained in the density cup to flow through the funnel was also determined and recorded in Table 4.4. A comparison of the results obtained by these two separate methods of measuring flow rate was now possible since,

$$\text{volume flow} = \frac{\text{weight flow}}{\text{apparent density}} \qquad (1)$$

From Table 4.4,

$$\text{volume flow} = \frac{25\ cm^3}{42\ s} = 0.595\ cm^3/s$$

$$\text{weight flow} = \frac{50\ g}{29.2\ s} = 1.712\ g/s$$

and apparent density = 2.96 g/cm^3,

$$\text{hence, } 0.595\ cm^3/s = \frac{1.712}{2.96} = 0.578\ cm^3/s$$

It can therefore be seen that the results correspond reasonably well with one another.

TABLE 4.4

Physical Properties of AHC 100.29 Iron Powder

Property	Average of experimental values	Hoganas values
Flow rate	29.2 s/50 g	28 s/50 g
Flow rate	25 cm^3/42 s	-
Apparent density	2.96 g/cm^3	2.95 $^{+\ 0.10}_{-\ 0.05}$ g/cm^3
Tap density	3.75 g/cm^3	

Unlike the measurement of apparent density, where it was necessary to ensure the complete absence of any vibration, the tap density was determined by deliberately vibrating a known weight of powder in a measuring cylinder until the volume of the material became constant. In order to perform this non-standard test, a 100 cm^3 measuring cylinder was approximately half-filled with powder, and the weight of powder determined. The cylinder was then gently tapped and vibrated until the powder had completely settled, whereupon its volume was noted and divided into its weight to give the value of tap density shown in Table 4.4.

4.3 Sieve Analysis of AHC 100.29 Iron Powder

The sieve analysis was carried out to establish the particle size distribution of the bulk powder. The test sieves used complied with B.S. 410: 1976, ISO/R565 and ASTM Specification E11. The method of sieving was in general accordance with ASTM B-214-64 and MPIF 5-62. Since the apparent density of the powder was greater than 1.5 g/cm^3,

then a sample of 100 g was weighed out for sieving[82]. A stack of suitable sieves, see Table 4.5, was arranged with the coarsest at the top and the finest at the bottom. A receiving pan was fitted to the bottom of the stack, and the sample of powder poured onto the top sieve, and a lid placed in position. The stack was then clamped in place on the shaker, see Figure 4.2, which was normally used for fatigue testing so that the frequencies and amplitudes could be varied over a wide range. It was found by trial and error that the optimum frequency at which to operate the shaker was 15 Hz with a total vertical displacement of approximately 18 mm.

Sieving took place for 15 minutes, after which the quantity remaining on each sieve, together with that in the receiver, was weighed and the results tabulated as shown in Table 4.5. This method of recording the results is in accordance with the recommendation of ASTM B-214-64.

TABLE 4.5

Sieve Analysis of AHC 100.29

Retained on Sieve	Passing Sieve	Percentage by Weight
ASTM Sieves (Specifications E.11)		
No. 80 (180 μm)	--------	0.3
No. 100 (150 μm)	No. 80 (180 μm)	12.1
No. 120 (125 μm)	No. 100 (150 μm)	18.8
No. 170 (90 μm)	No. 120 (125 μm)	34.38
No. 270 (53 μm)	No. 170 (90 μm)	25.96
--------	No. 270 (53 μm)	8.45
	Total ----------	99.99

Fig. 4.2 POWDER SHAKER

A histogram[83] showing the various powder fractions was then plotted as shown in Figure 4.3. These fractions will be referred to in the subsequent sections dealing with compaction and mechanical testing. Particular attention will be focussed on the coarse fraction (150 to 180 μm) referred to as the "first fraction" Figure 4.3, since, as already mentioned in Section 3.1, the possibility of using such a fraction for powder forging could offer distinct economic advantages.

In plotting the histogram use was made of the screen analysis provided by Hoganas which stated that there were no powder particles greater than 65 Tyler mesh i.e. 210 μm.

The ogive[84] or cumulative underweight curve Figure 4.4 was plotted using the data provided in Table 4.5. From this curve the median particle size i.e. the size corresponding to 50% underweight, or overweight, was determined as being 108 μm. The cumulative underweight curve was also used to provide the data for Figure 4.5, i.e. the Particle Size Frequency Curve.

The actual procedure used to plot this latter curve, which is based on a class interval of 10 μm, is illustrated in Figure 4.4, where, for example, it can be seen that the difference in percentage underweight lying between 130 μm and 140 μm is 8%. It can therefore be argued that 8% of the powder by weight has an average particle size of 135 μm. This procedure was repeated over the whole size range, and the ensuing results plotted as shown in Figure 4.5.

4.4 Sub-Sieve Analysis

The fines of sub-sieve fraction i.e. particle size $< 53\ \mu$m, shown in Figure 4.3 was further analysed for particle size and distribution, by means of a Fisher Sub-Sieve Sizer[85, 86] and a Coulter Counter[87]. Whereas the former gave the "mean particle diameter", the

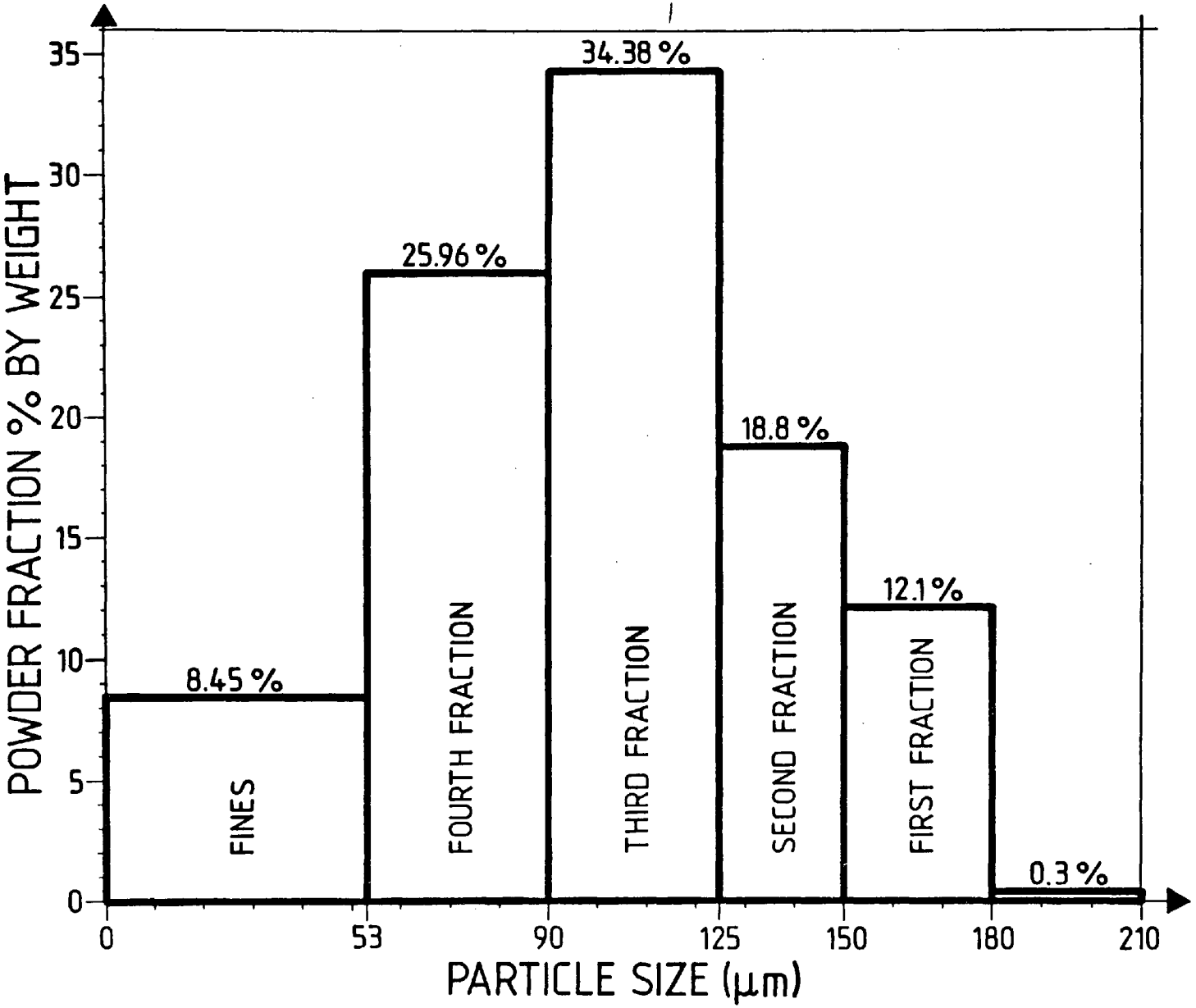

FIG. 4.3 HISTOGRAM OF PARTICLE SIZE DISTRIBUTION (AHC 100.29)

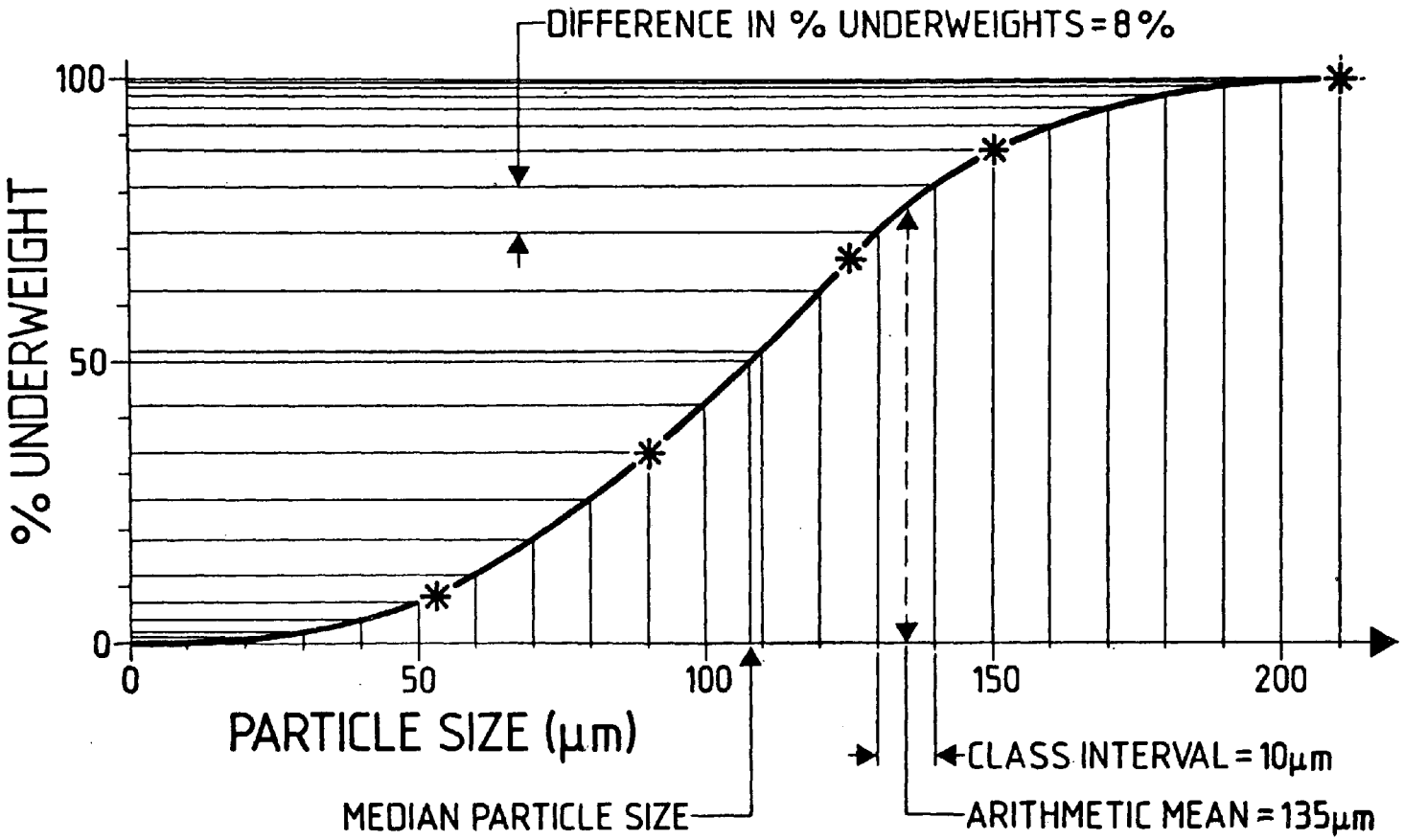

FIG. 4.4 OGIVE OR CUMULATIVE UNDERWEIGHT CURVE (AHC 100.29)

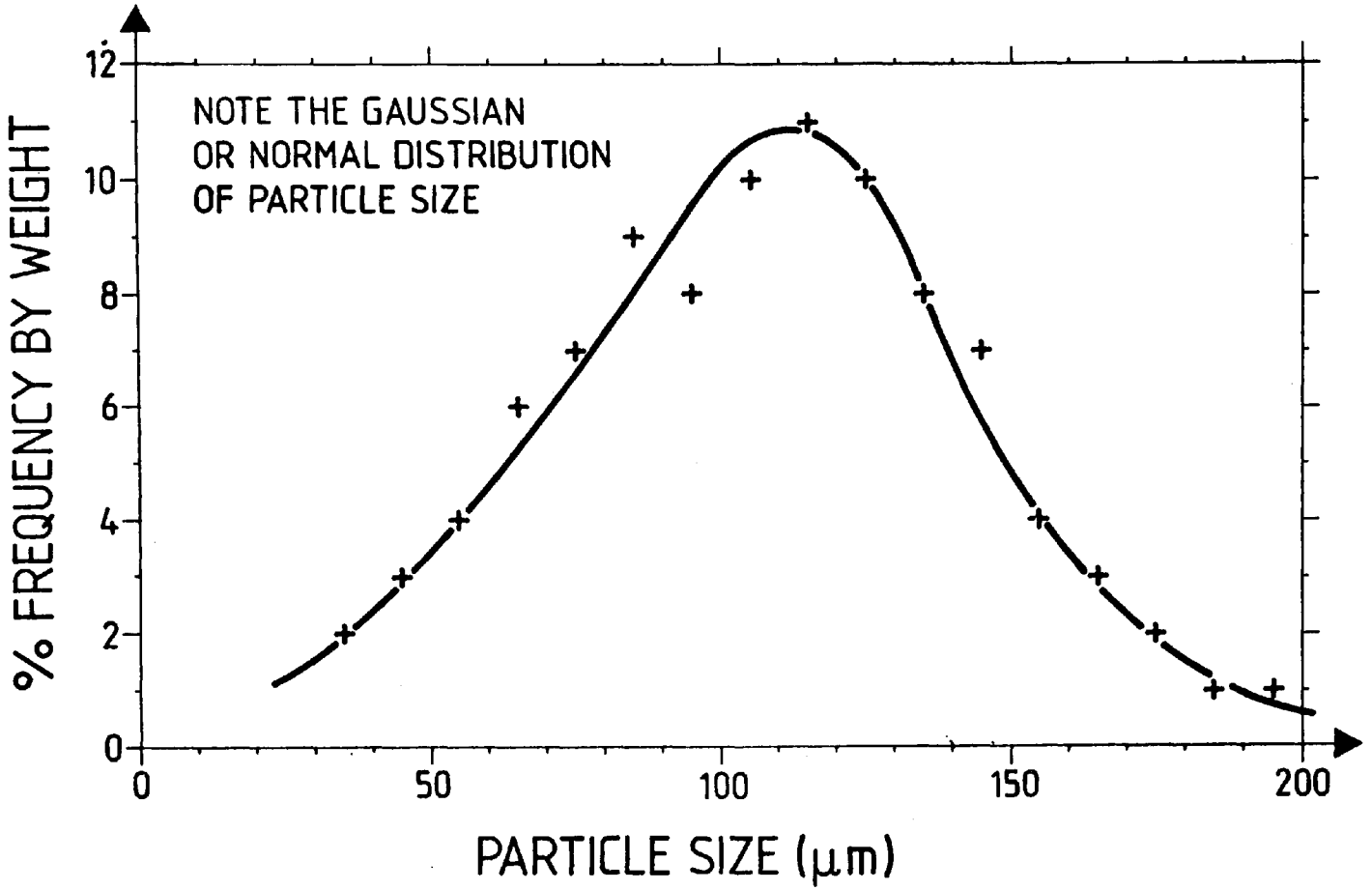

FIG. 4.5 PARTICLE SIZE FREQUENCY CURVE BASED ON A CLASS INTERVAL OF 10 μm

(AHC 100.29)

latter provided the particle size distribution.

The Fisher Sub-Sieve Sizer provided a dry method of particle size analysis based on the air permeability principle. The instrument was first calibrated using the Calibrator supplied, which was in the form of a synthetic ruby jewel with a precision orifice mounted in a tube similar to the sample tube. With the constant pressure dried air flowing through this orifice, the standardizing needle valves were adjusted until the manometer reading coincided with the porosity value of 0.75 engraved on the Calibrator, 7.8 g of powder, i.e. a mass numerically equal to the true density of iron, was then weighed out and placed into the sample tube the lower end of which had been fitted with a filter disc and porous plug. The open end of the tube was then closed in a similar manner and the tube placed in the rack and pinion compression device. Here the powder was compacted, by means of a torque screwdriver, to a known porosity which was read off the chart at a point corresponding to the height of the compact. The sample tube was then clamped in position, and the dried air allowed to pass through it. When the liquid level in the manometer tube reached its maximum position, the corresponding average particle size was read directly form the appropriate curve on the calculator chart. The procedure was repeated for different torque readings on the calibrated screwdriver in order to determine the optimum compacting pressure to suit the powder sample i.e. the torque at which the average particle size is a minimum. This was found to be 20 lbf in, whereupon tests were then performed on a number of different powder samples to provide the results shown in Table 4.6.

TABLE 4.6

Results of Fisher Sub-Sieve Tests on AHC 100.29 Fines

Sample No.	Porosity	Average Particle Size (μm)
1	0.53	12
2	0.54	12
3	0.54	12
4	0.54	12.1
5	0.54	12.5
6	0.535	12.6
7	0.54	12.5
	Mean	12.24 μ m

The Coulter Counter provided a wet method of particle size analysis based on the principle of electric flow modulation. The instrument used was a Coulter Counter Model TA, sixteen channel fully solid state particle size analyser. A small quantity of the sample to be checked was firstly mixed with the dispersant Isoterge and then suspended in the electrolyte Isoton. A 70 μ m diameter aperture, Serial no. 6102032 was used for the test. After being placed into the instrument, the particles suspended in the electrolyte were forced through the aperture across which a flow of electric current was induced by means of two immersed electrodes positioned on either side of the aperture. As each particle passed through the aperture, the volume of electrolyte displaced produced a voltage pulse proportional in magnitude to the particle volume. The instrument was set to count 10^5 particles after which the stored information was printed directly in the form of the histrogram, Figure 4.6(a) and the ogive or cumulative

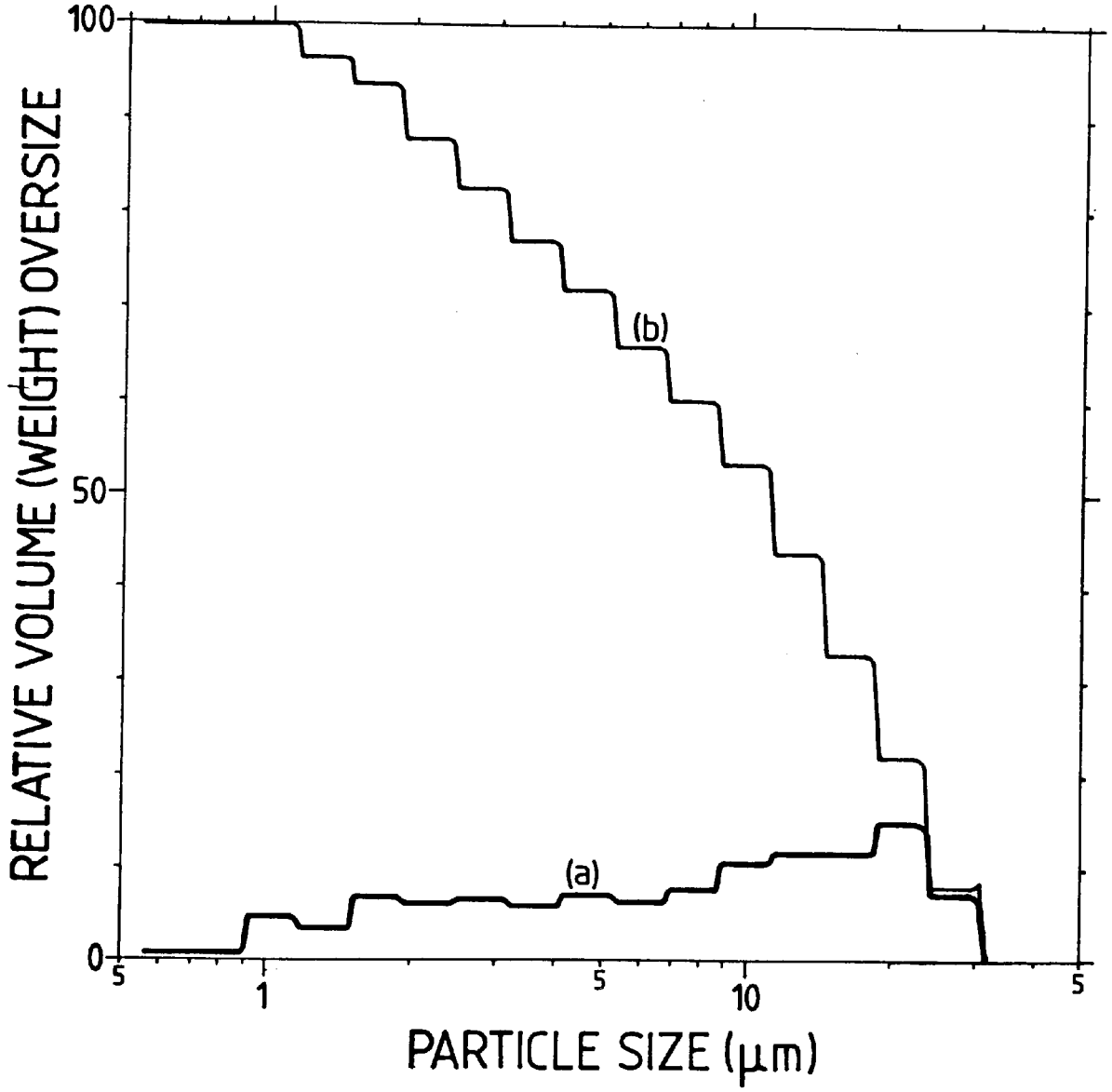

FIG. 4.6 (a) Coulter Counter histogram of sub-sieve particle size distribution (AHC 100.29)
(b) Coulter Counter ogive or cumulative overweight curve for sub-sieve particle sizes (AHC 100.29)

overweight plot, Figure 4.6(b). From Figure 4.6(b) it can be seen that the median particle size corresponding to 50% overweight is 12.3 μ m, which compares favourably with the Fisher Sub-Sieve average result of 12.24 μ m.

4.5 Use of Scanning Electron Microscope (S.E.M.)

Widespread use is now being made of the S.E.M. for the appraisal of PM starting-material[88]. For the purpose of this present programme of work it was used to gain a qualitative appreciation of the powder particle morphology, and to a limited extent give some indication of powder particle size and distribution. The instrument used was "The Cambridge S150". A small quantity of the fines, together with the fractions, No's. 1, 2 and 3, were individually mounted on stubs by means of conductive paint. Each of the samples in turn was loaded into the S.E.M., and then carefully examined before representative photographs were taken on an automatic 35 mm camera at very slow scan rates. These micrographs appear as Figure 4.7 to 4.12 and indicate that although the bulk of the larger particles are irregular in shape, which is desirable for good mechanical interlocking during compaction, the particles tend to become smooth and spherical, as the particle size diminishes.

4.6 Powder Mixing

Mixing is defined as "the thorough intermingling of powders of two or more materials", whereas Blending is defined as "the thorough intermingling of powders of the same composition"[89]. The degree of mixing is referred to as "mixedness" (M), which starts off as M = 0 and tends towards M = 1 for the ideal case of complete uniform mixing[90].

An Apex[6] stainless steel Y cone blender was used for mixing the

S.E.M. photographs showing the various fractions of AHC 100.29 iron powder

Fig. 4.7 FINES OR SUB-SIEVE FRACTION ($< 53\ \mu m$) Mag. x 1000

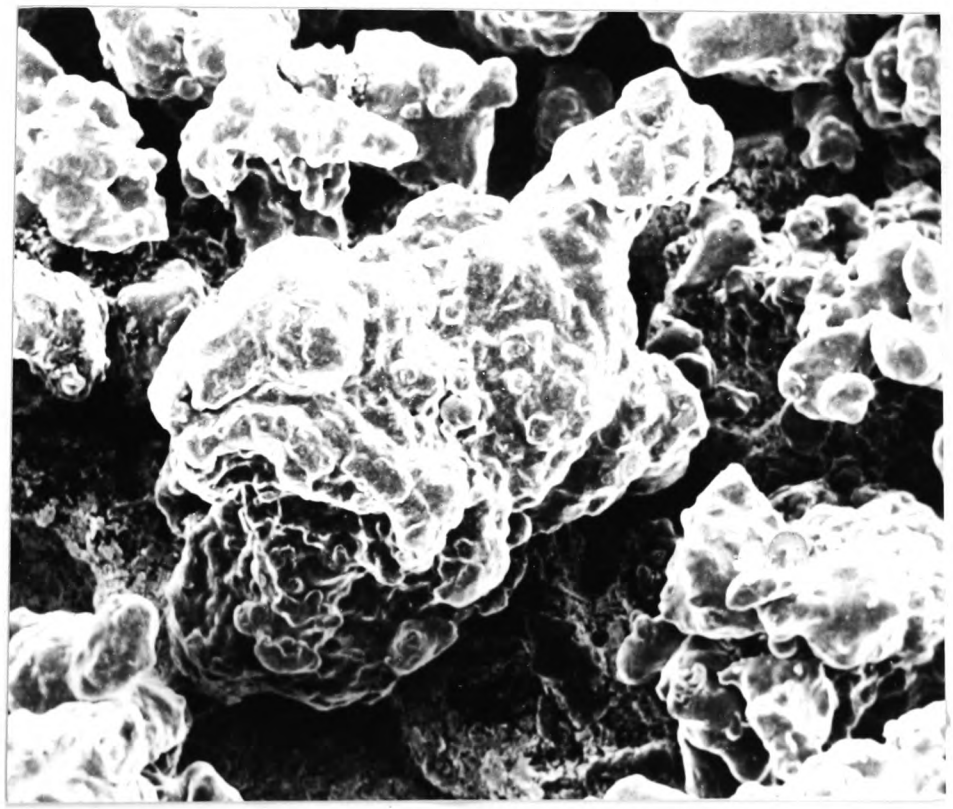

Fig. 4.8 FIRST FRACTION (150 - 180 μm) Mag. x 500

S.E.M. photographs showing the various fractions of AHC 100.29 iron powder

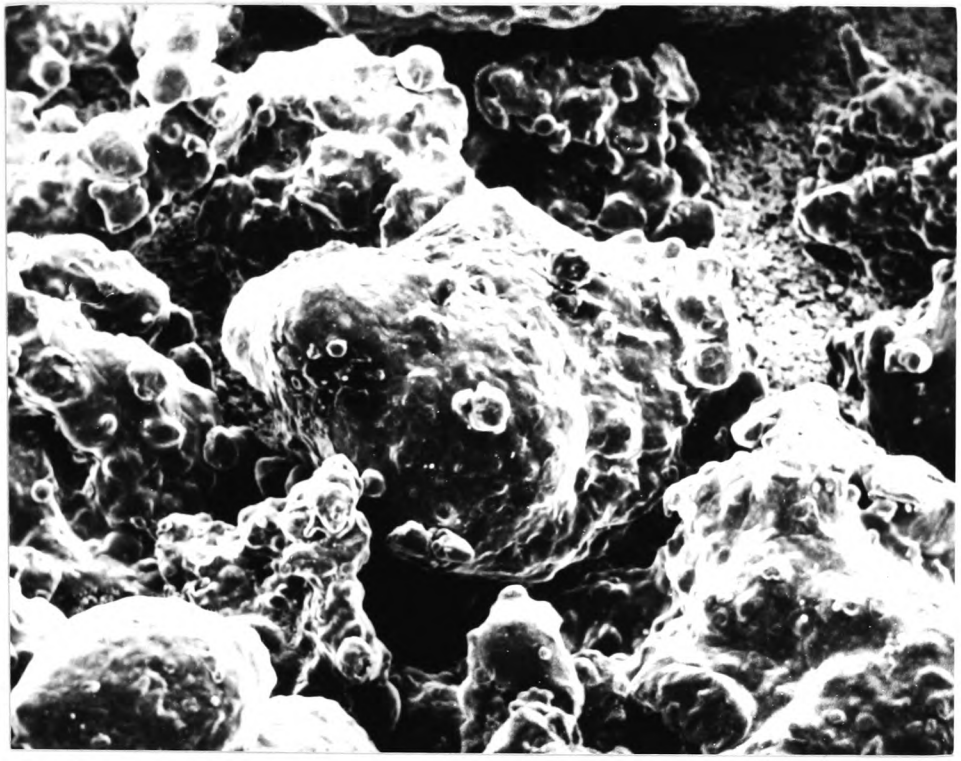

Fig. 4.9 SECOND FRACTION (125 - 150 μ m) Mag. x 500

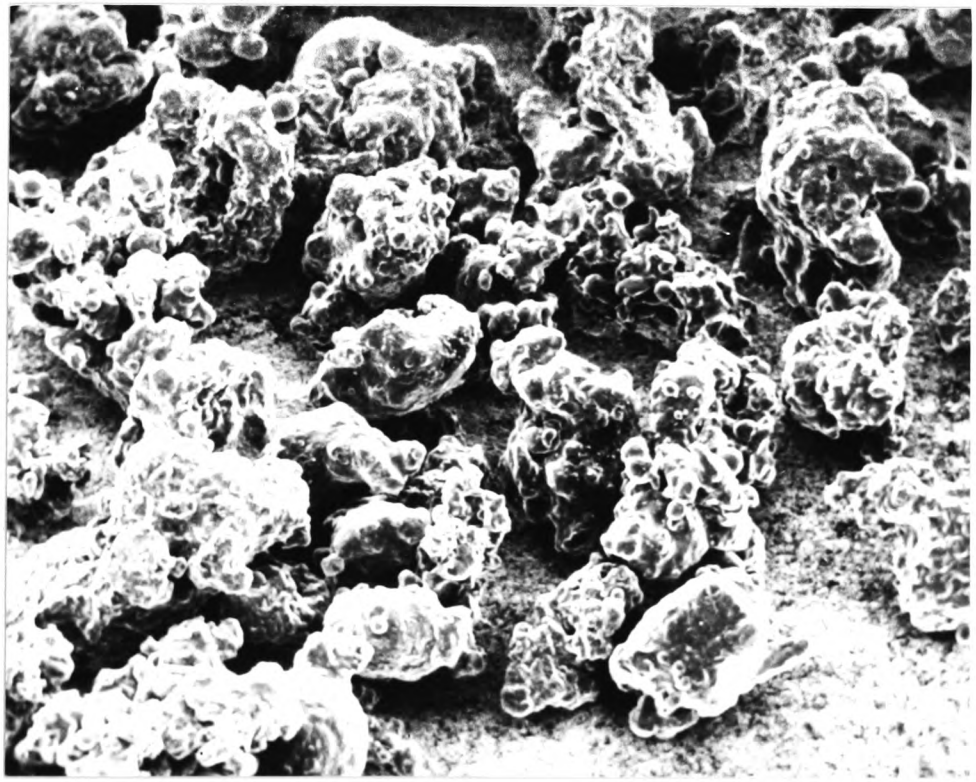

Fig. 4.10 THIRD FRACTION (90 - 125 μ m) Mag. x 200

S.E.M. photographs showing the various fractions of AHC 100.29 iron powder

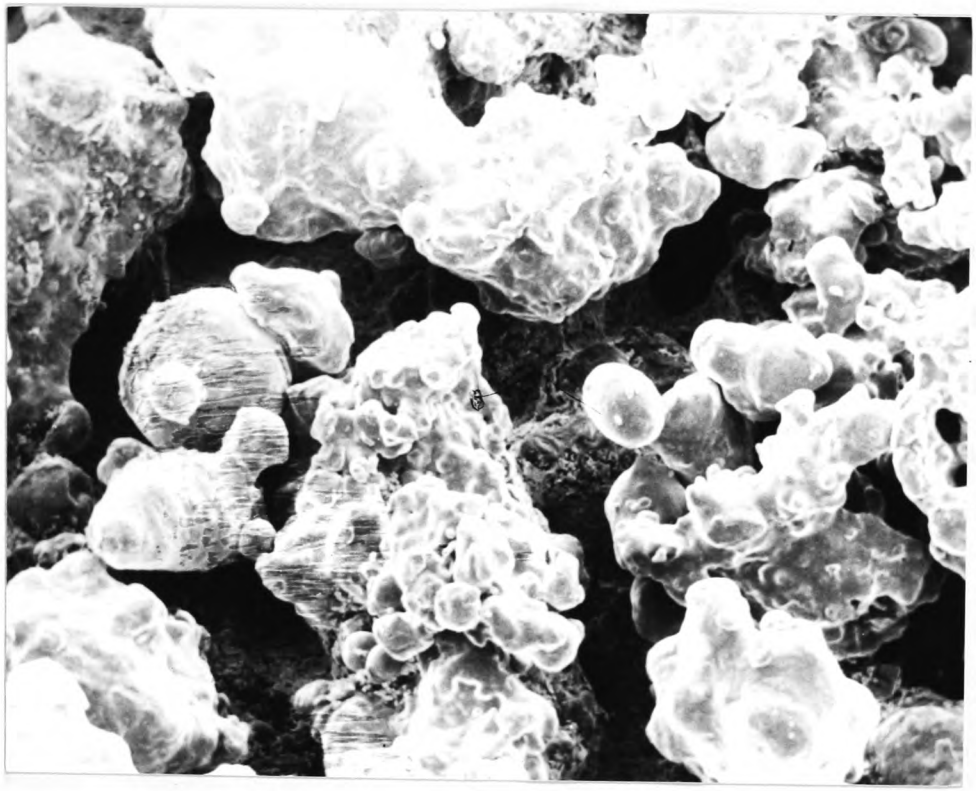

Fig. 4.11 FOURTH FRACTION (53 - 90 μ m) Mag. x 500

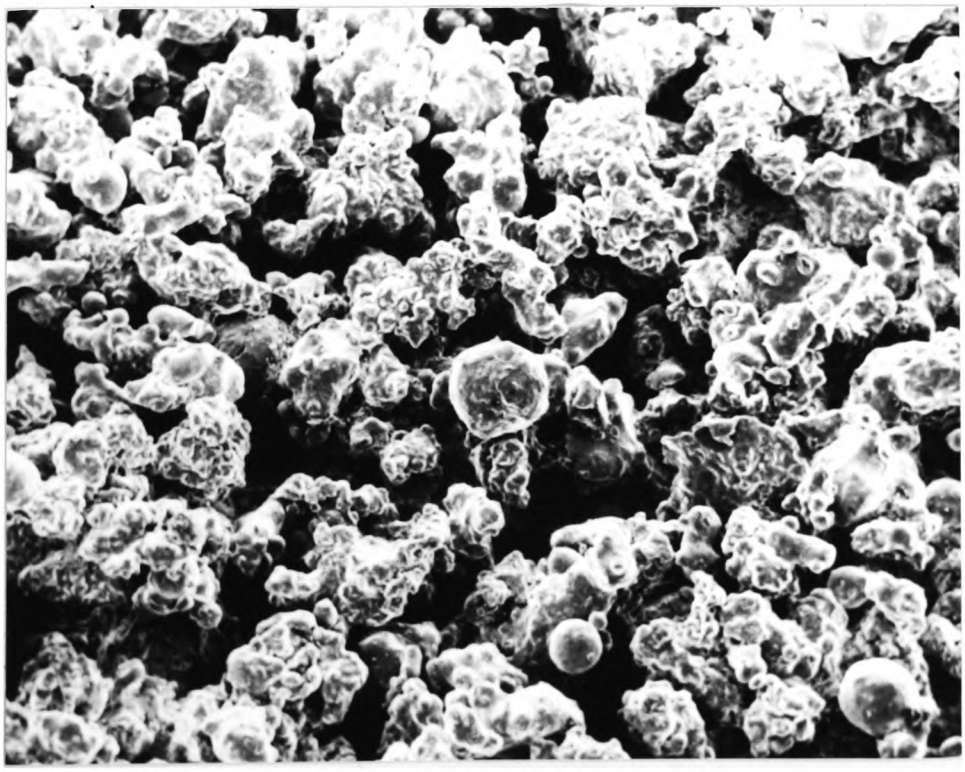

Fig. 4.12 FOURTH FRACTION (53 - 90 μ m) Mag. x 200

iron powders with 1% zinc stearate and amounts of graphite varying from 0 to 1% by weight. The quantities of powder were carefully weighed out on the Sartorius top pan balance before being introduced into the Y cone, which was then sealed with a cover and rotated at 39 rev/min. The capacity of the Y cone was 0.7 l, and the maximum quantity of powder mixed at any one time never exceeded 1 kg. The gentle mixing action of the Y cone is necessary for iron powders, to prevent the liklihood of work hardening which would reduce the compressibility of the powder during compaction. During the mixing, the Y cone shape offers a number of curved surfaces at constantly changing angles which deflect the powder, particularly in the horizontal plane, to achieve rapid and intimate mixing[91]. The two arms of the Y allows the powder to be sub-divided during rotation, and then to be reunited again in the space where the arms join.

Although no tests were performed to accurately establish an optimum mixing time, it was found that rotating for 20 minutes produced a powder mix which behaved satisfactorily during compaction and sintering.

The graphite used was Kropfmuhl 'UF4' 96/96% C which was a natural graphite of Bavarian origin, available from Woodstock (London) Ltd.

CHAPTER 5

Powder Compaction

5.1 Compaction Presses

All the powder compaction, together with much of the subsequent mechanical testing and powder forging, was carried out with the aid of two, single-acting, hydraulically operated presses.

The first of these was an Avery-Denison Type 7113 DCJ Universal Testing Machine, No. P4786. Although this machine had a maximum capacity of 600 kN, any one of five load ranges could be selected, to give full scale deflections of 30, 60, 120, 300 or 600 kN. The accuracy and repeatability of the machine was re-verified annually, and fulfilled the requirements of B.S. 1610: 1964.

The second press was manufactured in its original form by Armstrong (Leeds) Ltd., in 1967, in accordance with a design specification proposed by Dr. M. B. Bassett. The manufacture of the press was financed by the Science Research Council[28], and it can be seen in its modified form in Figure 5.1. It has a maximum capacity of 3 MN and consists of four vertical pillars which support the fixed platen and load cell at the top and which also act as guides for the lower, moving platen. The main ram is housed near the base of the machine together with two smaller hydraulic cylinders used for the return stroke.

Owing to the need for rapid ram speeds for hot working e.g. hot extrusion[92] and powder forging, it was necessary to modify the hydraulic circuit to include two nitrogen filled accumulators. Each accumulator had a maximum capacity of 45 litres and could be charged to a pressure of 345 bars. This charge could be released into the main ram very rapidly by a suitable arrangement of solenoid valves. Furthermore, the

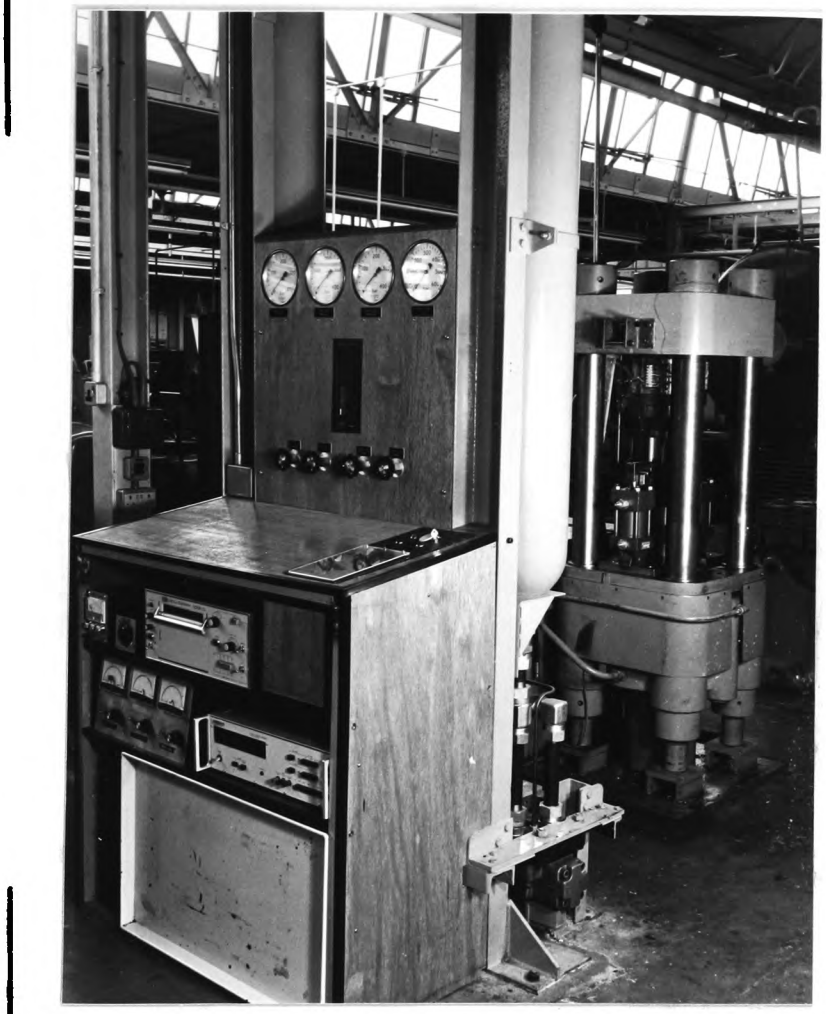

Fig. 5.1 MODIFIED "ARMSTRONG" 3 MN HYDRAULIC RESEARCH PRESS AND INSTRUMENT CONSOLE

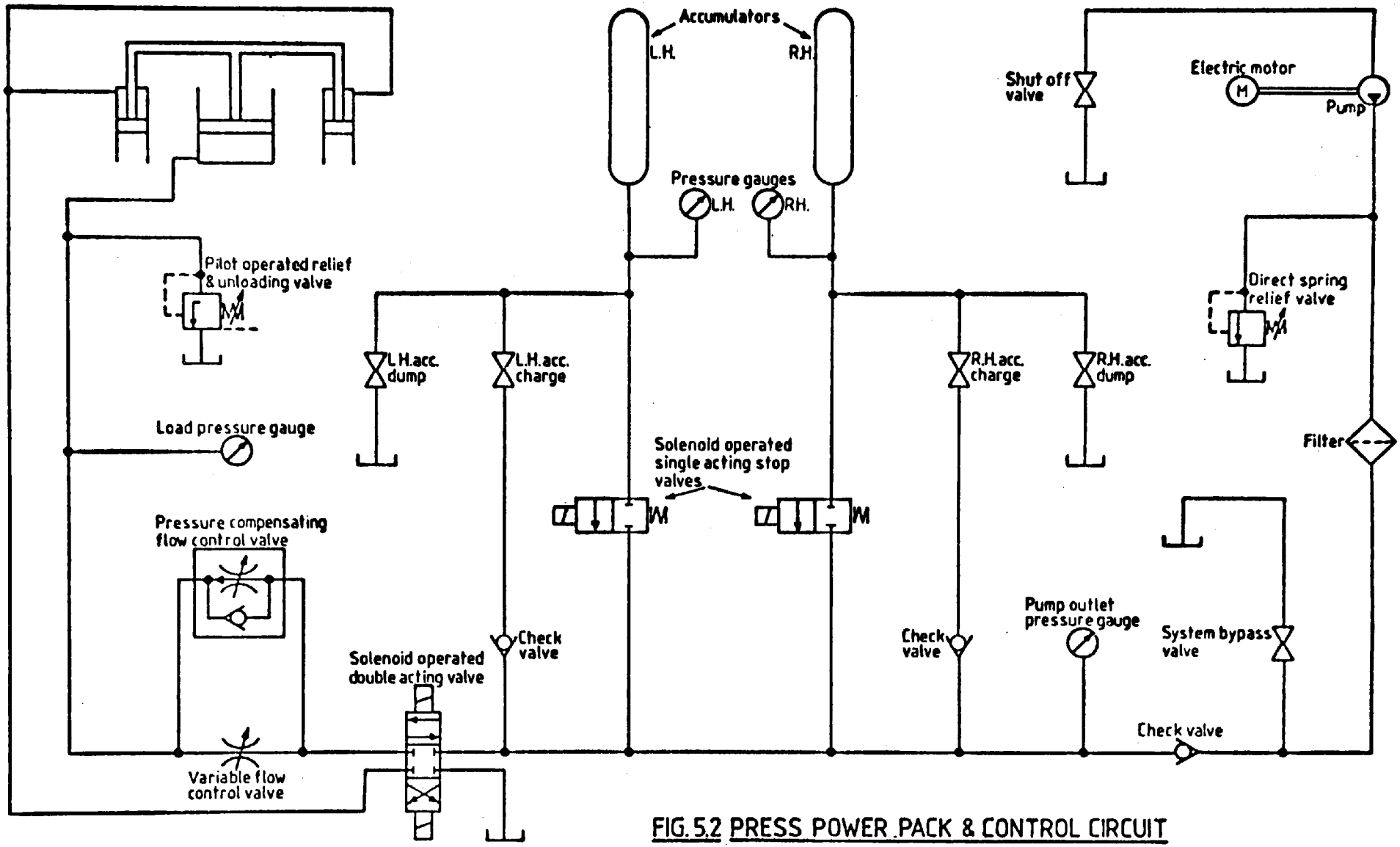

FIG. 5.2 PRESS POWER PACK & CONTROL CIRCUIT

original hydraulic power pack which was driven by a 5 hp motor, was replaced by a larger unit driven by a 30 hp motor. Although the writer can claim some involvement in helping to engineer these modifications, the design of the new hydraulic circuit, shown in Figure 5.2, was entirely the work of Mr. A. H. Richards, Principal Lecturer at The Polytechnic of Wales.

Equally so, the instrumentation of the press was developed by Dr. C. Holloway[92] whilst undertaking a programme of post graduate work.

The test results were recorded on a twelve channel SE 3006 Ultra-Violet (U.V.) recorder, whilst the force acting on the ram was measured by means of a resistance type load cell. Details of the load cell together with the calibration procedure appear in Appendix E. Alternatively, the load could be read directly off a Bourdon type gauge.

5.2 Compaction Tools for Pilot Study

Figure 5.3 shows details of the compaction tool used to produce preforms for the pilot study[28] undertaken in collaboration with South Wales Foregmasters Ltd., Cardiff. It was made from a low-alloy steel and consisted of a die and two punches. The die was in the form of an annular ring of material measuring approximately 250 mm outside diameter, 100 mm bore and 100 mm long and weighing approximately 30 kg, hence the need for the lifting and carrying handles. The upper punch was a plain cylinder of material whereas the lower punch had a recess with a 10° draft angle machined out of its top face. The reason for this was to produce the boss on the two stage compact needed in this case. Although the initial weight of the compact produced was approximately 900 g the final weight of the preform required was only 414 g. The surplus metal was machined off after sintering, which unfortunately was carried out rather crudely in a muffle furnace, which it was realized would result

Fig. 5.3 POWDER COMPACTION TOOLS USED FOR PILOT STUDY OF PREFORM DESIGN

(Ref. 28)

in considerable decarburization hence the need for the surplus material to combat the problem.

Preforms of densities ranging from $\rho_* = 0.72 - 0.83$ (Ref. 21) were then produced at compaction pressures ranging from 210 MN/m^2 to 420 MN/m^2, as shown in Figure 5.4, with the quantity of powder being introduced into the die on a constant volume basis. Difficulty was experienced with the production of blanks at 210 MN/m^2 owing to the boss separating from the flange as a result of poor compaction in this region. Double ended compaction would have undoubtedly produced a more satisfactory compact. After compaction, the tool was supported whilst the bottom platen was lowered sufficiently to allow the removal of the bottom punch, and the positioning of metal spacers between the platen and the underside of the die. The lower platen was then moved upwards so that the upper punch ejected the compact.

5.3 Compaction Tool for Test Specimen

Figures 5.5 and 5.6 show details of the compaction tool, together with a typical compact. The construction was more sophisticated than that of the previous compaction tool in as much as the die now consisted of a hardened and tempered alloy steel insert, which was a shrink fit into a mild steel shroud. The purpose of this was to introduce compressive stresses into the insert to enable larger compaction pressures to be used, since the accompanying tensile stresses would have to counteract these before the stresses in the die could themselves become tensile. The effect is similar to that obtained by using such techniques as wire winding or autofrettage in the construction of pressure chambers for isostatic presses. However, the mode of operation was still that of single ended compaction, with the lower punch being of sufficient length to eject the component after pressing. Since the

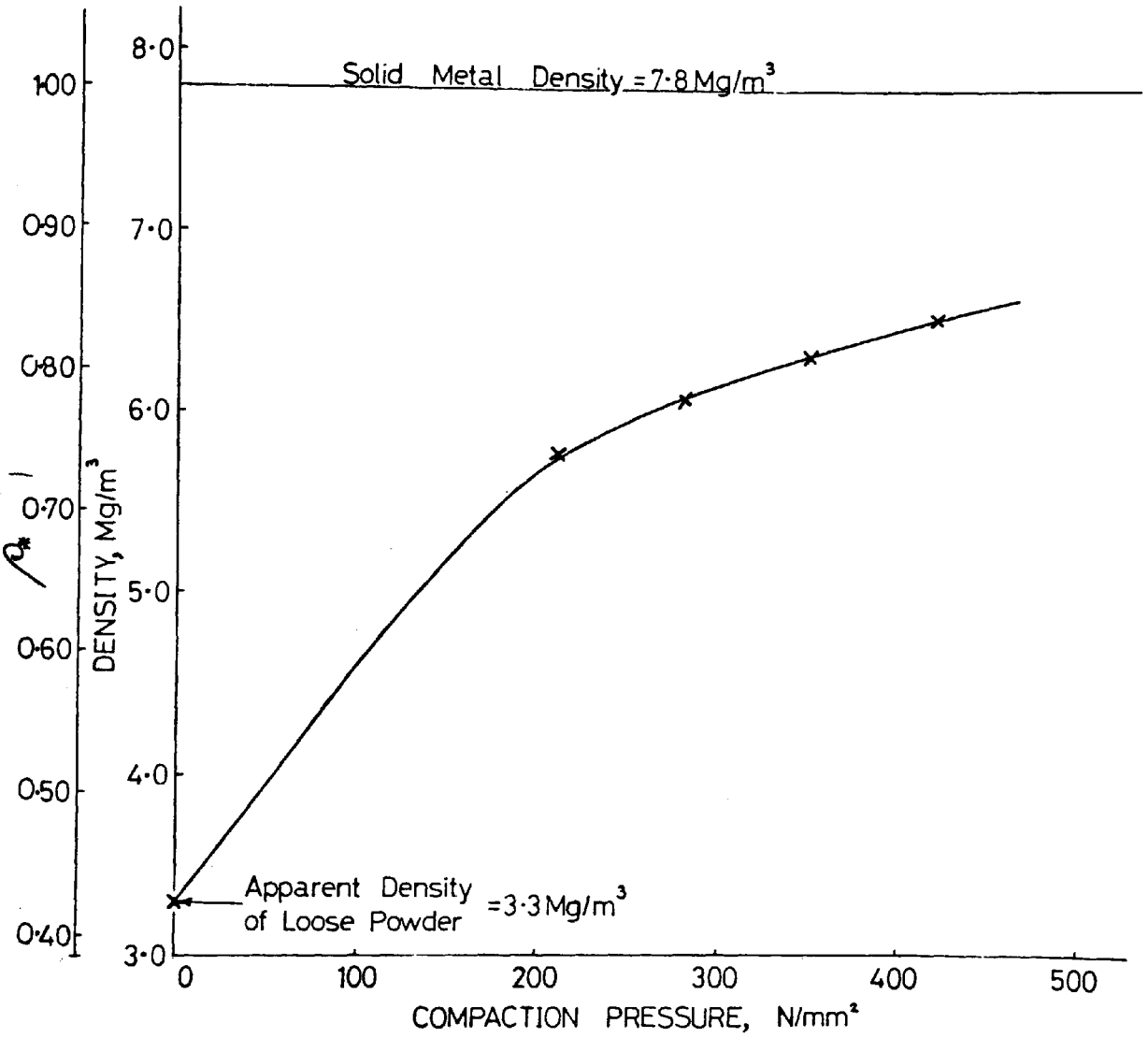

Fig. 5.4 Mean preform density vs. compaction pressure.

(MP 32, Ref. 28)

Fig. 5.5 COMPONENT PARTS OF SINGLE-ENDED COMPACTION TOOL TO PRODUCE "WAFER" SPECIMEN

Fig. 5.6 SINGLE-ENDED COMPACTION TOOL IN USE

components produced by this tool all had a high cross-section/height ratio, it was considered that the density distribution obtained was sufficiently uniform for the purposes intended. For the most part these included the manufacture of "wafers measuring approximately 5 - 6 mm thick to be used for tensile testing, and to establish hardness/density relationships. Rather thicker compacts were also produced for the manufacture of dilatometer specimen, and specimen for subsequent forging and fatigue testing. In practically all cases, the requisite quantities of powder were carefully weighed out before being introduced into the die.

5.4 Compaction Tool for Cylindrical Preforms

This was by far the most sophisticated compaction tool used in the project, see Figure 5.7. It was designed to produce compacts 40 mm dia. x 50 mm long, and to operate on the floating-die principle in order to overcome the limitations imposed by the use of a single acting press. With the floating-die mode, relative movement is obtained between the lower punch and the die as well as the upper punch and the die. This is brought about by virtue of the frictional forces acting between the powder compact and the die walls during the actual pressing operation. In order to take advantage of this, and thereby simulate double ended compaction and the accompanying benefits of a more uniform density distribution throughout the compact, it was necessary to just support the weight of the die on a suitable arrangement of springs. This is shown in Figure 5.8, whilst Figure 5.9 shows the die being supported on 3 small screw jacks to enable it to be used in the single-ended mode, so that the results of compacts produced by both methods could be compared to demonstrate the advantages offered by the former arrangement. With reference to Figure 5.7 it can again be seen that the

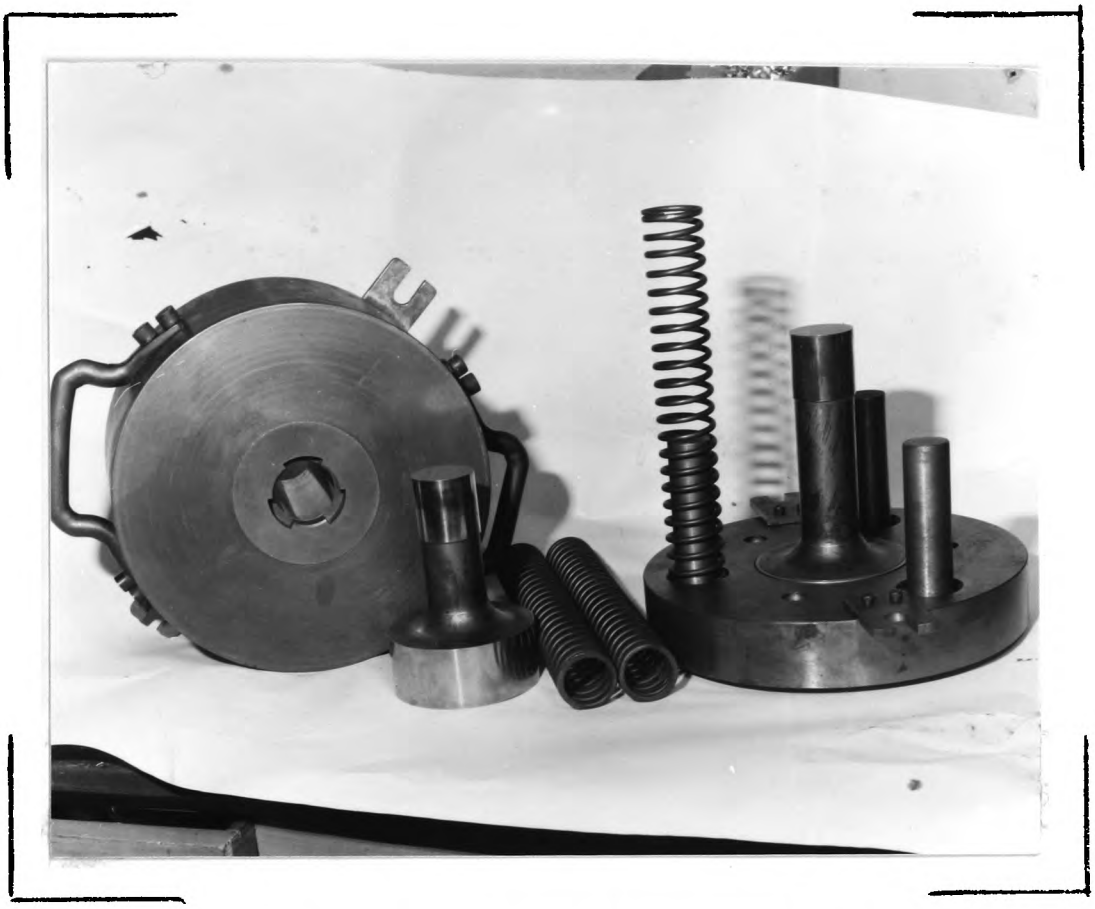

Fig. 5.7 COMPONENT PARTS OF "FLOATING DIE" COMPACTION TOOL

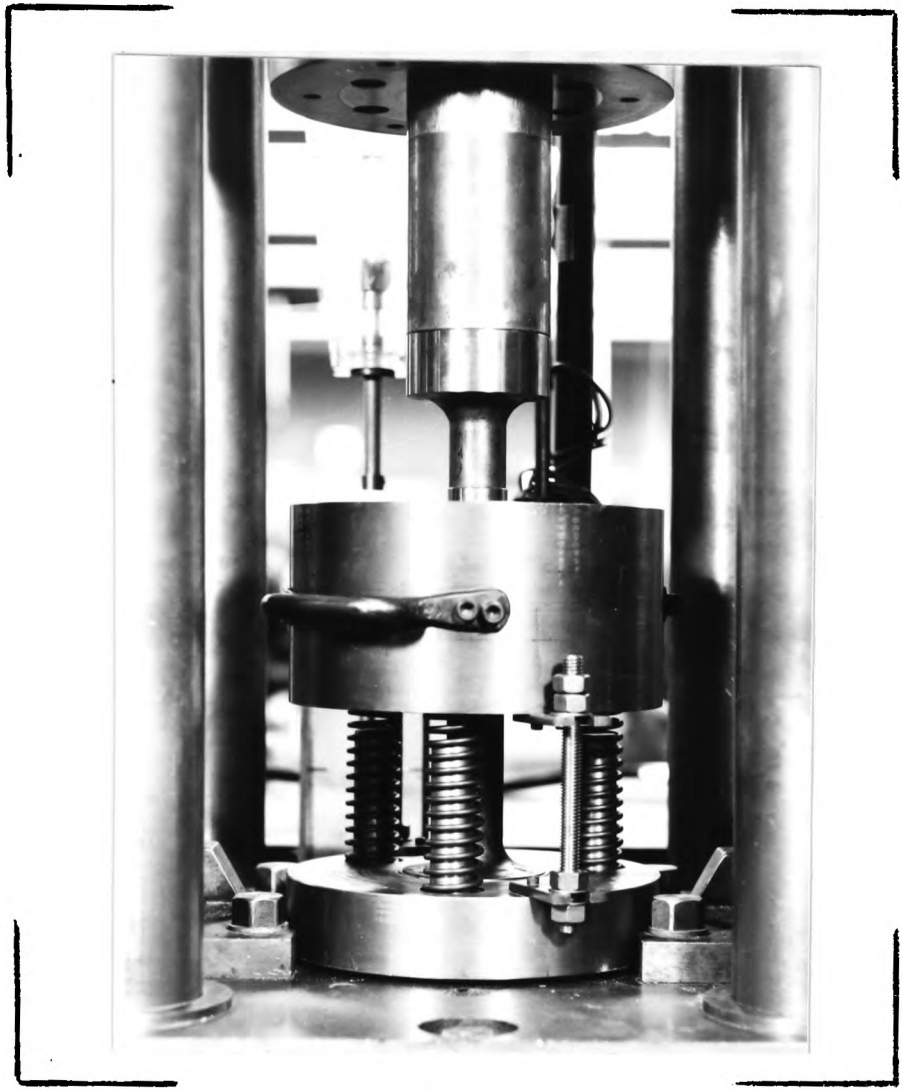

Fig. 5.8 "FLOATING DIE" TOOL USED IN DOUBLE-ENDED PRESSING MODE

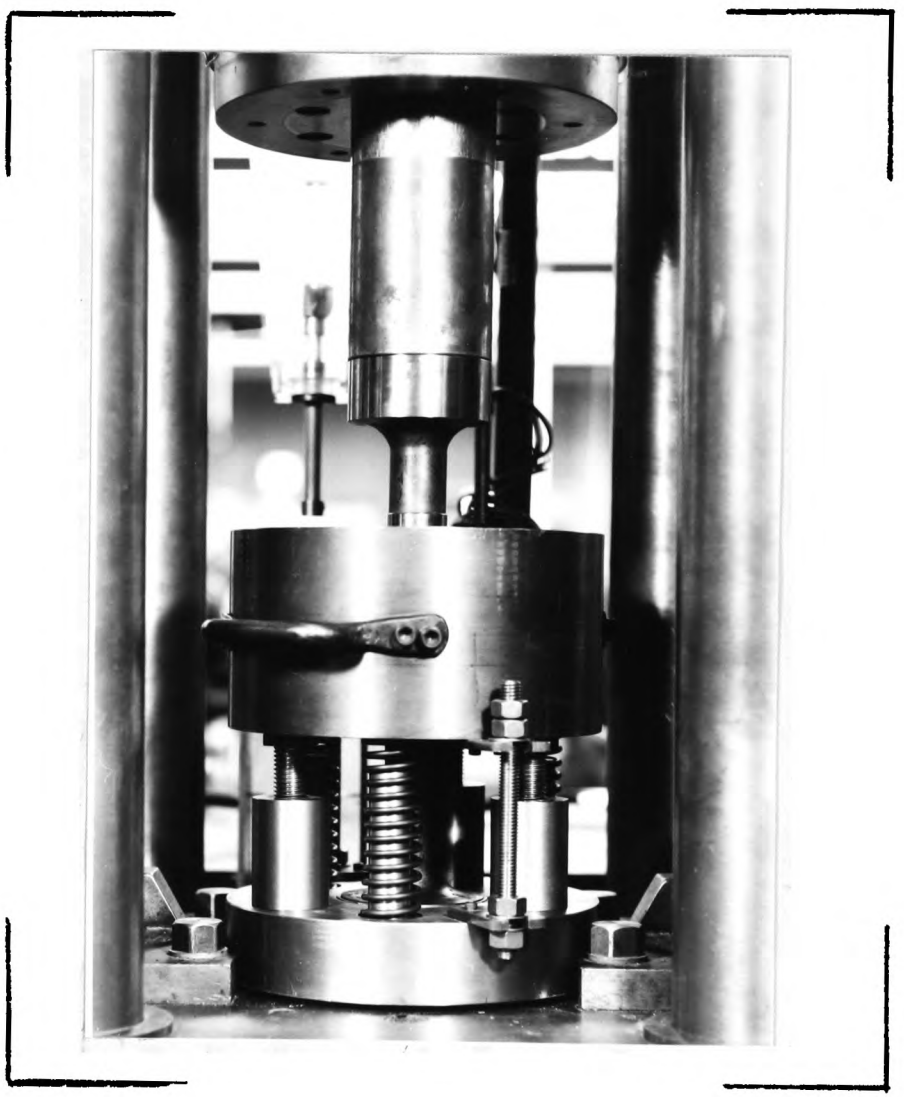

Fig. 5.9 "FLOATING DIE" TOOL USED IN SINGLE-ENDED PRESSING MODE

die consists of a hardened and tempered insert which is a shrink fit into a mild steel shroud. The stress calculations and details of this arrangement can be seen in Appendix F. As a point of interest, the shrink fit was achieved by the use of liquid nitrogen[94]. In this case the die assembly weighed approximately 50 kg, hence the necessity to fit handles for carrying and lifting.

The punches and die were made from W. L. Marrison's non-distorting tool steel, designated WLM 2014, which contained 2% carbon and 13% chromium. Hardening was carried out by preheating to 800°C and then to 950/1000°C, followed by cooling in air. The punches were tempered by heating to 400°C followed by quenching in oil to give a hardness of Rc 59. The die was quenched from 270°C, to give a hardness of Rc 62.

5.5 Powder Compaction Tests Involving the Production of "Wafers"

Initial tests were carried out using Rospol MP 32 iron powder mixed with 1% graphite and 1% zinc stearate by weight. A series of wafers similar to those shown in Figure 5.10 (a) were produced at different compaction pressures, and their relative densities determined by weighing and measuring. Typical results are shown in Figure 5.11. The Brinell hardness of these wafers was then determined in order to establish a relationship between hardness and density for future purposes, see Figure 5.12 and Section 5.6, respectively.

Attempts were made to analyse the compaction results in the manner suggested by Heckel[95] and Hewitt et al[96], namely, by determining the empirical constants H and F in the equation,

$$\ln \frac{1}{1-\rho_*} = H \Phi + F \qquad (2)$$

Hewitt et al[96] suggest that the compaction process can be sub-divided into three distinct regions corresponding to compaction pressures of 0 to 300 MN/m^2, 300 to 1000 MN/m^2 and above 1000 MN/m^2.

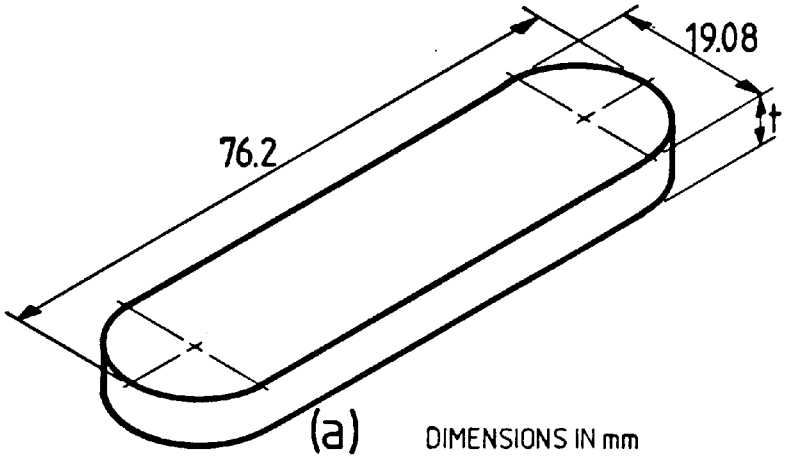

THICKNESS t (mm)	SPECIMEN USE			
6 (WAFERS)	HOT TENSILE TESTS SECTION 7.4 (HOUNSFIELD SPECIMEN FOR STRIP CHUCKS TYPE B)	POISSON'S RATIO SECTION 7.6 FIG. 7.7	ROOM TEMPERATURE TENSILE TESTS SECTION 7.10	
15	HOT TORSION TESTS SECTION 7.3	DILATOMETER TESTS SECTION 7.5	FATIGUE TESTS SECTION 8.6 FIG. 8.11	HOUNSFIELD SPECIMEN No. 13 SECTION 8.6

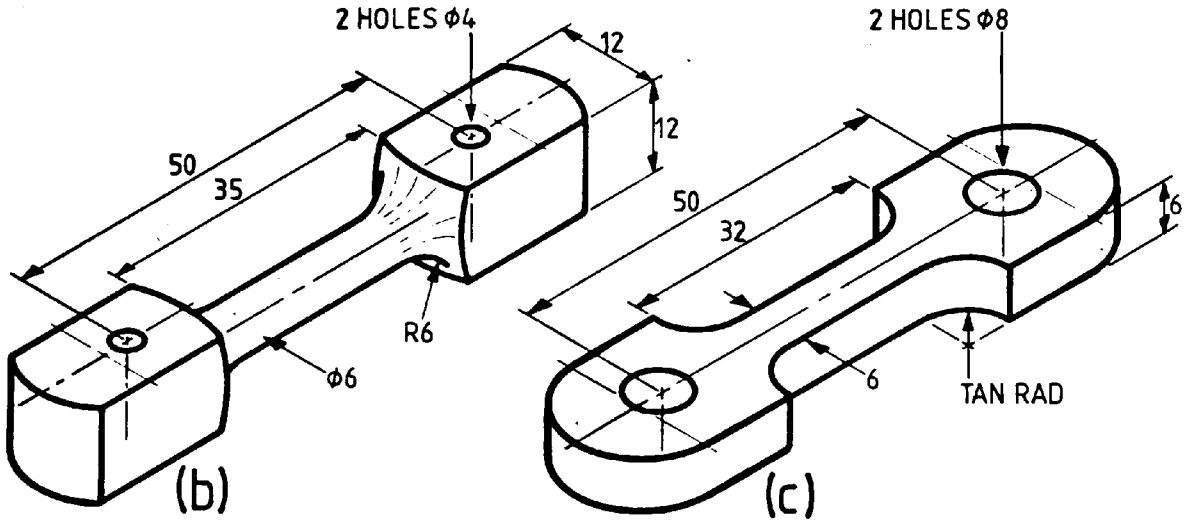

HOT TORSION SPECIMEN

SPECIMEN FOR ROOM TEMPERATURE TENSILE TESTS

FIG. 5.10 Details of test specimen used throughout project

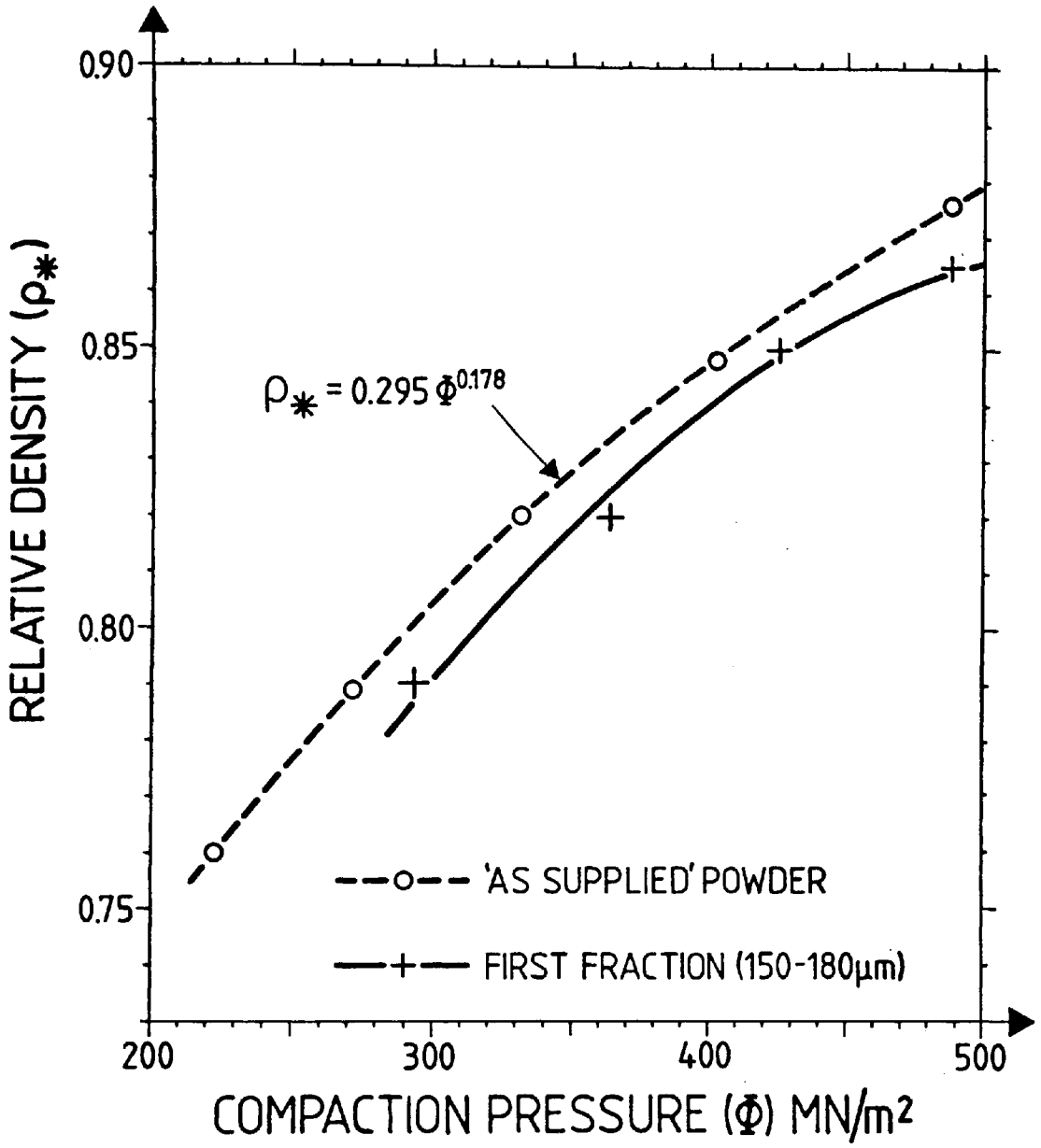

FIG. 5.11 COMPARISON OF COMPACTION BEHAVIOUR OF "AS SUPPLIED" AND "COARSE FRACTION" POWDERS

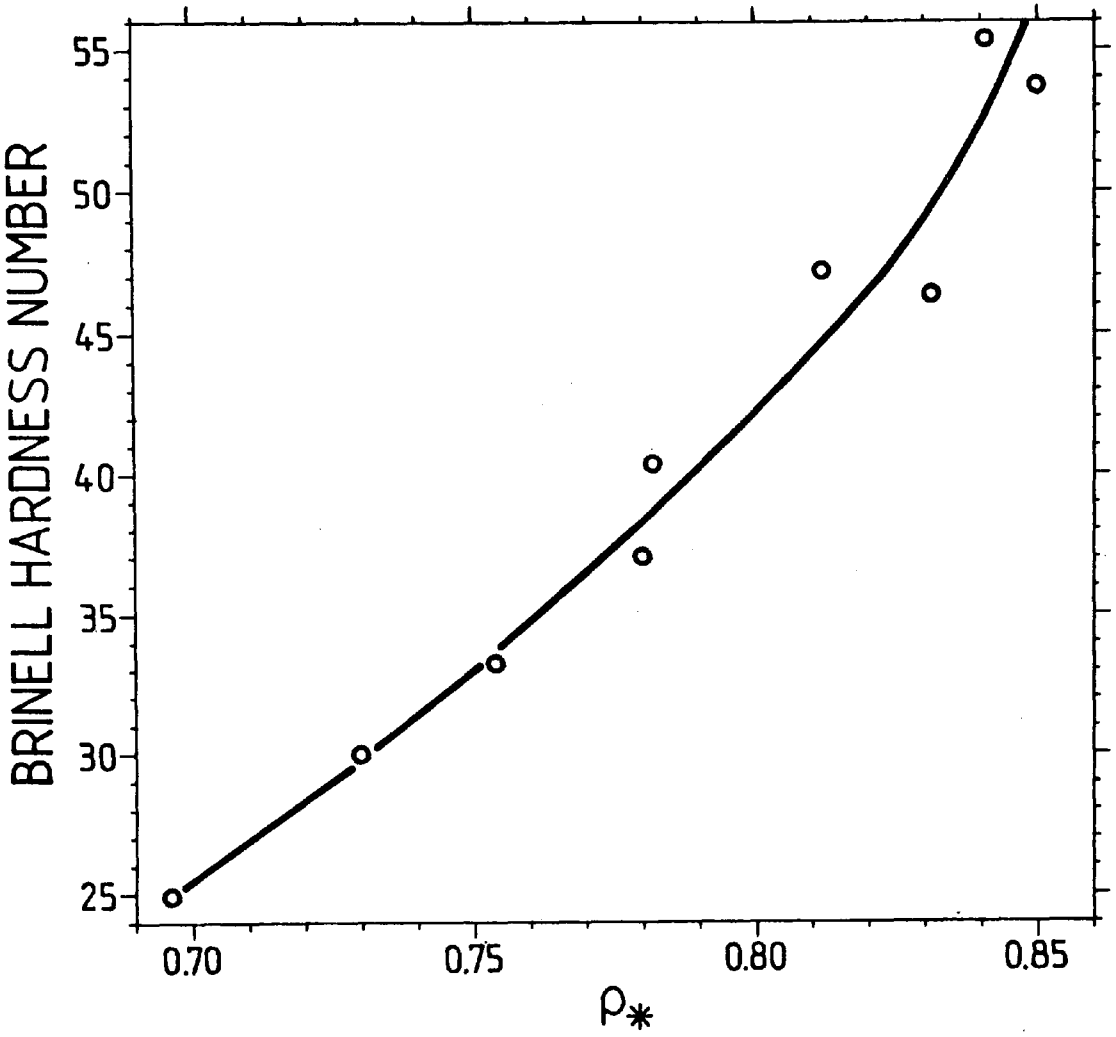

FIG. 5.12 BRINELL HARDNESS/RELATIVE DENSITY, CALIBRATION CURVE

It is further suggested that over these three regions, densification occurs initially as a result of re-stacking and re-orientation of the powder particles, followed by localised plastic flow, and finally, for the higher pressures, bulk plastic flow accompanied by a gradual decrease in pore size. Since Figure 5.11 shows that quite modest compaction pressures were used for the current series of tests, then it must be concluded that densification occurred merely as a result of re-stacking, re-orientation and some localised plastic flow. This is regarded as being quite adequate for preform production since the final consolidation is achieved by forging. Furthermore, these lower compaction pressures have greater commercial interest, since they neither impose excessive wear on tools, nor require the use of high capacity presses.

When further compaction tests were carried out on the same tool but using Hoganas AHC 100.29 iron powder mixed with 0.5% graphite and 1% zinc stearate by weight, it was found that ρ_* and ϕ (MN/m^2) could be connected by the empirical equation,

$$\rho_* = 0.295\,\phi^{0.178} \qquad (3)$$

or, by transposition,

$$\phi = 951\,\rho_*^{5.62} \ MN/m^2 \qquad (4)$$

The constants were determined by linear regression, see Section 7.10, after the equation had been linearized by taking lograthms of both sides. The purpose of adding 0.5% graphite was to simulate En8 (B.S. 970) which contains 0.35 - 0.4% C, and is widely used throughout the forging industry. It was considered that a small portion of the graphite would be lost during sintering, so that the final microstructure would probably contain $\sim$ 0.4% C in an associated form.

Further compaction tests were carried out using the various fractions of AHC 100.29 obtained from the earlier sieving see Figure 4.3, each fraction also being mixed with 0.5% C and 1% zinc stearate. The coarse or first fraction (150 - 180μm) is the one of main interest owing to its possible commercial application. The compaction curve for this fraction can be seen in Figure 5.11, where it is compared against the "as supplied" powder. As might be expected, it does not compact as well as the latter due to the absence of the smaller fractions and fines needed to fill the interstices between the relatively coarse particles.

As a matter of interest, it was observed that as the fractions became finer, so did their compaction curves tend to approach that of the "as supplied" powder, which gave the best result. A surprising exception was that the "fines" exhibited the poorest compressibility of all the fractions tested. This is probably due to the fact that the fines contained the highest proportion of spherical particles, see Figure 4.7.

5.6 Tests Conducted Using "Floating-Die" Tool

Rospol MP 32 iron powder with 1% C and 1% zinc stearate was used for the early compaction tests conducted with this tool.

Preliminary tests were carried out using the tool in both the single ended and floating-die mode of operation. Figures 5.13 and 5.14 show the relative movements of the punches for both types of operation, together with corresponding densities achieved. After compaction, the compacts were sectioned and the central portions removed, polished and then mounted with aid of a magnetic block, on to the indexing device shown in Figure 5.15. By altering the two screws of known pitch, arranged at right angles to one another, it was possible to obtain the

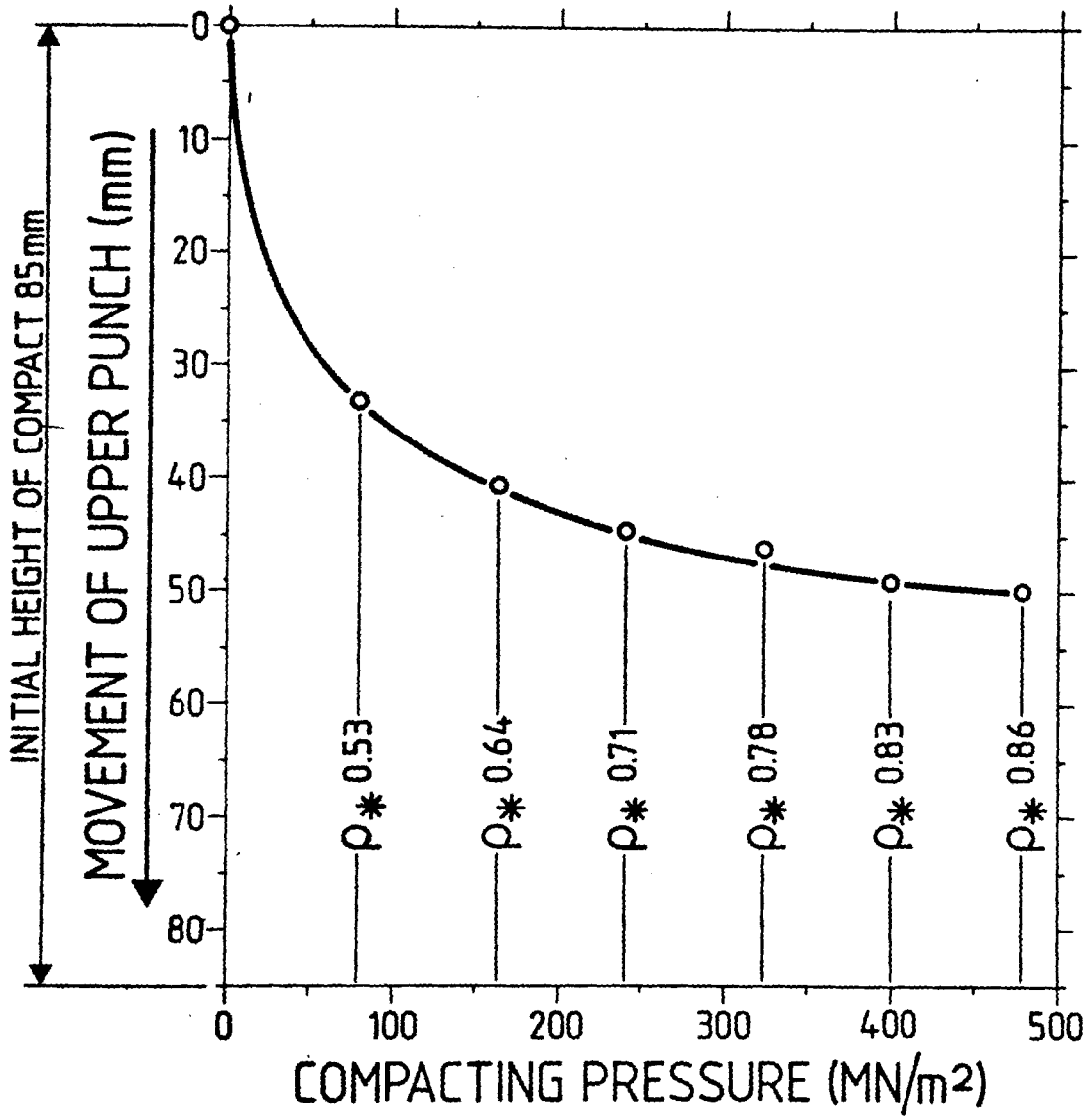

FIG. 5.13 RELATIVE MOVEMENT OF PUNCHES VS. AVERAGE COMPACT DENSITY FOR SINGLE-ENDED PRESSING MODE

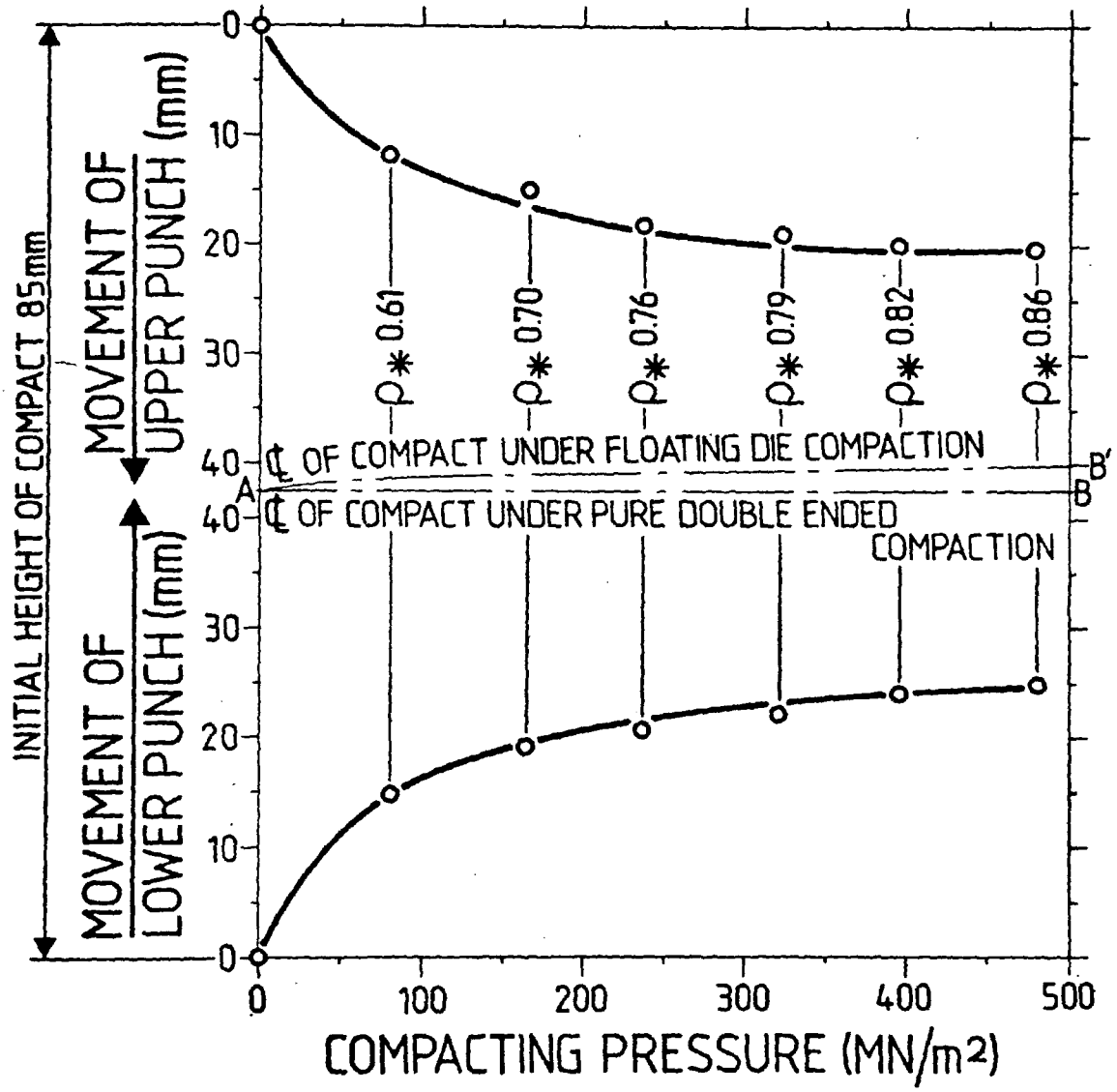

FIG. 5.14 RELATIVE MOVEMENT OF PUNCHES VS. AVERAGE COMPACT DENSITY FOR DOUBLE-ENDED PRESSING MODE

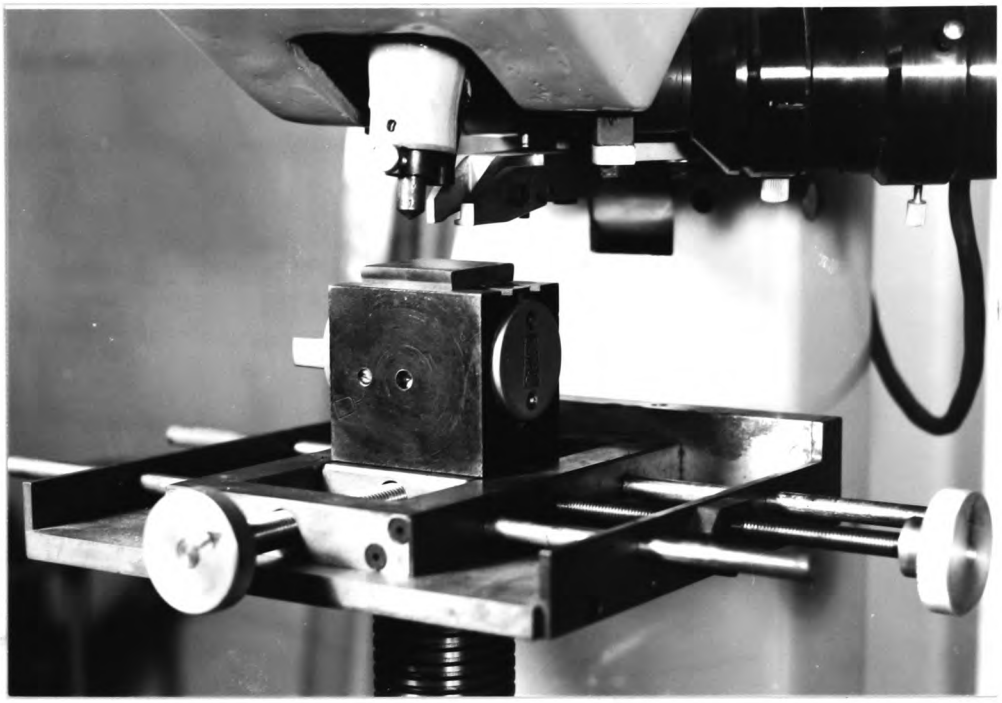

Fig. 5.15 EQUIPMENT USED TO CONDUCT HARDNESS SURVEY.

Section of green compact shown mounted on magnetic block

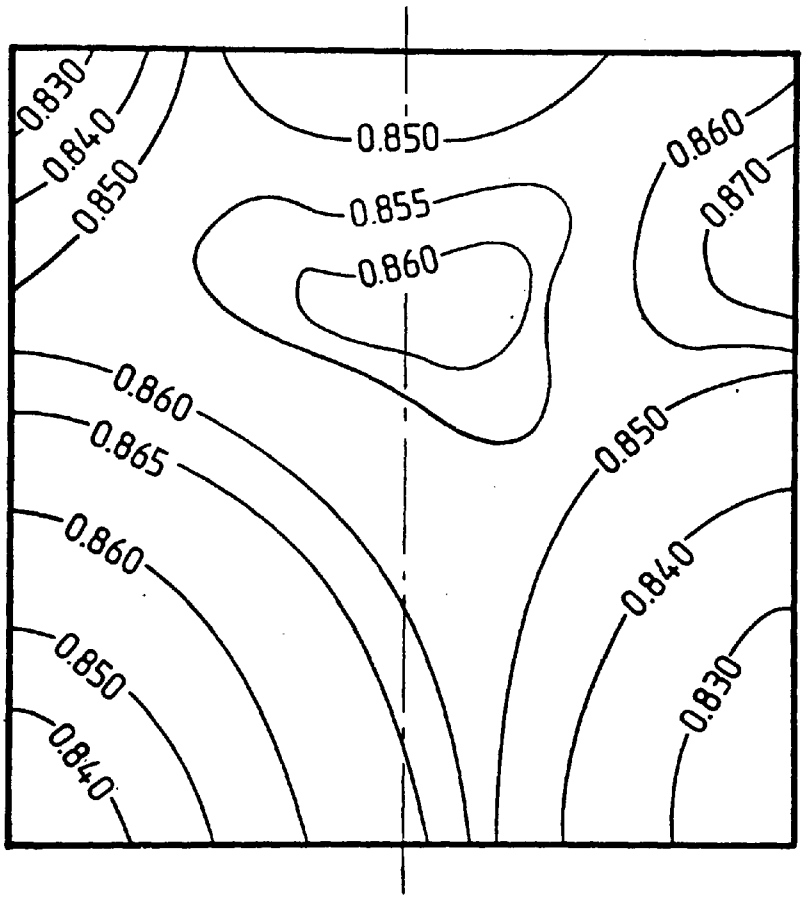

FIG. 5.16 RELATIVE DENSITY DISTRIBUTION THROUGHOUT COMPACT PRODUCED BY SINGLE-ENDED PRESSING

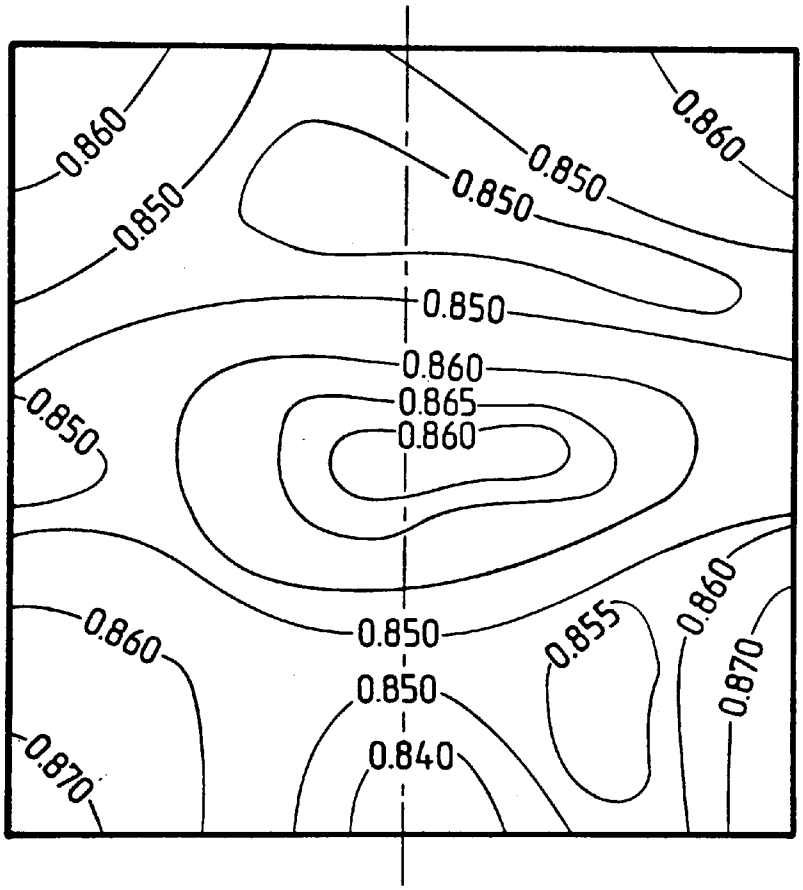

FIG. 5.17 RELATIVE DENSITY DISTRIBUTION THROUGHOUT COMPACT PRODUCED BY DOUBLE-ENDED COMPACTION

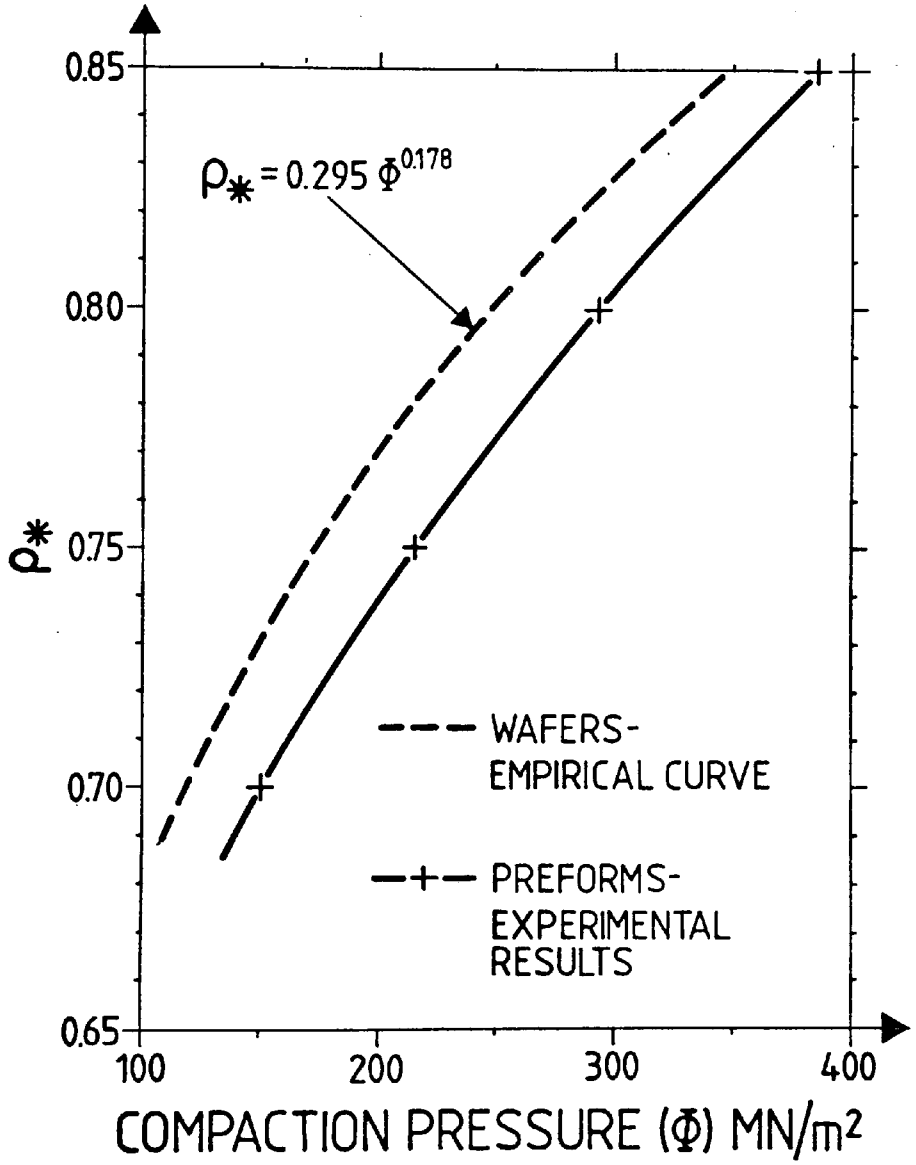

FIG. 5.18 COMPARISON OF RELATIVE DENSITY VS. COMPACTION PRESSURE CURVES FOR PM "WAFERS" AND CYLINDRICAL PREFORMS

Brinell hardness readings of the surface, in a grid pattern. These hardness readings were then converted to relative densities using the calibration curve, Figure 5.12. Finally density distribution contours were drawn as shown in Figures 5.16 and 5.17.

These compare favourably with similar contours shown in Jones[98] and Sands and Shakespeare[99], and clearly show the improved density distribution obtained with the "floating-die" as opposed to single ended compaction.

Cylindrical preforms for powder forging were made from AHC 100.29 iron powder mixed with 0.5% C and 1% zinc stearate. These were compacted with the tool used in the floating-die mode, and the powder introduced on a constant mass basis, in accordance with the final relative density required, plus the fact that all the preforms were required to be 50 mm long. The resulting compaction curve is shown in Figure 5.18, where it is compared with that obtained for the wafers produced from the same powder mix. The difference in the two curves is due to the different geometries of the two compacts, which, in the case of the cylindrical preform, results in a larger lateral surface area of compact in contact with the die wall.

A series of preforms were also compacted from the coarse powder fraction.

CHAPTER 6

Sintering

6.1 Firth Cleveland Sintered Products

A fairly comprehensive discussion of sintering phenomena has already been included in Section 2.10, whilst Section 3.1 draws attention to the lack of the specialised equipment available to exercise careful control over the heating operations, which unfortunately also included sintering. However, this obstacle was overcome by the willingness of Firth Cleveland Sintered Products Ltd., Treforest, to undertake the major part of the sintering required throughout the project, see "Acknowledgements".

This sintering was carried out on continuous belt-type sintering furnaces under production conditions in accordance with standard industrial practice. The atmospheres used were mixtures of air and propane in the approximate ratio of 7 to 1. These mixtures were passed through an endothermic atmosphere generator employing a nickel catalyst, to provide a product gas consisting largely of CO, H_2 and N_2. These generators were operated to give dew points of approximately + 1°C. A typical sintering operation included heating to 760°C to preheat and "dewax" followed by sintering for 28 minutes. During this time the specimen passed through three, 4 foot zones which collectively make up the sintering region of the furnace. Typical temperatures for each of the zones were 1130°C, 1139°C and 1040°C. After sintering, the specimens were passed through a gas protected cooling region, before being discharged from the furnace.

6.2 Improvised Sintering for Pilot Study[28]

As stated in Section 2.11, earlier sintering of the blanks required

for the pilot study[28], was carried out in an electrically heated muffle furnace. The compacts were produced from Rospol MP32 iron powder, see Sections 4.1 and 5.2, which was admixed with 1% zinc stearate and 1% graphite, originally intended to simulate E_n8 (B.S. 1970). The seemingly high quantity of graphite was considered necessary, since the following improvised sintering technique made it uncertain as to how much associated carbon would remain in the final microstructure.

Prior to sintering, the blanks were heated in air to approximately 400°C to remove the zinc stearate, after which they were cooled and coated with Birkatekt 22. The sintering was then carried out in the muffle furnace which was occasionally purged with nitrogen. The blanks were heated to 1130°C, soaked for 30 minutes, and then removed from the furnace and buried in sand to cool.

Upon examination, the blanks did not appear to be excessively scaled, see Fig. 6.1.a, whilst a sectioned blank revealed a decarburized zone to a depth of $\sim$ 3-5 mm. However, this decarburization was of little consequence in this instance, since approximately 50% of the weight of the blank was removed when machining to the required preform size, shown in Fig. 6.1(b).

6.3 Construction of Bench Top Tube Furnace

Whilst undertaking the three month study tour[6] referred to in Section 1.4, the writer acquired the twin horizontal tube sintering furnace shown in Fig. 6.2, with a view to restoring it to working order. However, since it later became apparent that it was at least 30 years old, it was considered more expedient to undertake the construction of an entirely new furnace.

As a preliminary measure, the small bench top tube furnace shown

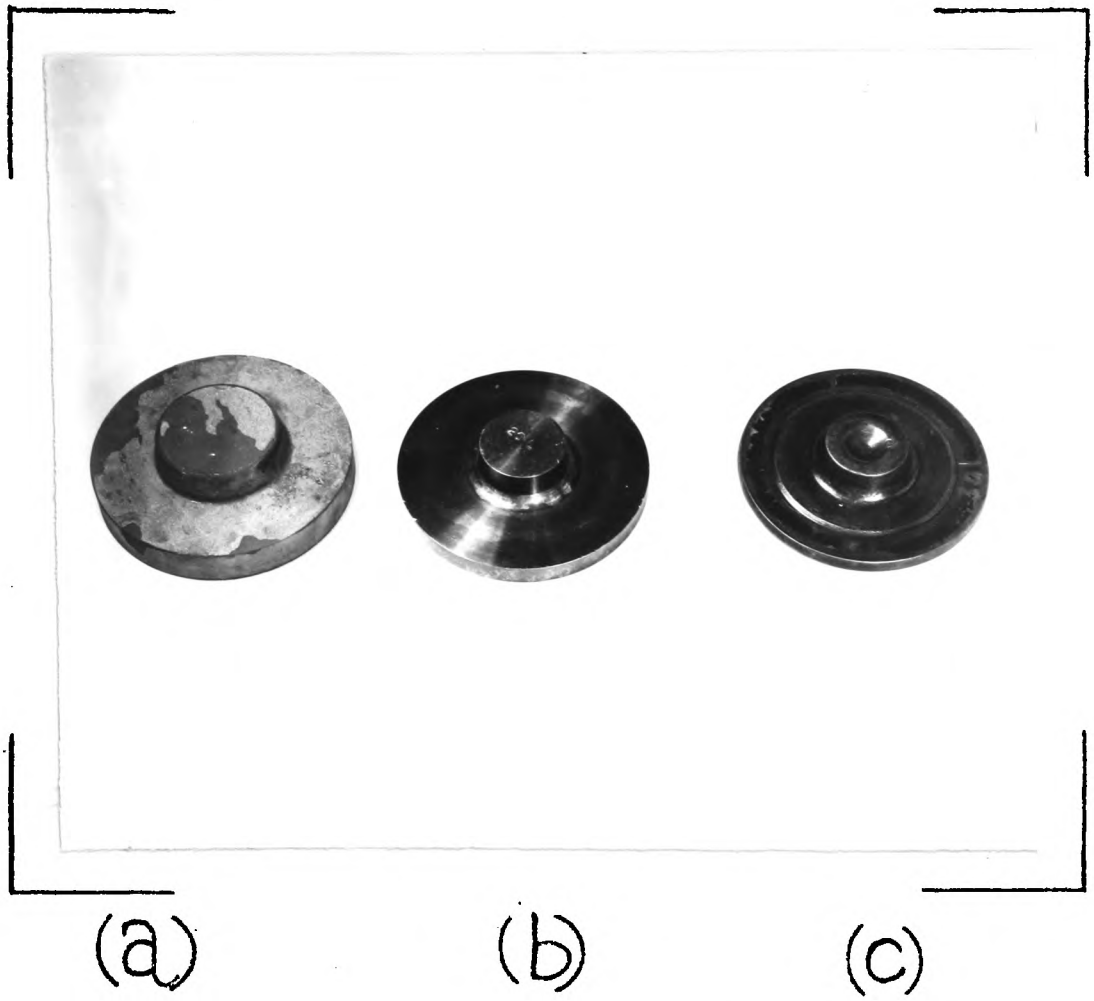

Fig. 6.1 THREE STAGES IN THE MANUFACTURE OF THE POWDER FORGED TURBINE HUB

(a) sintered blank

(b) machined preform

(c) final forging

(Ref. 28)

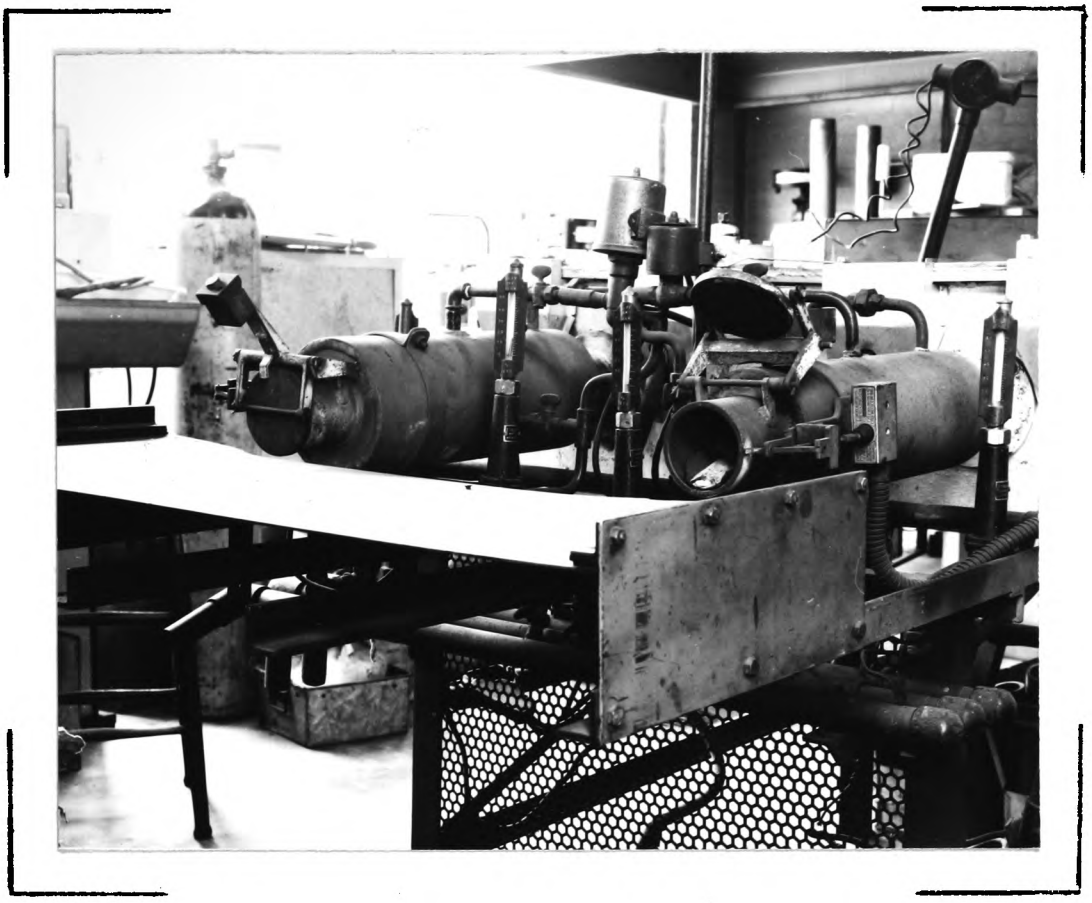

Fig. 6.2 TWO VIEWS OF TWIN HORIZONTAL TUBE SINTERING FURNACE

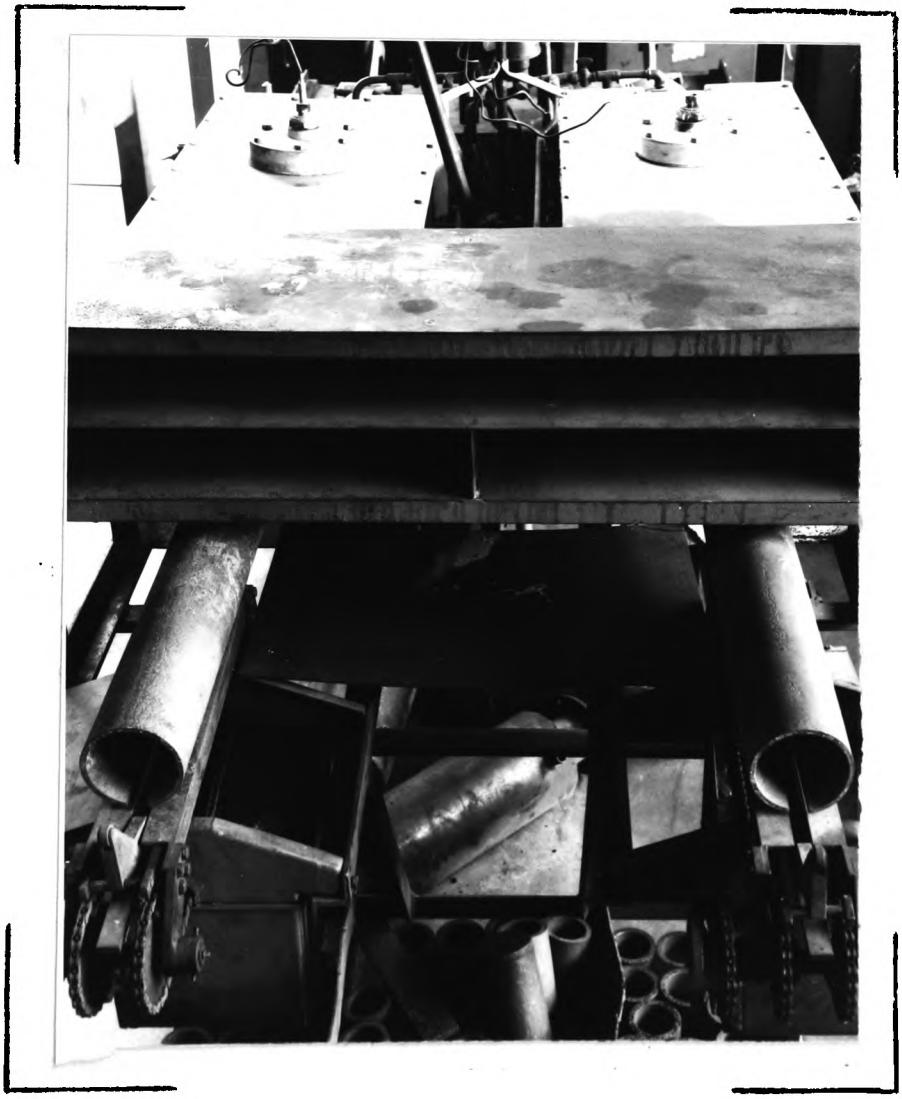

in Fig. 6.3 was constructed. This consisted of an impervious mullite tube inserted into a single phase 750 watt Kanthal wound annular heating furnace, just capable of attaining the sintering temperature. The furnace assembly was mounted on an angle iron cradle, and the temperature controlled by means of a Eurotherm temperature controller used in conjunction with a chromel alumel thermocouple located near the outer surface of the mullite tube, at its mid-length. The furnace end caps were made from aluminium and these carried the seals necessary to exclude the surrounding atmosphere. These end caps were water-cooled to prevent the seals from becoming damaged by over heating. The caps were designed to allow the protective atmosphere to flow through the mullite tube, and also to allow ease of access for the components with the minimum of disturbance to the seals. The temperature profile along the furnace tube was checked with the aid of a previously calibrated Cambridge chromel/alumel thermocouple, and the results are shown plotted in Fig. 6.4.

The furnace performed quite satisfactorily when used in conjunction with the Admix Mark 2, gas mixing system described in Appendix G. However, it was only intended to be a forerunner of the more ambitious, larger tube furnace described in Appendix H. Unfortunately, however, the construction of this latter furnace was not completed in time to allow it to be used for the present programme of work.

6.4 Micro-examination of Sintered Material

Four specimen were selected for micro-examination. Two of these were for the "as supplied" Hoganas A.H.C. 100.29 iron powder, and a further two for the coarse fraction (150-180 μm) of the same powder. In each case the samples were admixed with 0.5% graphite and 1% zinc stearate, and sintered as described in Section 6.1. The "as supplied"

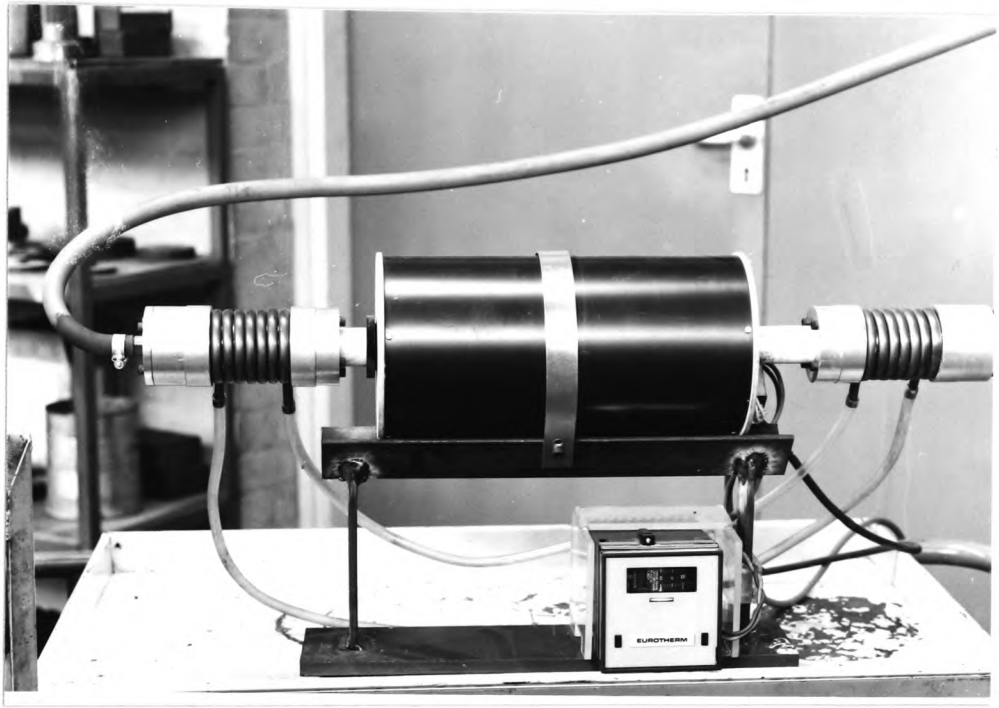

Fig. 6.3 BENCH TOP TUBE FURNACE

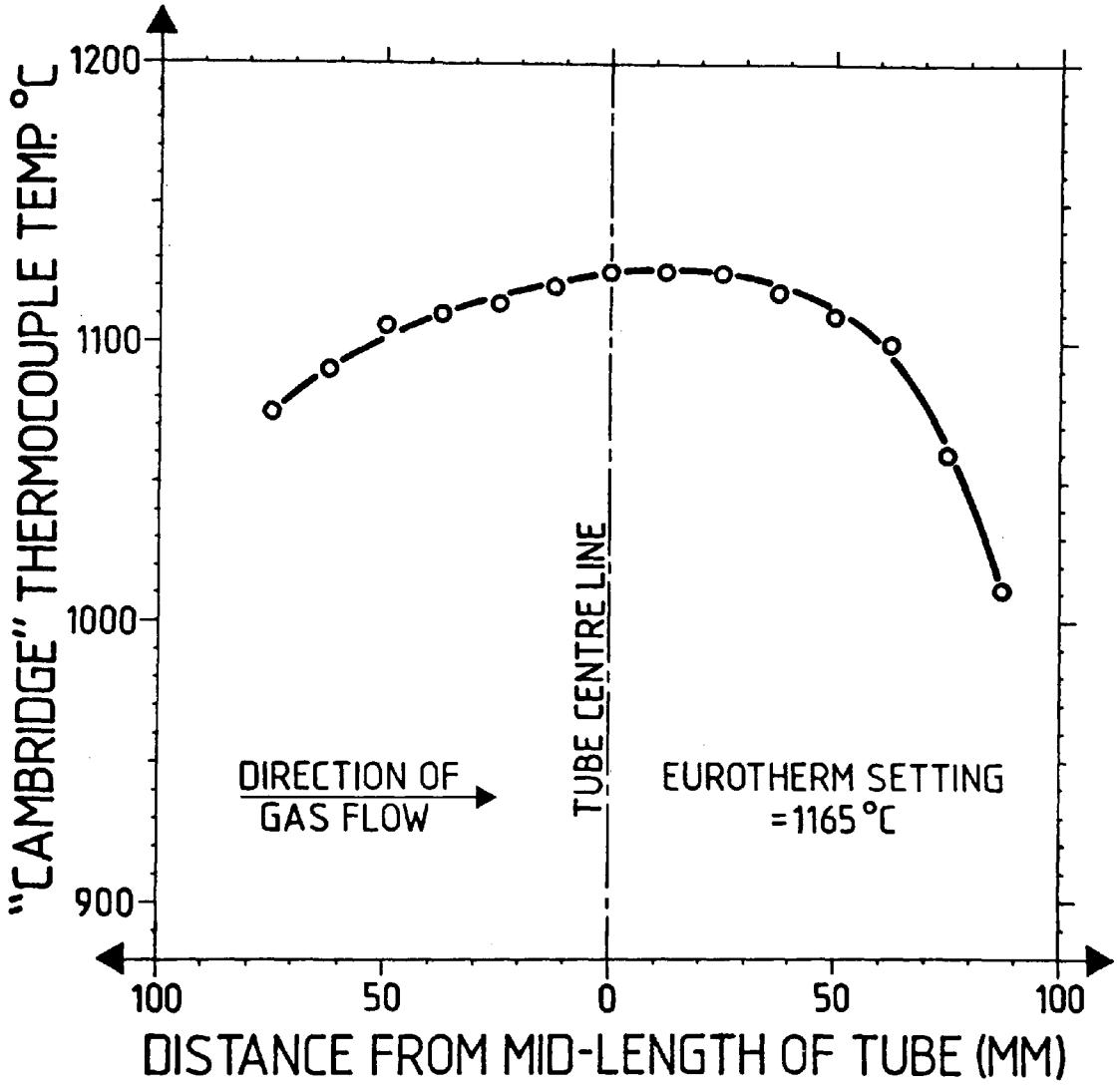

FIG. 6.4 TEMPERATURE PROFILE ALONG WORKING REGION OF BENCH TOP TUBE FURNACE

specimen had relative densities (ρ_*) of 0.76 and 0.876, whilst the "coarse fraction" specimen had relative densities (ρ_*) of 0.79 and 0.865 respectively.

The specimen were prepared for micro-examination by firstly being hot mounted in a transparent thermoplastic mounting medium together with an identification disc. They were then lightly ground on a belt linisher followed by wet pre-grinding by hand on four successively finer grades of metallographic paper, the actual grades being 240, 320, 400 and 600. This was followed by polishing on two rotating disc polishing machines with cloths impregnated with 6 micron and 1 micron diamond paste. The specimen were carefully washed between each successive stage of polishing, and finally degreased and blown dry.

The polished specimen were then examined and photographed on a Vickers Fifty-Five projection microscope (Serial No. M550030), in order to gain an appreciation of the morphology and distribution of the porosity contained in each specimen. These are shown as Figs. 6.5 to 6.8 inclusive, where it can be seen that the porosity occurring with the "as supplied" powder specimen is finer than that obtained from the "coarse fraction" powder, for similar values of ρ_*.

The specimen were then etched in 3% nital for times varying from 30 to 45 seconds depending upon the degree of porosity, and re-photographed. This was followed by a second etch which involved boiling for 10 minutes in alkaline sodium picrate, after which the same areas were photographed as for the nital etch. A comparison of the results of the two different etches are shown as Figs. 6.9(a) and (b) to Fig. 6.12(a) and (b) inclusive.

Figs. 6.9(a) and 6.10(a) show white bands around the grains suggesting the presence of free cementite in the form of a carbide

Photomicrographs of polished sintered specimen produced from various iron/graphite powder mixes, see Section 6.4 for details

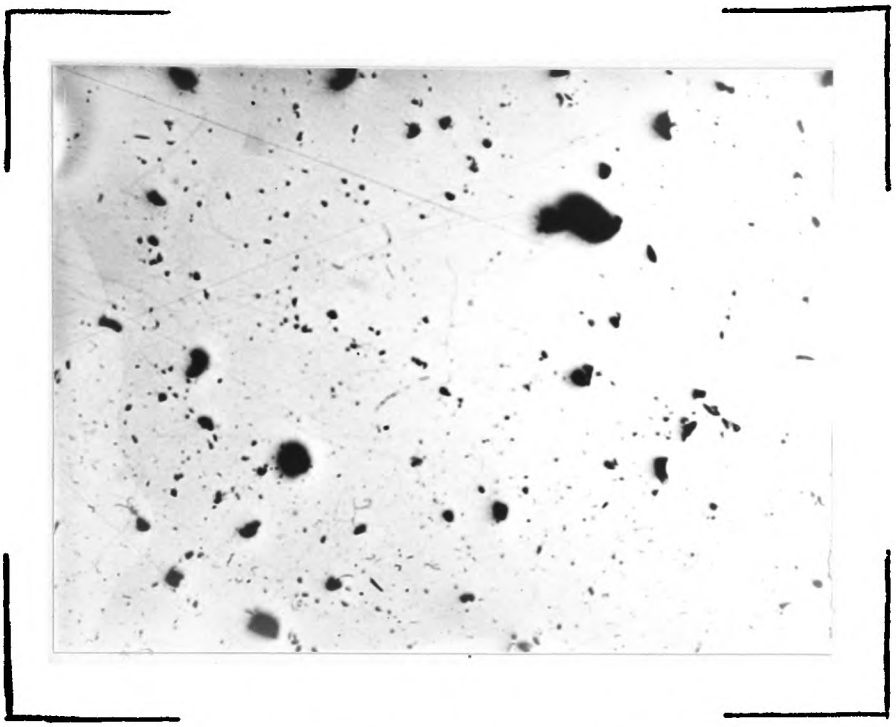

Fig. 6.5 "AS SUPPLIED AHC 100.29 IRON POWDER
P = 0.24, Mag. x 100

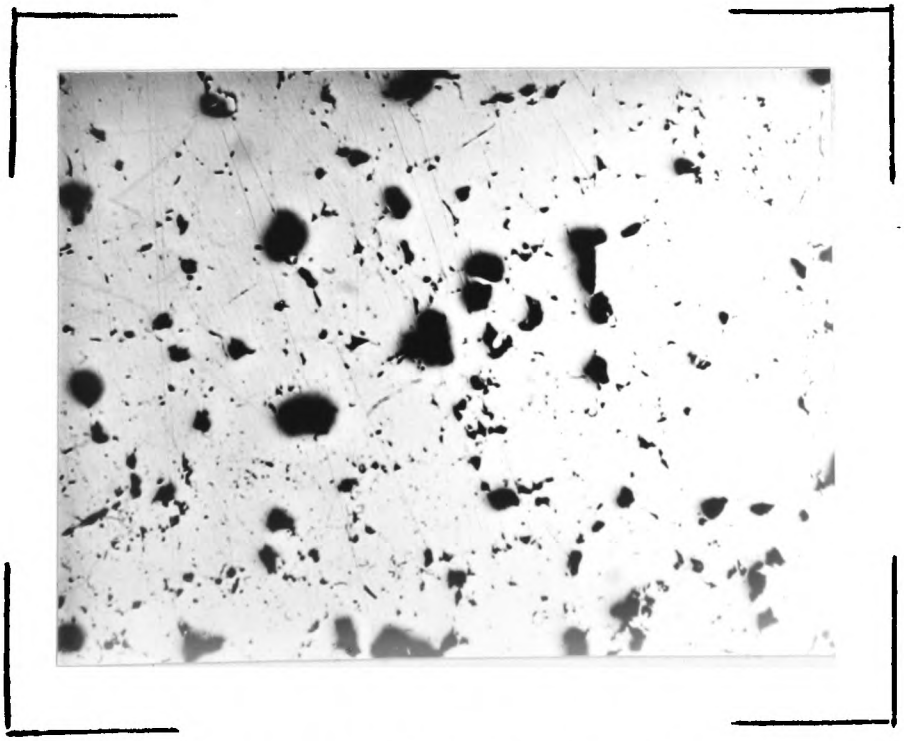

Fig. 6.6 "COARSE FRACTION" (150 - 180 μm) IRON POWDER
P = 0.21, Mag. x 100

Photomicrographs of polished sintered specimen produced from various iron/graphite powder mixes, see Section 6.4 for details

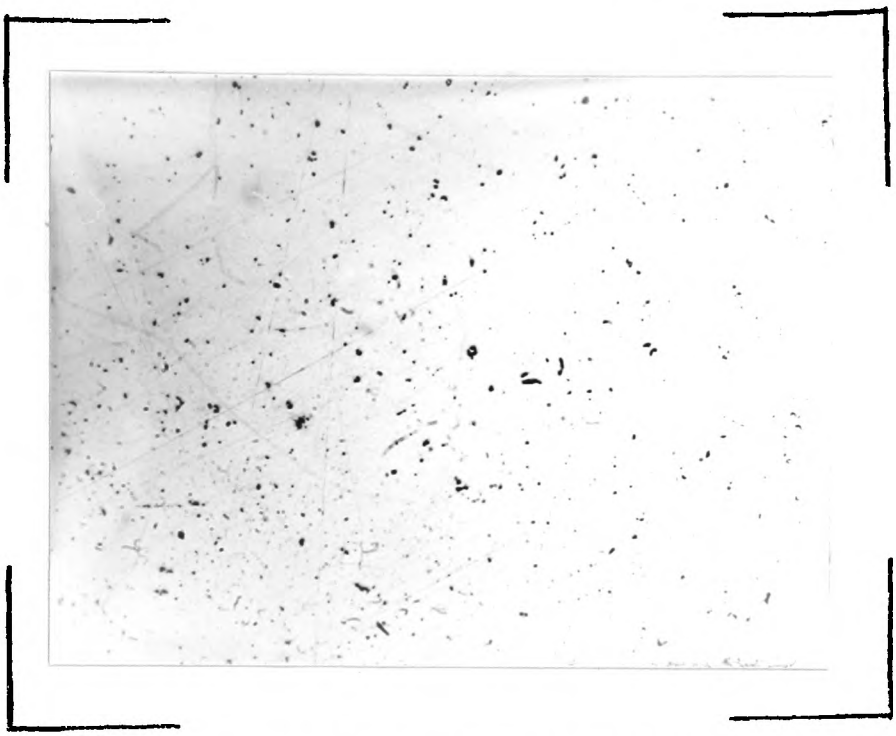

Fig. 6.7 "AS SUPPLIED" AHC 100.29 IRON POWDER
P = 0.124, Mag. x 100

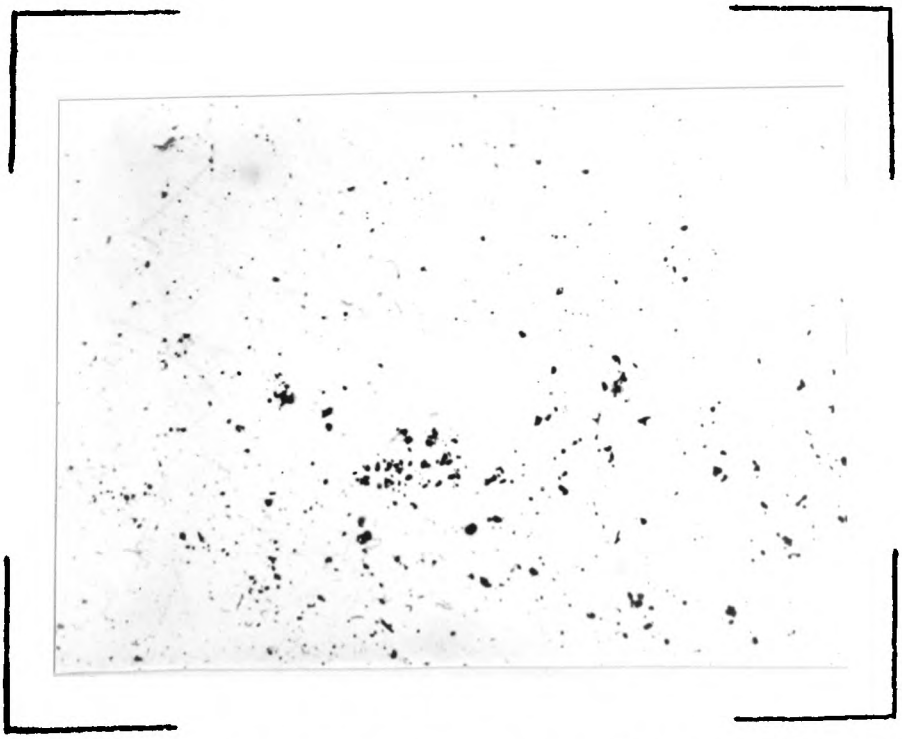

Fig. 6.8 "COARSE FRACTION" (150 - 180 μm) IRON POWDER
P = 0.135, Mag. x 100

Photomicrographs of polished and etched sintered specimen produced from iron/graphite powder mixes, see Section 6.4 for details

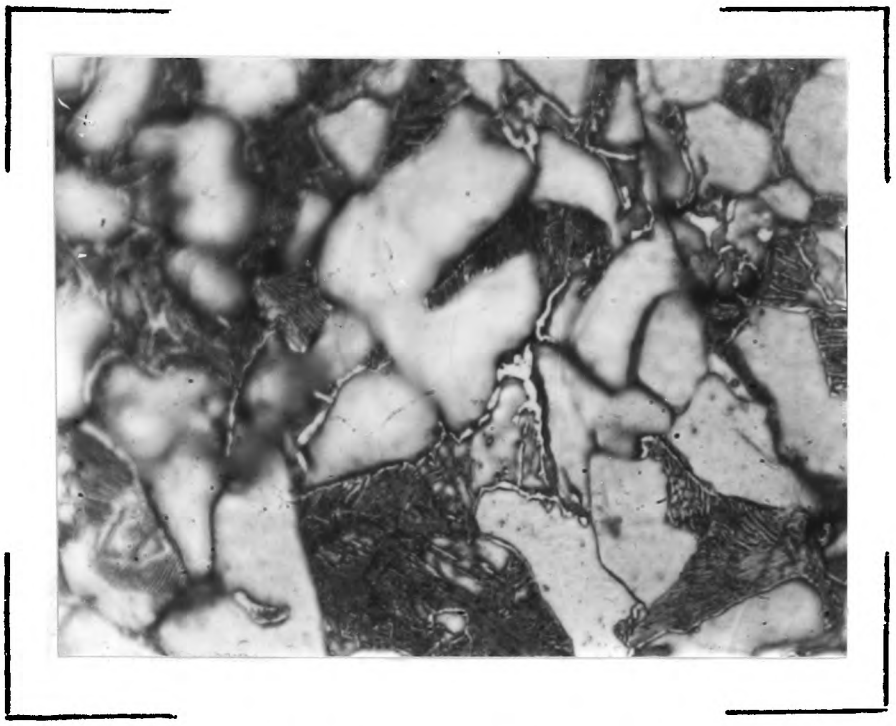

Fig. 6.9(a) "AS SUPPLIED" AHC 100.29 IRON POWDER
P = 0.24, Mag. x 1000, nital etch

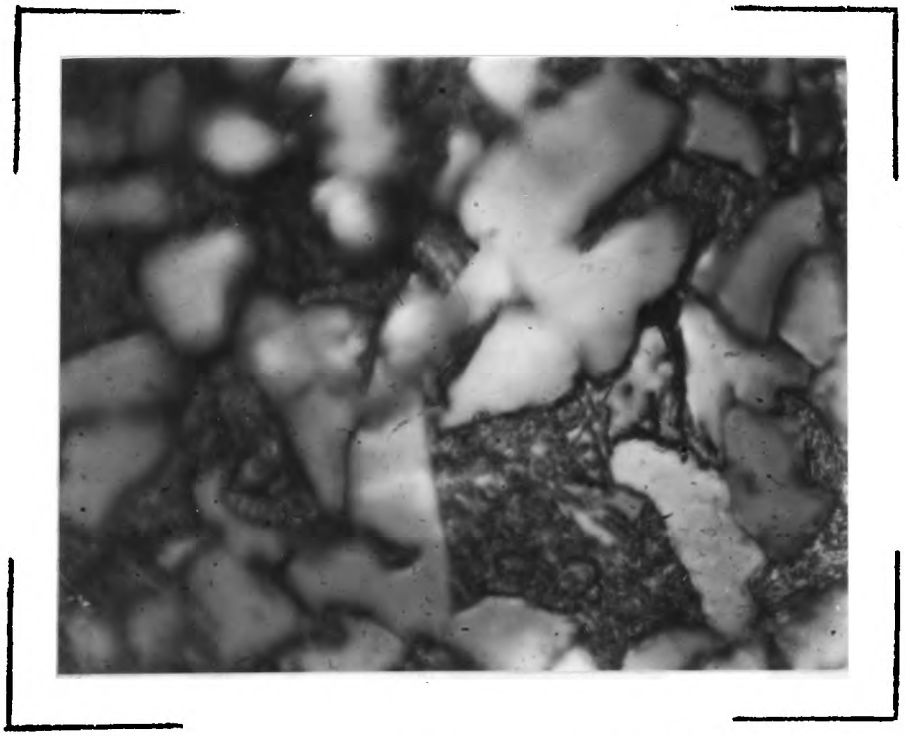

Fig. 6.9(b) "AS SUPPLIED" AHC 100.29 IRON POWDER
P = 0.24, Mag. x 1000, picrate etch

Photomicrographs of polished and etched sintered specimen produced from iron/graphite powder mixes, see Section 6.4 for details

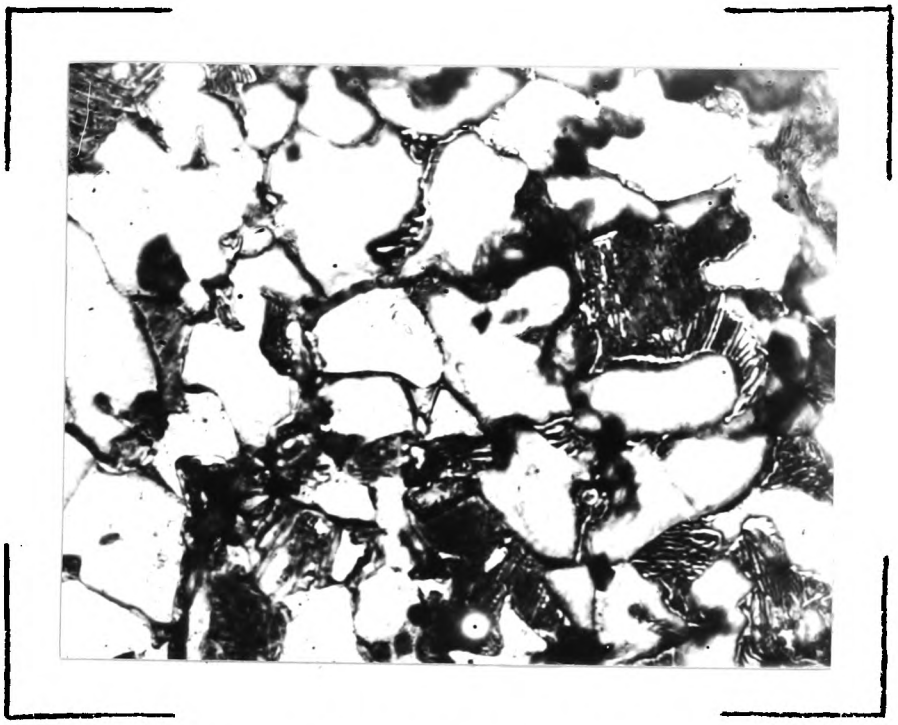

Fig. 6.10(a) "AS SUPPLIED" AHC 100.29 IRON POWDER
P = 0.124, Mag. x 1000, nital etch

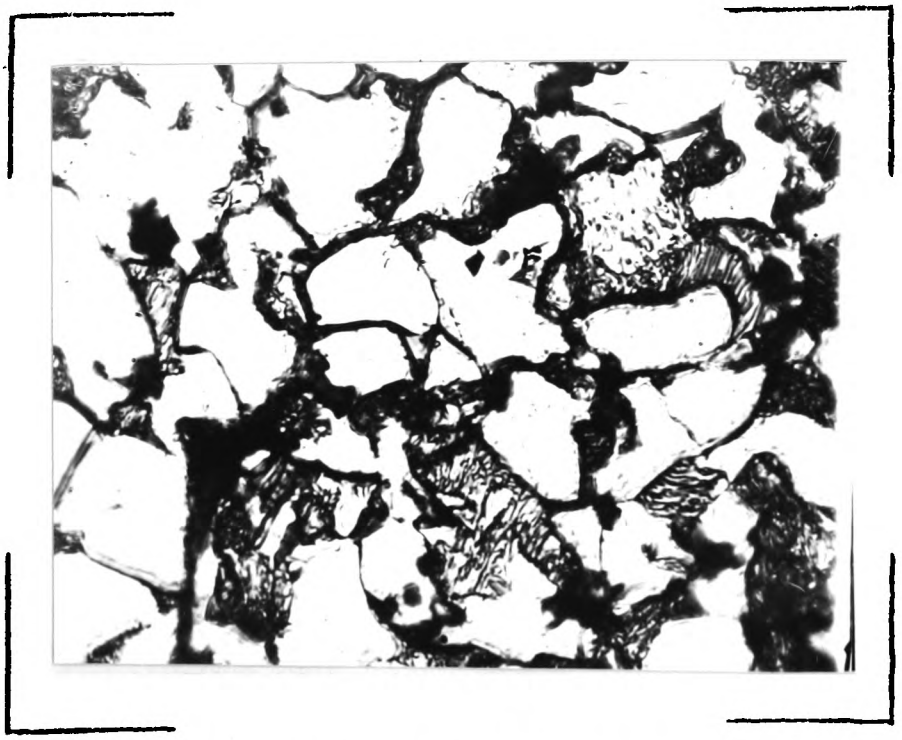

Fig. 6. 10(b) "AS SUPPLIED" AHC 100.29 IRON POWDER
P = 0.124, Mag. x 1000, picrate etch

Photomicrographs of polished and etched sintered specimen produced from iron/graphite powder mixes, see Section 6.4 for details

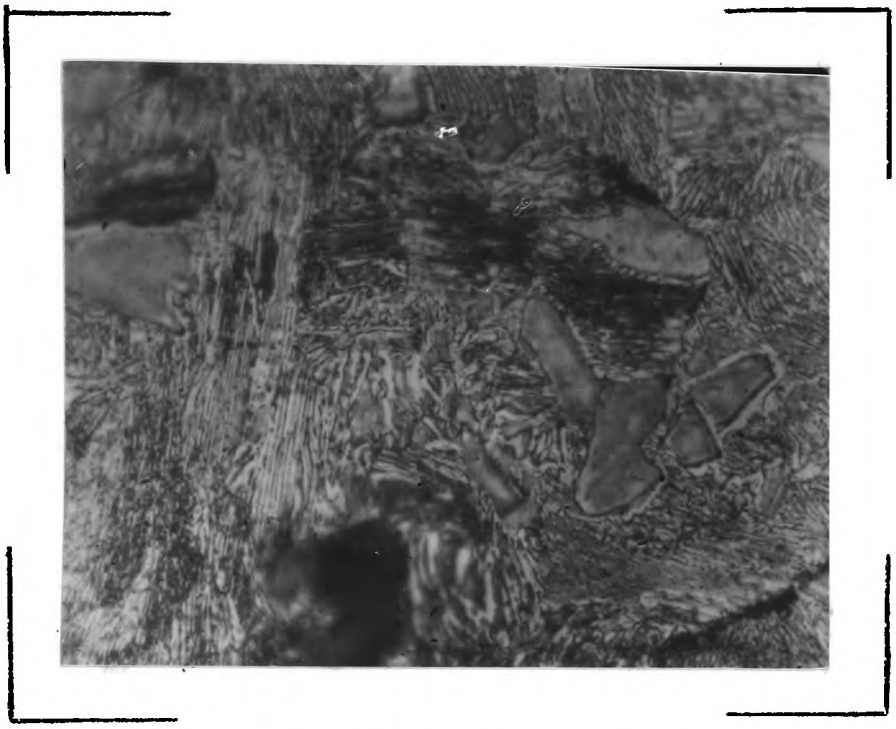

Fig. 6.11(a) "COARSE FRACTION" (150 - 180 μ m) IRON POWDER
P = 0.21, Mag. x 1000, nital etch

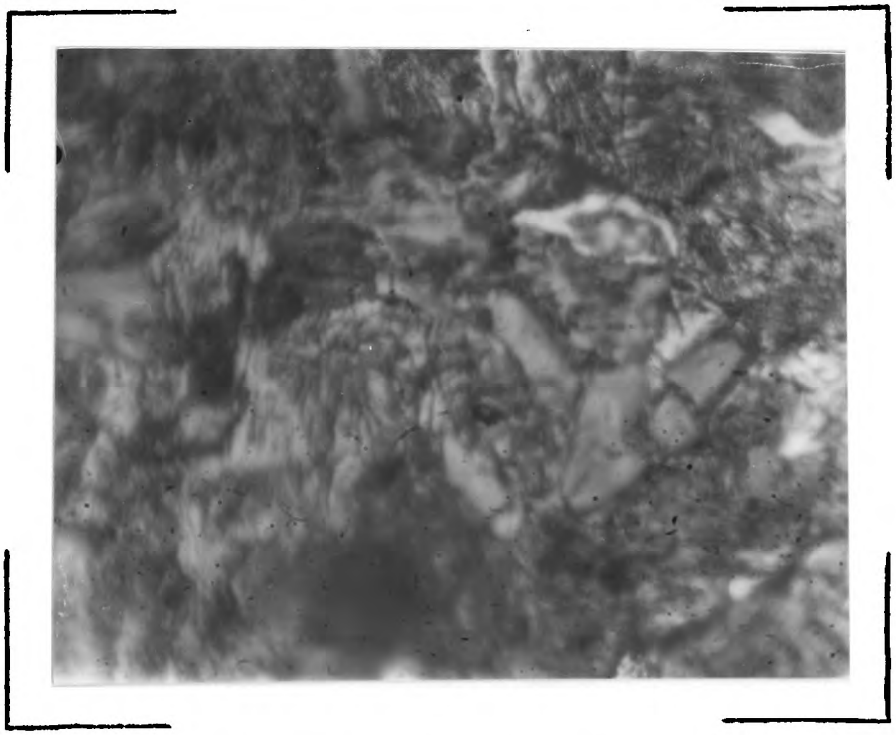

Fig. 6.11(b) "COARSE FRACTION" (150 - 180 μ m) IRON POWDER
P = 0.21, Mag. x 1000, picrate etch

Photomicrographs of polished and etched sintered specimen produced from iron/graphite powder mixes, see Section 6.4 for details

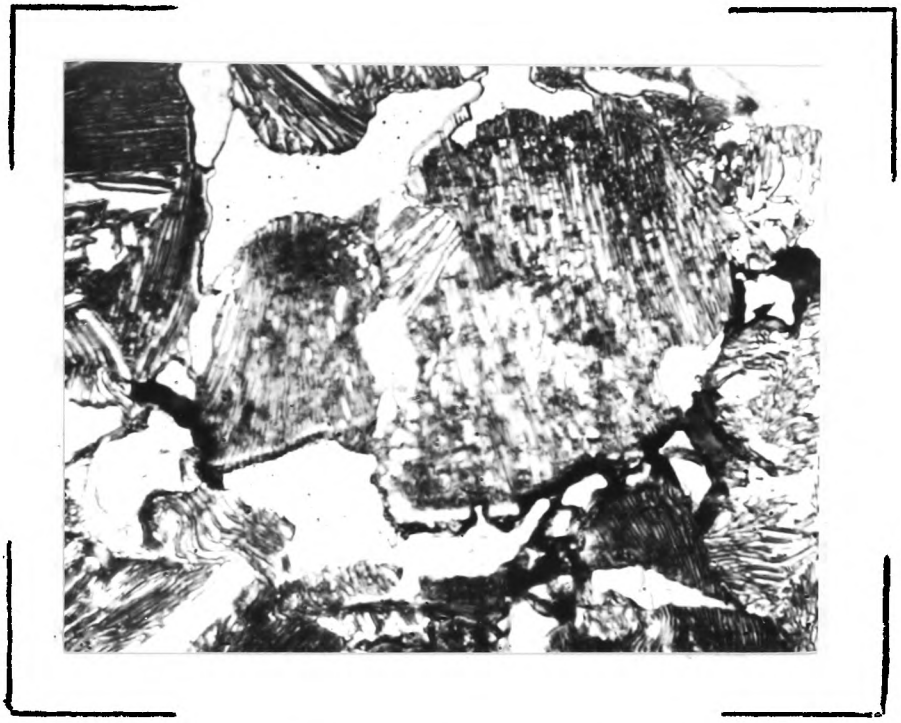

Fig. 6.12(a) "COARSE FRACTION" (150 - 180 μm) IRON POWDER
P =0·135, Mag. x 1000, nital etch

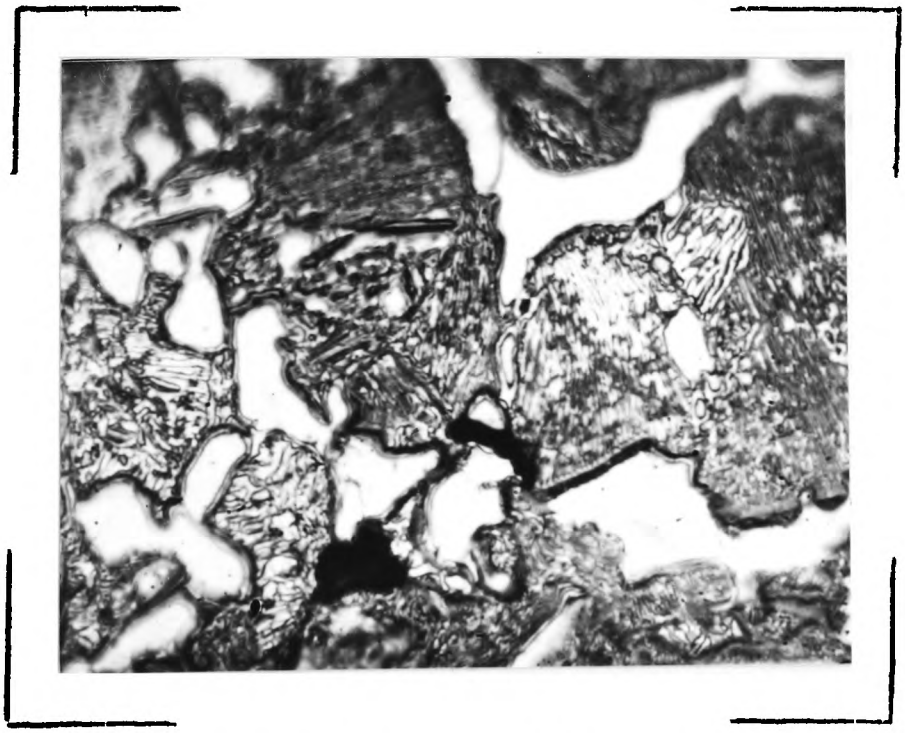

Fig. 6.12(b) "COARSE FRACTION" (150 - 180 μm) IRON POWDER
P = 0.135, Mag. x 1000, picrate etch

network. In Figs. 6.9(b) and 6.10(b) the white bands have darkened as a result of the alkaline sodium picrate etch, thereby confirming the presence of free cementite in the microstructure. Figs. 6.11 and 6.12 indicate that there is far less evidence of free cementite plus the fact that it is quite apparent that there is considerably more pearlite present in the material.

Since the same quantity of graphite was admixed with each sample prior to compaction and sintering, it must therefore be concluded that more carbon has diffused into the iron in the case of the coarse particles, as compared to the "as supplied" powder. It would therefore appear that coarse powder particles seem to offer definite advantages from the point of view of homogenization.

The reasons for this may be that the finer dispersion of porosity resulting from the use of "as supplied" powder makes it difficult for the reducing atmosphere to efficiently permeate throughout the material. Hence the oxide films trapped in these fine dispersions of porosity are not effectively reduced, and therefore act as diffusion barriers[100], requiring prolonged sintering before their eventual breakdown. It must therefore be assumed that the coarser porosity occurring in the "coarse fraction" compacts, result in less entrapped oxide layers. Additionally, this coarser porosity will present a higher surface area within the compact, which will greatly assist surface diffusion, and hence homogenization.

CHAPTER 7

Appraisal of Preform Material

7.1 Introduction

It was considered necessary to examine the preform material in some detail in order to gain an appreciation of its properties and characteristics, and thereby gain a better understanding of its behaviour during the forging operation. Furthermore, such information would be helpful in the development of analytical approaches to preform and tool design. For the purpose of this study it was decided to carry out tests at room temperature and at elevated temperatures, since it is a well known fact that temperature has a marked effect on the plastic behaviour of metals[101]. In the case of ferrous materials, increases in temperature result in a lowering of the yield point and the rate of work hardening. However, since the thermally activated processes which bring about these effects are time dependent, the yield point and tensile strength will be influenced by the rate at which the material is being strained. From this it follows that too high a strain rate may cancel out some of the advantages of working at elevated temperatures, whereas on the other hand, a low rate of straining will result in chilling. In practice therefore, it is necessary to obtain the correct balance between these various considerations. Although, due to lack of sophisticated equipment it was not possible to carry out an exhaustive programme of work along these lines, nevertheless it was possible to conduct some meaningful tests which provided useful data directly applicable to the forging process.

7.2 Forgeability

Although forgeability does not have a standard definition it is

generally agreed that it relates to flow stress, ductility and coefficient of friction[102]. Furthermore, although there are no standard tests to ascertain forgeability, hot torsion tests appear to be favoured as providing a good indication of optimum forging temperature. The advantages of such tests are that they allow specimen to be subjected to a considerable amount of strain with virtually no change in specimen geometry. Other tests which are considered useful are hot tensile tests[28] and cylinder upset tests[103].

7.3 Hot Torsion Tests

The specimen used for these tests were manufactured from A.H.C. 100.29 iron powder mixed with 0.5% C and 1% zinc stearate. After compacting to the relative densities (ρ_*) of 0.75, 0.8 and 0.85 the specimen were sintered to produce the blanks shown in Fig. 5.10(a) These were then machined to produce the hot torsion specimen shown in Fig. 5.10(b). The hot torsion test rig shown in Fig. 7.1 was designed and constructed solely for the purpose of carrying out these tests. With reference to Fig. 7.1 it can be seen to consist of two chucks with square recesses to accommodate the ends of the specimen, and apply the torque. One of these chucks is rigidly secured to the rear of the machine by means of a steel bar of sufficient length to enable the furnace to be slid clear of the chucks to facilitate loading and unloading. The other chuck is driven by means of a constant speed geared motor rotating at 39 rev/min. This rotating chuck is attached to a sliding, spring loaded shaft. It is necessary to compress the spring in order to load the specimen into position, so that the specimen is subjected to a slight axially applied tensile load; hence the need for pinning the specimen to the chucks. This sliding shaft carries a drive dog which, when the specimen is loaded into place, engages with a

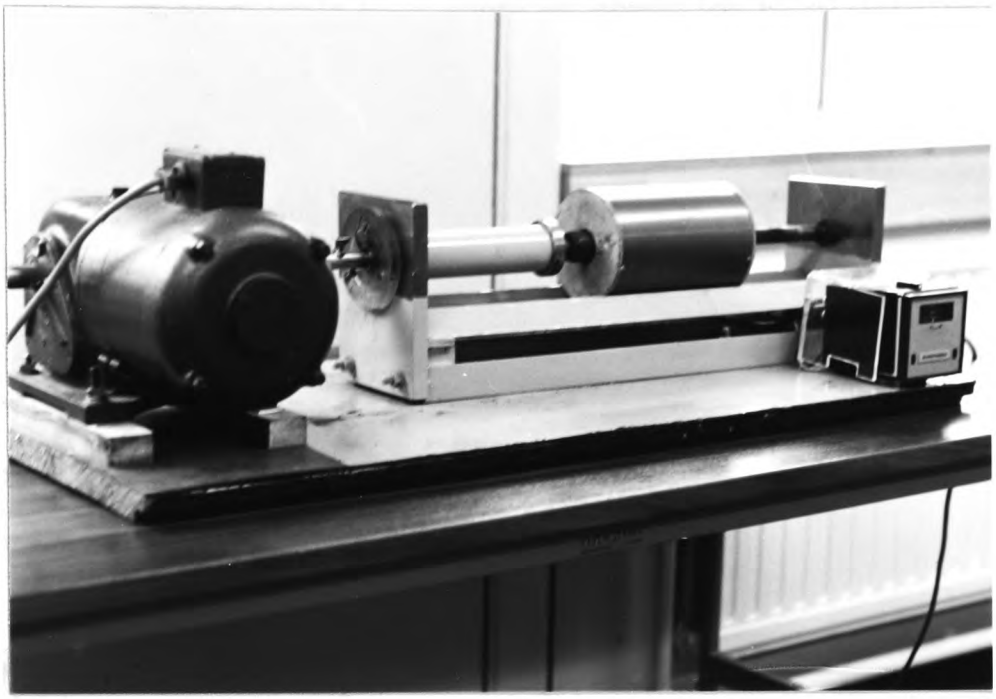

Fig. 7.1 HOT TORSION TEST RIG

moveable pointer on the protractor scale. However, when the specimen breaks in torsion, the compression spring expands to its free length and disengages this drive dog, so that the pointer will remain stationary, indicating the angle of twist at which the specimen broke.

Owing to the relatively slow speed of operation no difficulty was experienced in manually counting the whole number of revolutions completed by the specimen.

The specimen was heated by means of a single phase 500 W Kanthal wound tube furnace capable of temperatures in excess of 1100°C. Temperature control was achieved by means of a chromel/alumel thermocouple used in conjunction with a Eurotherm temperature controller. The furnace was supported on a vee slide arrangement made from angle iron, which constituted the bed of the machine, and along which the furnace could be traversed to facilitate loading and unloading.

Owing to the simplicity of the equipment, it was virtually impossible to introduce and maintain a suitable atmosphere e.g. argon, to protect the specimen from internal and external oxidation during the heating period prior to testing. The specimens were therefore coated with Birkatekt which proved to be perfectly satisfactory for the purpose.

Tests were carried out over the temperature range 800 - 1000°C at temperature intervals of 50°C, with specimen of all three relative densities, and the results recorded are shown in Fig. 7.2.

These results compare very favourably with those determined by Antes[104], and indicate that forgeability increases with increasing preform density and suggests that the optimum forging temperature commensurate with the maximum angle of twist is $\sim$ 920°C.

7.4 Hot Tensile Tests

The powder used to produce the hot tensile test specimens was

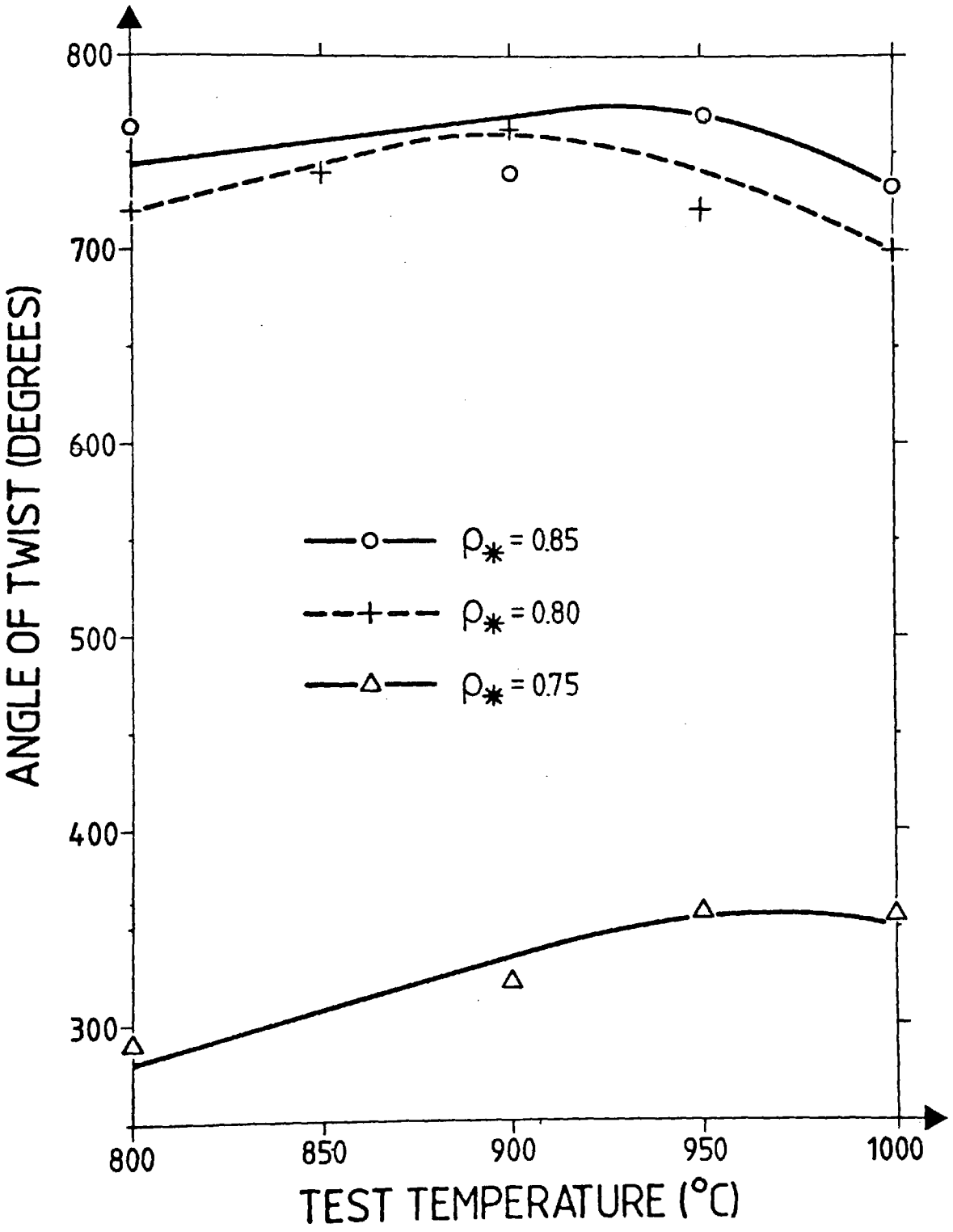

FIG. 7.2 RESULTS OF HOT TORSION TEST, ANGLE OF TWIST VS. TEMPERATURE

Rospol MP32 iron powder which was premixed with 1% C and 1% zinc stearate. After compacting to relative densities (ρ_*) of 0.72, 0.77, 0.81 and 0.84, sintering was carried out for 20 minutes at 1120°C in an endothermic atmosphere, dew point - 1°C.

The tensile test specimen, see Fig. 5.10, were then machined from the sintered "wafers" see Fig. 5.10(a) on a MOOG Numerically Controlled (NC) 2-axes milling machine. To facilitate comparison with bulk material, a batch of mild steel specimen were also prepared.

The tests were carried out on a motorized Hounsfield tensometer fitted with an automatic recorder, Fig. 7.3. An electrically heated Wild-Barfield tube furnace was used in conjunction with the tensometer, and the temperature of the furnace, and hence that of the specimen was measured by means of a thermocouple.

All the specimen were coated with Birkatekt to provide protection from oxidation during heating which varied from approximately 30 to 60 minutes depending upon the test temperature.

Specimens of each preform density were tested over the temperature range 700 - 1000°C in increments of 100°C, whereas the mild steel specimen were tested over the same temperature range, but in increments of 50°C. The results obtained are shown in Fig. 7.4.

It was not envisaged that any direct correlation between the tensile strengths obtained from these tests and those occurring during an actual forging operation, would be possible, because of the difference in strain rates involved, the tests being conducted at a strain rate of only $0.046s^{-1}$ as compared with 10 - $100s^{-1}$ for forging. However, Kalpakjian[102] suggests that, for wrought materials at least, the strengths obtained at room temperature for normal tensile testing could, as a first approximation, be regarded as being representative of those obtained at

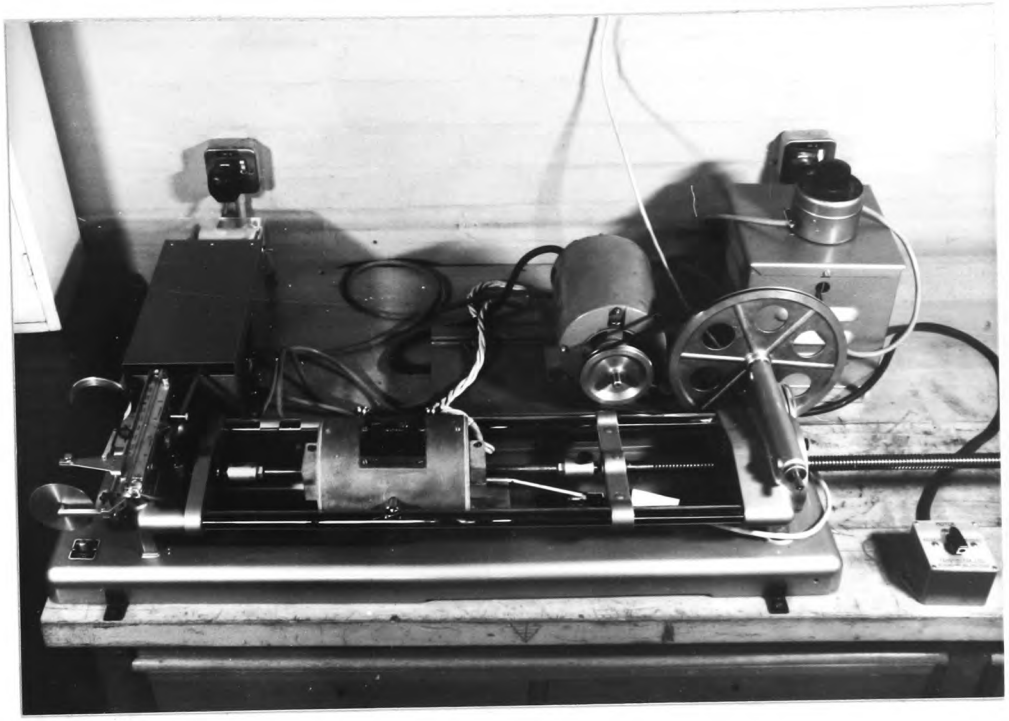

Fig. 7.3 MOTORIZED HOUNSFIELD TENSOMETER FITTED WITH AUTOMATIC RECORDER, AND SHOWING ARRANGEMENT OF TUBE FURNACE USED FOR HOT TENSILE TESTING

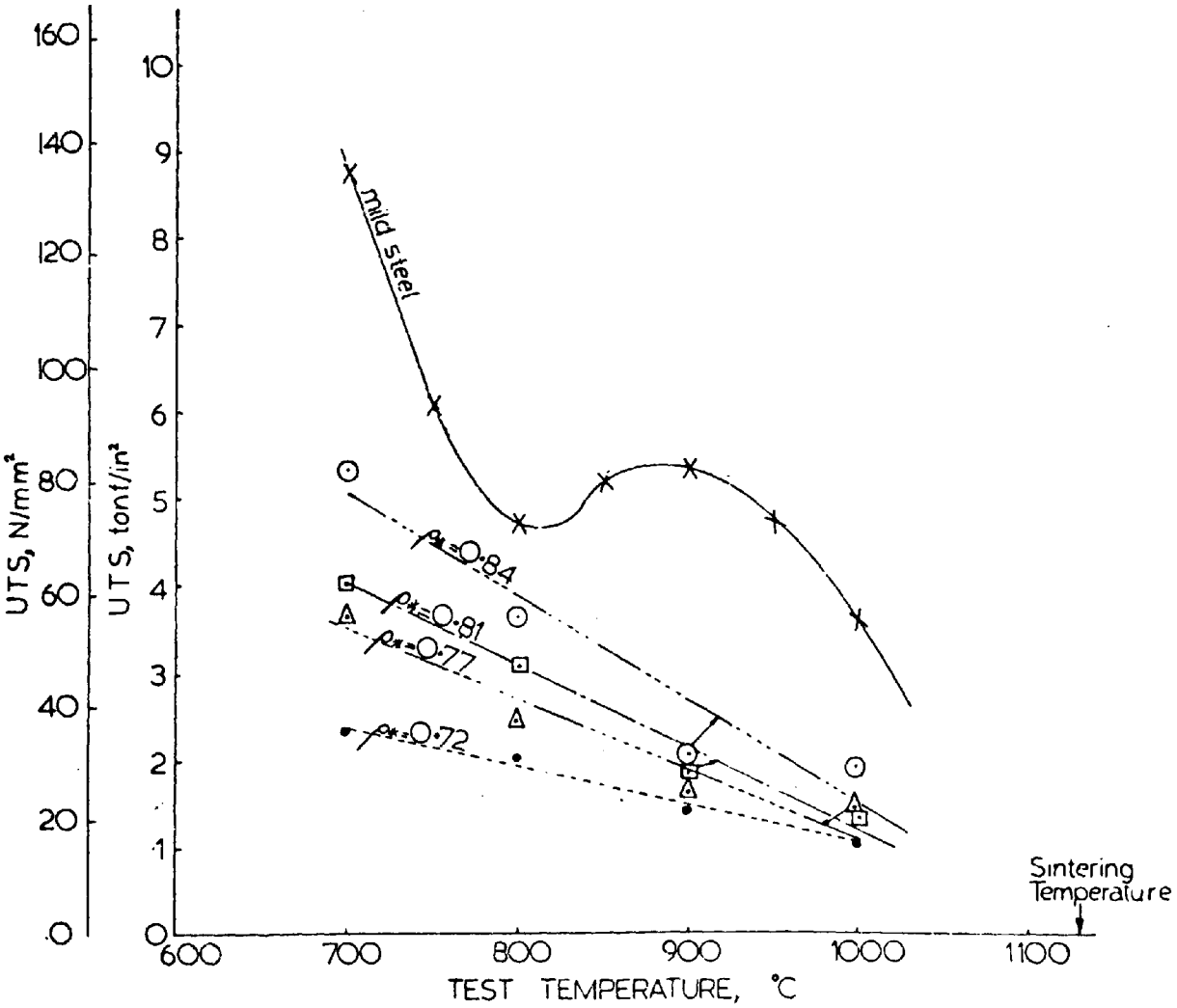

Fig. 7.4 Curves showing variation of UTS with test temperature. (ref. 28)

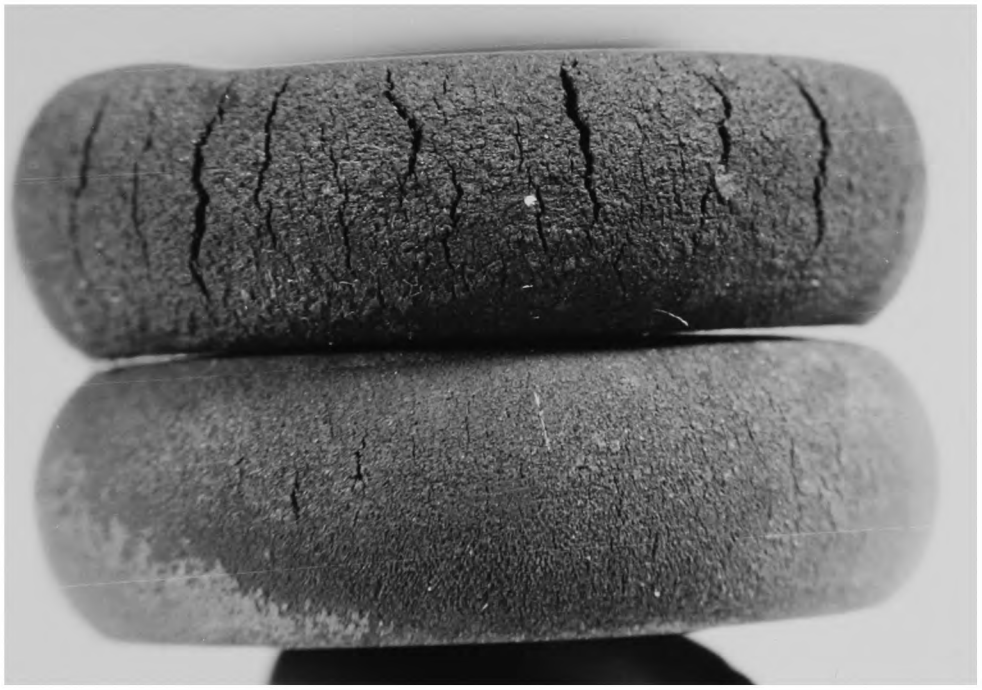

Fig. 7.5 COMPARISON OF PERIPHERAL CRACKING IN CYLINDRICAL PREFORMS OF INITIAL RELATIVE DENSITY $\rho_* = 0.77$ WHEN SLOWLY UPSET TO 54% OF THEIR ORIGINAL HEIGHTS

INITIAL TEMPERATURE OF UPPER PREFORM = 1050°C
INITIAL TEMPERATURE OF LOWER PREFORM = 950°C

elevated temperatures for rapid strain rates. Furthermore, Keane et al[105] state that the effect of increased strain rate on iron is to increase its ductility, as well as its strength, and they demonstrate that the percentage elongation of iron has a very pronounced peak value in the temperature range 850 - 900°C. With reference to Fig. 2.10 it can be seen that the percentage elongations of the sintered material all tend to reach a peak value at the same temperature of $\sim$ 800°C hence suggesting an optimum forging temperature to obtain maximum ductility. The fact that this temperature is below that of Keane et al's and that obtained from the hot torsion tests, is merely due to the higher carbon content of the material which it is widely acknowledged, reduces the forging temperature[102].

Additional tests involving the slow upsetting of hot blanks of the same material with a relative density $\rho_* = 0.77$ to 54% of their original height, revealed that whereas no peripheral cracking was evident with blanks whose initial temperature was 950°C, it did occur for those heated to 1050°C, see Fig. 7.5. Bockstiegel and Olsen[106] and Cull[21] also draw attention to the risk of cracking increasing with increasing temperature, again suggesting an optimum temperature for maximum ductility. The peripheral cracking of the preform is due to the unsupported peripheral surface of the preform being subjected to circumferential tensile stresses as the outward speading of the preform material takes place during the upsetting stage of the forging process. The fact that the UTS curve for mild steel shown in Fig. 7.4. compares favourably with similar curves obtained by Keane et al provides evidence to suggest that all the results obtained from these hot tensile tests are quite valid.

7.5 Dilatometer Tests

Dilatometer tests were conducted in order to gain an understanding

of the thermal expansion properties of the sintered preform material. The tests were carried out on specimen made from the same powder mix, and sintered in the same manner as the hot tensile specimen. The finally machined dilatometer specimen measured 50 mm long x 12 mm diameter, with a blind hole drilled axially for approximately half its length. The tests were carried out using a Griffin and George dilatometer in which the specimen was contained in an electrically heated silica tube, surmounted by a dial test indicator to measure thermal expansion, and fitted with a thermocouple to record the temperature. The purpose of the blind hole in the specimen was to accommodate the hot junction of the thermocouple.

In addition to the tests which were carried out on the sintered PM specimen compacted at various pressures, tests were also conducted on some wrought steel specimen, by way of comparison. There was no appreciable variation in the results over the range $\rho_* = 0.77 - 0.84$, as compared with those obtained from 0.6% carbon steel. Typical experimental curves are shown in Fig. 7.6 where it can be seen that for all practical purposes, the two curves compare quite favourably. This indicates that in the first instance, the 1 in 60 contraction allowance normally used in the design of conventional hot forging tools for wrought metals, can also be applied to those designed for powder forging.

It is considered that the precise amount of thermal contraction of the powder forging is of paramount importance in the design of forging tools to produce precision forgings. In addition to the preform temperature, see Section 2.13, the amount of contraction will be governed by the thermal expansion properties and the amount of preheating of the die, together with the elastic properties of both the die and

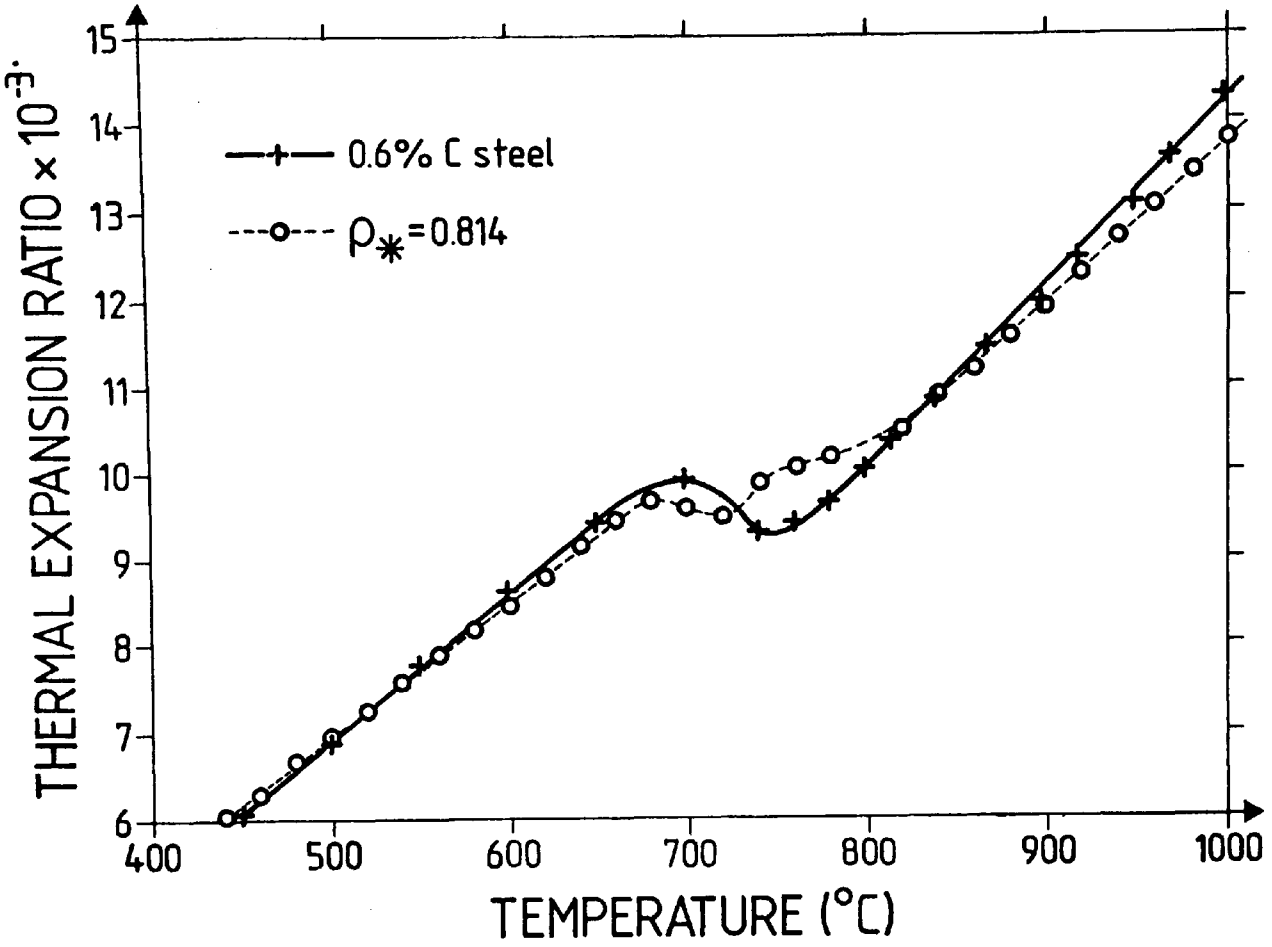

FIG. 7.6 RESULTS OF DILATOMETER TESTS

preform material.

The thermal expansion/contraction behaviour of the forging is further complicated by the volumetric changes which occur at the A_1 point, Fig. 1.1, when the γ - α allotropic transformation occurs. At this point the material will expand, as shown in Fig. 7.6 due to the atomic arrangement changing from the close packed face centred cubic, to the body centred cubic form. Such a transformation is accompanied by a change in the radii of the atoms occurring in each allotropic form, for the following reasons[107].

Firstly, the equilibrium distance between the centres of two adjacent atoms may be considered to be the sum of their radii. This distance, and consequently the atomic radius, can be increased by temperature, and manifests itself as thermal expansion. Additionally, the size of the atom is further affected by the coordination number i.e. the number of near neighbours that the atom has. In the case of the α phase the coordination number is 8, whereas for the γ phase it is 12, thereby causing a slight increase in the atomic radius. From this it follows that some of the volumetric expansion accompanying the re-stacking of the atoms due to the γ - α phase change, is offset by the associated decrease in atomic radius. During an actual forging operation it will be difficult to precisely predict the temperature at which this transformation occurs due to thermal lag arising from the relatively rapid cooling rates. However, some preliminary calculations are shown on p. 73 of Van Vlack[107], by way of example of the changes that can occur.

7.6 Measurement of Strain Components due to Uniaxial Tensile Stress.

PM preform material may be regarded as a two-phase material consisting of a mixture of matrix metal and pores. Since tensile fracture occurs with very little macroscopic deformation, it is

generally regarded as being a brittle material. However, in order to check the validity of this first impression, it was decided to conduct a series of direct tensile tests at room temperature in order to gain a better understanding of the deformation of the matrix material.

This entailed the use of electrical resistance strain gauges to measure the longitudinal and lateral strains occurring in the material during the tests. The specimen, together with the arrangement of strain gauges is shown in Fig.7.7, whilst the load was applied by means of a Hounsfield tensometer. The specimens were manufactured from Hoganas A.H.C. 100.29 iron powder, mixed with 0.5% graphite and 1% zinc stearate. Sintering was carried out as described in Section 6.1.

Fig. 7.8 shows typical results of longitudinal strain vs lateral strain for three specimen of relative densities (ρ_*) 0.76, 0.82 and 0.88, respectively, for apparent stresses of up to 40 MN/m^2. It can be seen that the line drawn through the origin of the graph to represent the elastic Poisson's ration (ν_e) of 0.3 for iron and steel, is tangential to the curves representing the two denser specimen, indicating that the material behaves in a purely elastic manner at very low stress levels. However, as the stress increases, the corresponding longitudinal strain becomes too large in relation to the accompanying lateral strain, to be explained in terms of pure elastic or bulk plastic deformation. The only plausible explanation therefore, is that the volume of the material has increased as a result of an increase in the porosity or individual pore size, obviously accompanied by a reduction in the relative density ρ_*. Similar effects have been observed with grey cast irons due to void formation around the graphite flakes[108, 109]. The porosity must have therefore become

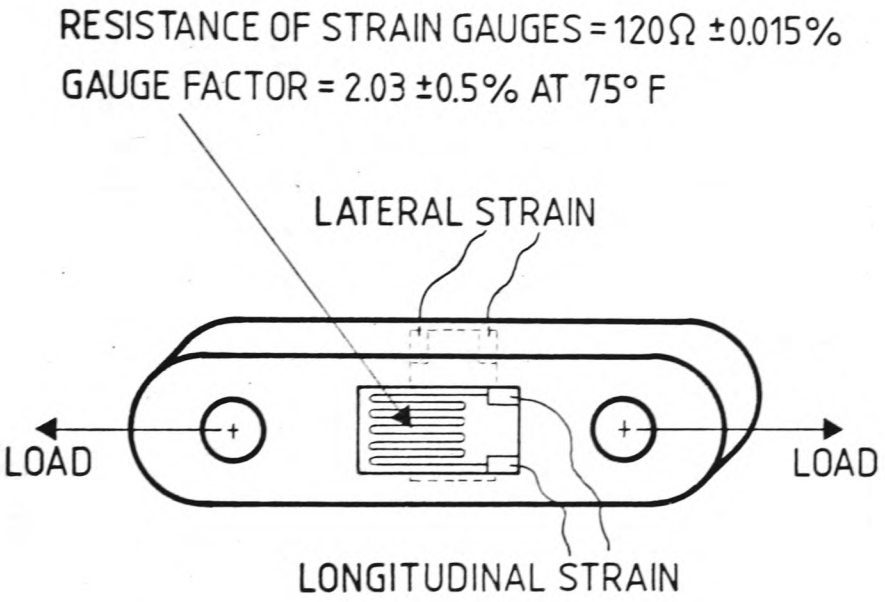

EACH GAUGE CONNECTED IN HALF BRIDGE ARRANGEMENT WITH EXTERNAL DUMMY GAUGE.

STRAIN MEASURED ON VISHAY PORTABLE STRAIN INDICATOR MODEL P-350A

FIG. 7.7 ARRANGEMENT OF ELECTRICAL RESISTANCE STRAIN GAUGES BONDED TO "WAFER" SPECIMEN TO DETERMINE LONGITUDINAL AND LATERAL STRAIN COMPONENTS DUE TO UNIAXIAL TENSILE STRESS

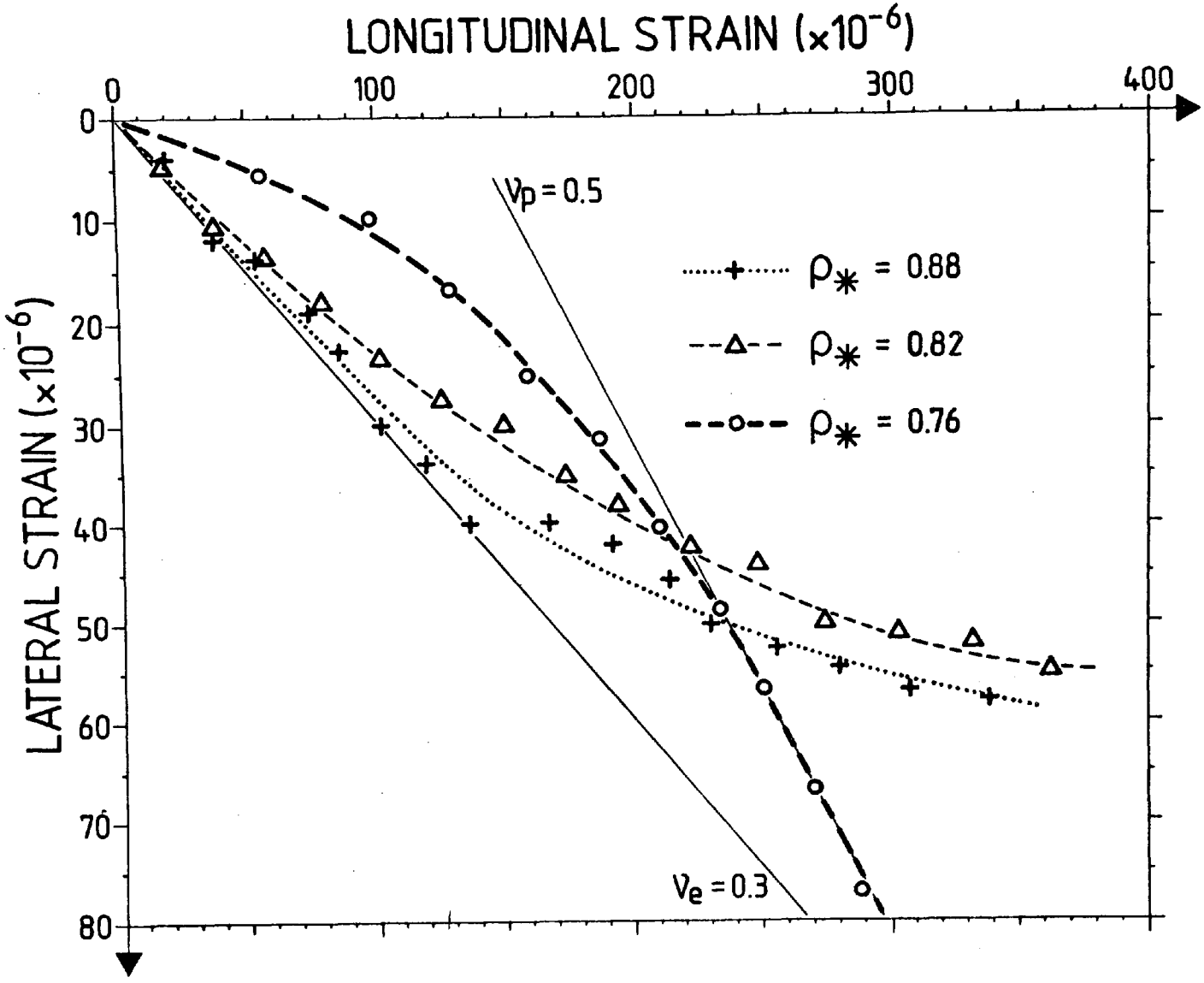

FIG. 7.8 CURVES OF LATERAL STRAIN VS. LONGITUDINAL STRAIN FOR POROUS PREFORM MATERIAL SUBJECTED TO UNIAXIAL TENSILE STRESS

elongated in the direction of the applied load, so that the matrix material immediately adjacent to the pores, undergoes localised plastic deformation due to the stress concentration effects associated with the pore geometry. As the porosity increases, the pore separation distances diminish, and the stress concentrations will begin to interact between adjacent pores at lower stress levels, thereby reducing the range over which the strain components can be solely attributed to elastic deformations. Some evidence of this is provided by comparing the two curves already examined. However, with reference to the curve plotted for the least dense specimen i.e. $\rho_* = 0.76$, it can be seen that there is a complete absence of any elastic region since the slope of the curve does not tend towards $\nu_e = 0.3$ at the origin. It must therefore be concluded that the stress interaction effect and the accompanying local plastic deformations occur almost immediately the load is applied to the specimen. It is interesting to note that in this case the slope of the curve rapidly tends towards 0.5, which is the plastic Poisson's ratio commensurate with volume constancy. It seems likely that the slopes of the other two curves would also tend towards 0.5 for higher stress values.

It can therefore be seen that although the porous preform material appears to be brittle on a macro-scale, implying that it obeys Hooke's law up to the point of fracture, this is not actually true, and in point of fact the matrix material behaves in a locally ductile manner.

This important conclusion will be used throughout the remainder of this Chapter in order to explain a number of phenomena associated with ferrous based, porous, sintered metals.

7.7 Derivation of Mathematical Models to Represent the Tensile Strength of Porous Preform Material

It would appear from Figs.6.5 to 6.8 that the porosity is

randomly disposed throughout the preform material. However, a more detailed study of the tensile strengths obtained for specimen manufactured from the various powder fractions, suggest that the distribution and morphology of the porosity behaves as if conforming to definite patterns, which can be represented by mathematically equivalent models[110].

In the first instance, it would be quite wrong to suppose that the PM material behaves as a homogeneous continuum since it would then appear that,

effective cross sectional area = $A_a \rho_*^{\frac{2}{3}}$ ----------(5)

which when coupled to the assumption that there are no stress concentrations, leads to highly exaggerated values for tensile strengths[111], curve (A), Fig.7.9.

As stated in Section 7.6 a more logical approach is to regard a PM material as a two phase material consisting of a mixture of matrix metal and pores. If isotropy and uniform density are assumed to prevail throughout, then,

average cross sectional area = $\rho_* = (1 - P)$ ----------(6)

This is shown as curve (B), Fig.7.9. However, neither curve (A) nor curve (B) has any practical significance, since the tensile strength depends upon (i) the minimum load bearing area, and (ii) the interaction of stress concentrations. Both (i) and (ii) are dependent upon the distribution and morphology of the porosity present within the component, whilst (ii) is also dependent upon the toughness of the matrix material i.e. its resistance to the propagation of cracks. In the case of metals, this toughness will depend upon the ductility of the matrix material, so that there may be instances when, due to a very ductile matrix, the stress interaction effects may be completely

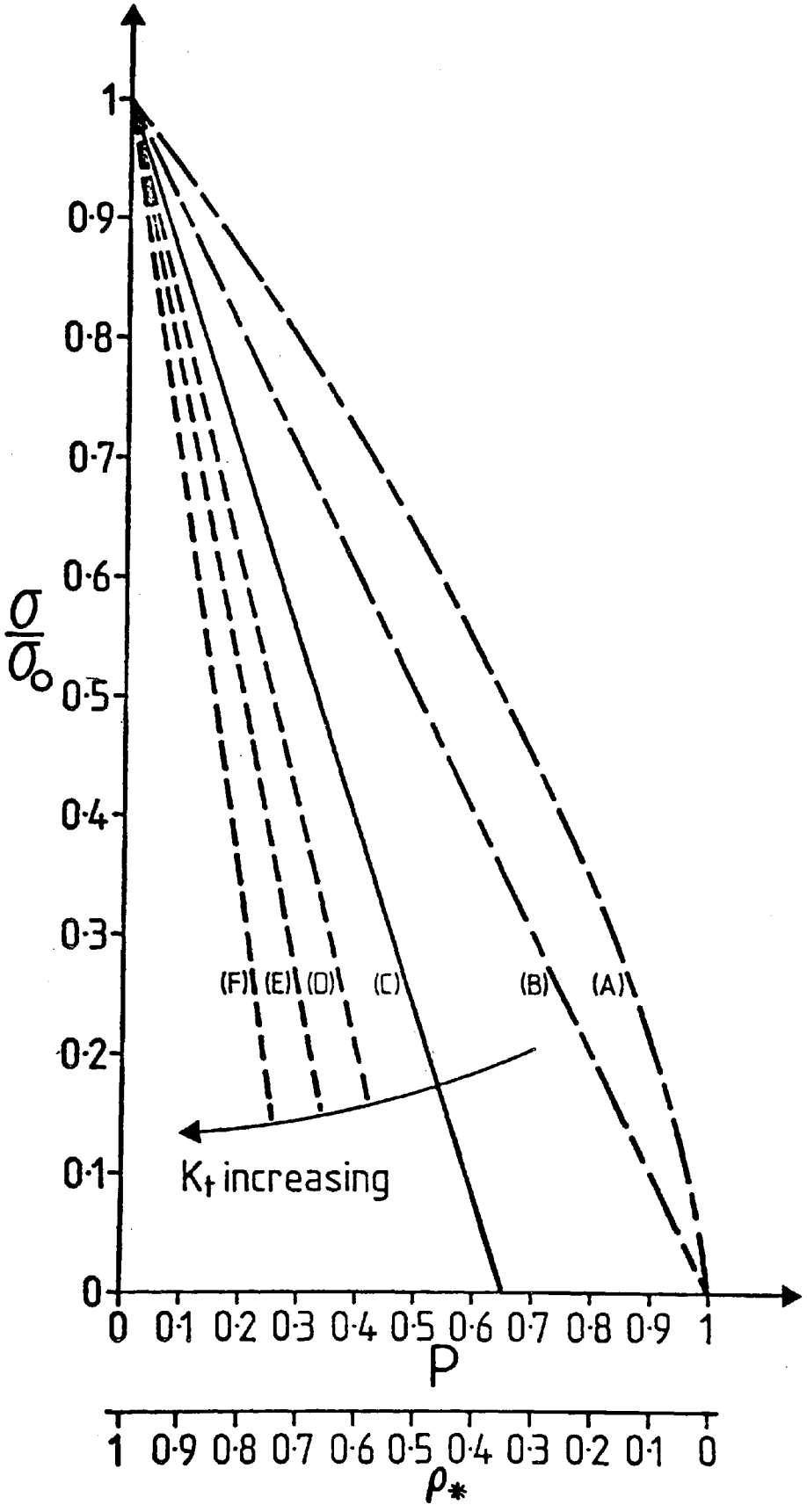

FIG. 7.9 COMPARISON OF PROBABLE RELATIVE STRENGTHS OF POROUS MATERIALS BASED ON VARIOUS CRITERIA

A: Homogenious continuum
B: Two phase material: average cross sectional area
C: Two phase material: no stress interactions
D:
E:
F: } Two phase material with stress interactions

neglected so that the tensile strength becomes solely dependent upon the minimum load bearing area.

For the purpose of quantifying these effects, it is a convenient and reasonable approximation, to regard the porosity as taking the form of either spherical or oblate ellipsoidal cavities, for which corresponding values for K_t are shown in Fig. 7.10. It is evident from this that the most favourable pore shape is a sphere, which is most likely to exist when the material has been fully sintered[113], and when $\rho_* > 0.9$ (Ref. 114).

As a first approximation in estimating the minimum load bearing area, it would seem reasonable to suppose that, $A_b \rightarrow 0$ as $\rho_* \rightarrow$ the apparent density of the loose powder, since lower densities imply some mysterious separation of the powder particles. Hence, for a ductile material e.g. elemental iron powder, $\sigma \rightarrow 0$ when $A_b \rightarrow 0$, which occurs when $\rho_* \rightarrow 0.35$ approx. In the absence of any further information, this is shown as the straight line (C) on Fig. 7.10.

If the circumstances were such that the stress interaction effects became significant, then the slopes of the $\frac{\sigma}{\sigma_0}$ Vs ρ_* curves, lines D, E and F, Fig. 7.10 will become progressively steeper, as the severity of the morphology, and hence the K_t values, increase.

Minimum load bearing areas may be estimated with the aid of mathematical models, devised by tessellating tiny fragments of material, which in themselves represent the three dimensional pore distribution under consideration. These fragments may be polyhedral or prismatic in shape, with the cavities centred around their respective vertices.

It is interesting to note that there are only 8 ways in which such solid tessellations[115] can occur viz. (i) cubes (ii) triangular

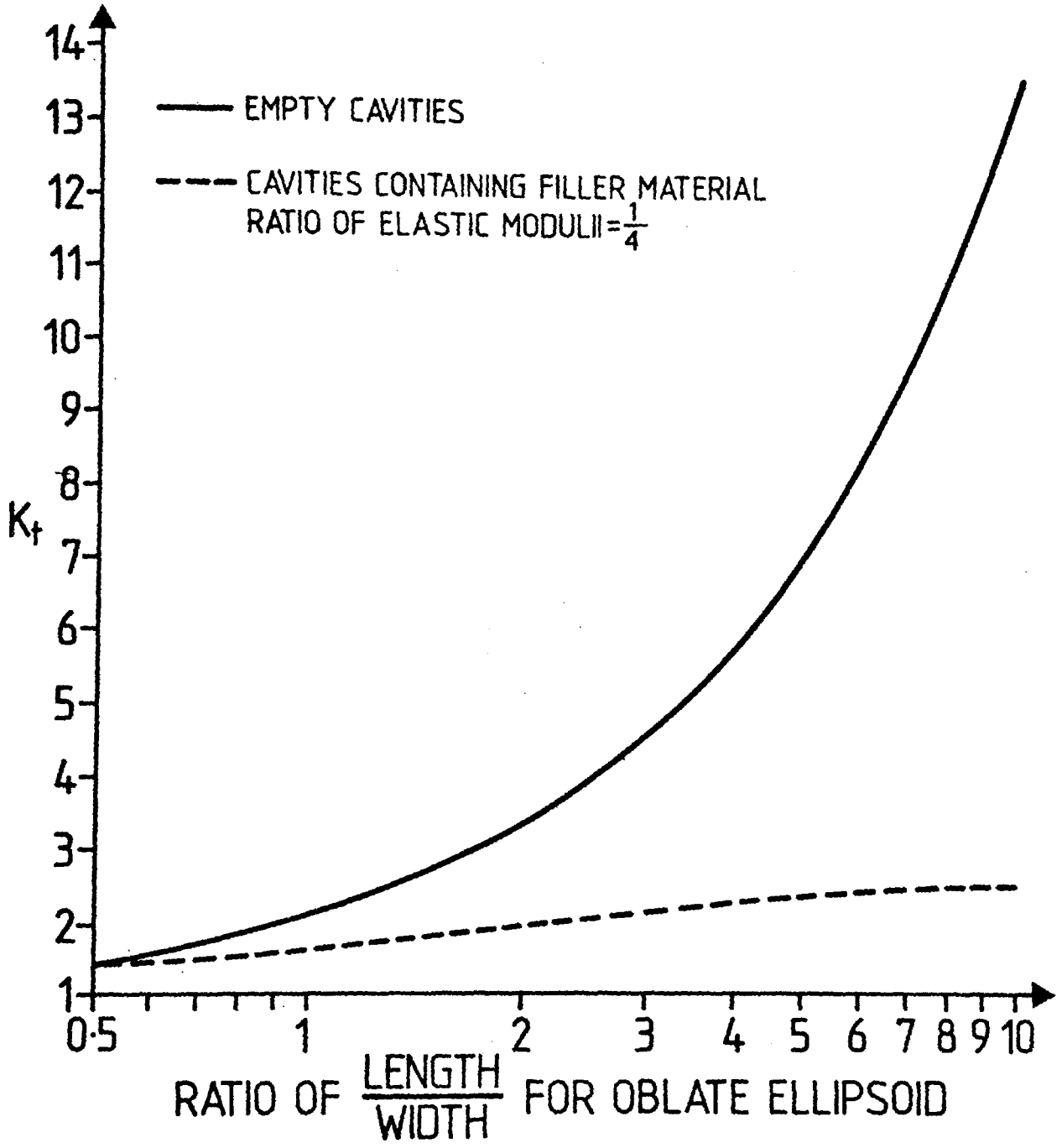

FIG. 7.10 GEOMETRIC ELASTIC STRESS CONCENTRATION FACTORS FOR ELLIPSOIDAL CAVITIES CONTAINED IN A MATERIAL SUBJECTED TO TENSILE STRESS (Ref. 112)

prisms (iii) hexagonal prisms (iv) rhombic dodecahedra (v) truncated octahedra (vi) tetrahedra and octahedra (vii) tetrahedra and truncated tetrahedra and (viii) octahedra and cuboctahedra. However, for present purposes it will only be necessary to consider a few of these.

General equations which take into account the quantity, distribution and morphology of the porosity present in such models, can now be established from the following considerations.

Volume of material contained in fragment $\propto p^3$

Volume of pore $\propto d^3$

Area of one face of fragment $\propto p^2$

Cross sectional area of pore $\propto d^2$

By inserting the constants of proportionality which take into account the geometries of both the fragments and the pores, then,

Volume of material contained in porous fragment $= bp^3 - cd^3$

hence $$\rho_* = 1 - \frac{c}{b}\left[\frac{d}{p}\right]^3 \qquad \text{---------- (7)}$$

minimum load bearing area $= fp^2 - gd^2$

$$\frac{A_b}{A_a} = 1 - \frac{g}{f}\left[\frac{d}{p}\right]^2 \qquad \text{---------- (8)}$$

from eqn. (7) $\left[\frac{d}{p}\right]^2 = \left[\frac{b}{c}P\right]^{\frac{2}{3}}$ subst. in eqn. (8).

hence, $$\frac{A_b}{A_a} = 1 - \frac{g}{f}\left[\frac{b}{c}P\right]^{\frac{2}{3}}$$

or $$\frac{A_b}{A_a} = 1 - kP^{\frac{2}{3}} \qquad \text{---------- (9)}$$

where $k = \frac{g}{f}\left[\frac{b}{c}\right]^{\frac{2}{3}}$

For a PM material with a very ductile matrix,

$$\frac{\sigma}{\sigma_o} = \frac{A_b}{A_a} = 1 - kP^{\frac{2}{3}} \qquad \text{---------- (10)}$$

An equation of this form was first suggested by Eudier[114], based

on an arrangement of spherical pores forming a simple cubic pattern, for which the calculated value for k = 1.209. Ishimaru et al[19] performed a series of tests on ferrous based powders, the results of which are summarised in Table 7.1. In this case the values obtained for k (or λ see ref.110) are empirical, and Ishimaru et al[19] offer no explanation for the fact that for the most part they are higher than the value calculated by Eudier[114]. The reason would seem to be that it is the result of the stress concentration effects associated

TABLE No. 7.1 - After Ishimaru et al[19]

$k(\lambda)$	Ferrous Powder Details
0.98	Carbonyl
1.7	Reduced + 0.5% C
1.71	Reduced
1.82	Atomised 325 - 400 mesh
1.94	Atomised -100 mesh
1.96	Atomised 200 - 250 mesh
2.04	Atomised + 0.5% C
2.12	Atomised 2% Ni alloy
2.16	Atomised 100 - 145 mesh

with the pore geometry. It is therefore a remarkable coincidence that the form of the equation which was derived by ignoring stress concentration effects, still manages to take them into account. Figs. 7.11, 7.12, 7.13 & 7.14 show various mathematical models together with their respective k values. In all cases the pores are assumed to be spherical, and stress concentration effects have been ignored. The ideal model Fig. 7.11 is interesting although in fact regular

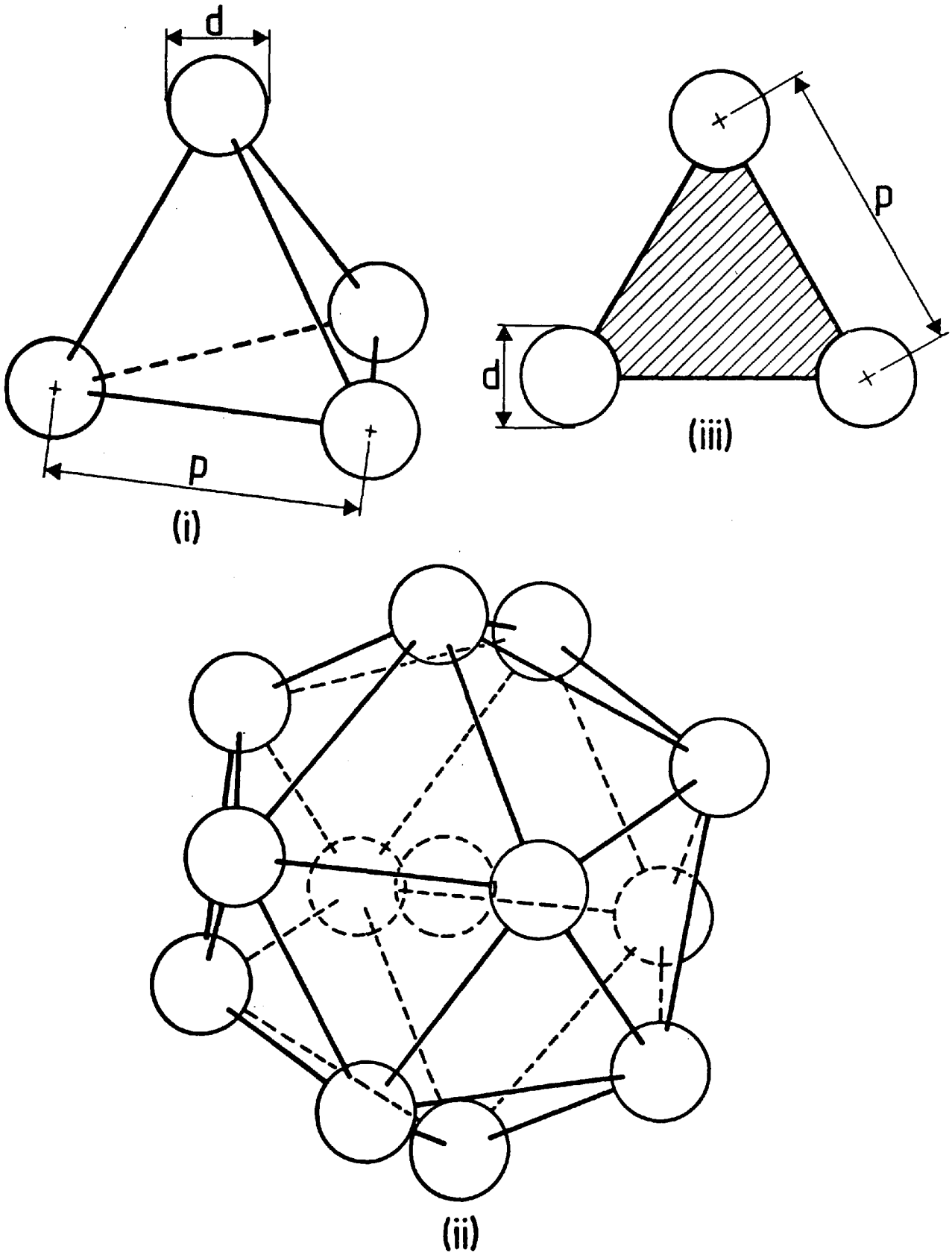

FIG. 7.11 IDEAL MODEL, k = 0.981

(i) Regular tetrahedron
(ii) Icosahedron
(iii) Minimum load bearing area

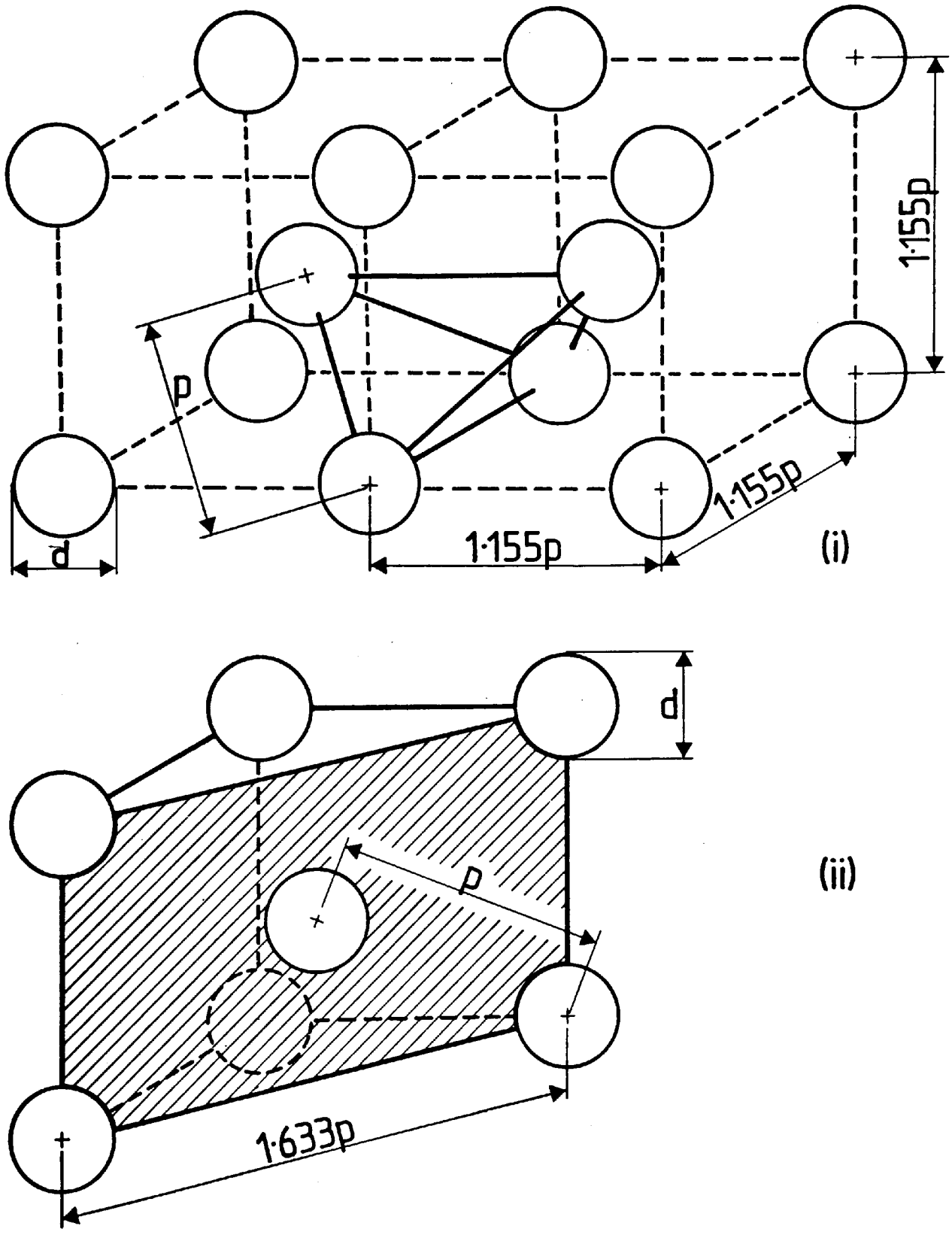

FIG. 7.12 MODIFIED IDEAL MODEL, k = 1.077

(i) Irregular tetrahedron
(ii) Minimum load bearing area i.e. (110) plane

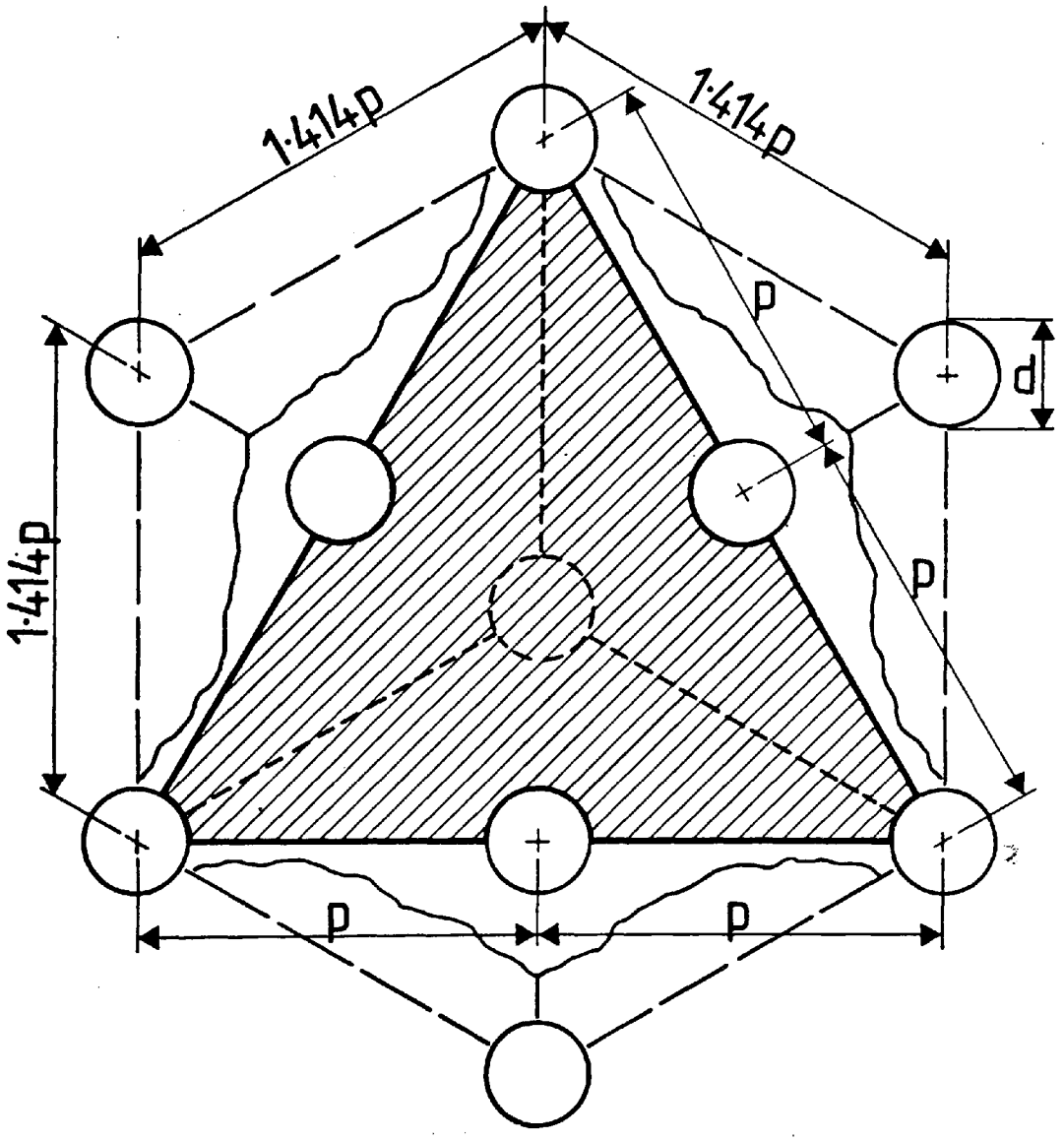

FIG. 7.13 CLOSE-PACKED CONFIGURATION, k = 1.109. FACE CENTRED CUBIC ARRANGEMENT SHOWING MINIMUM LOAD BEARING AREA i.e. (111) PLANE

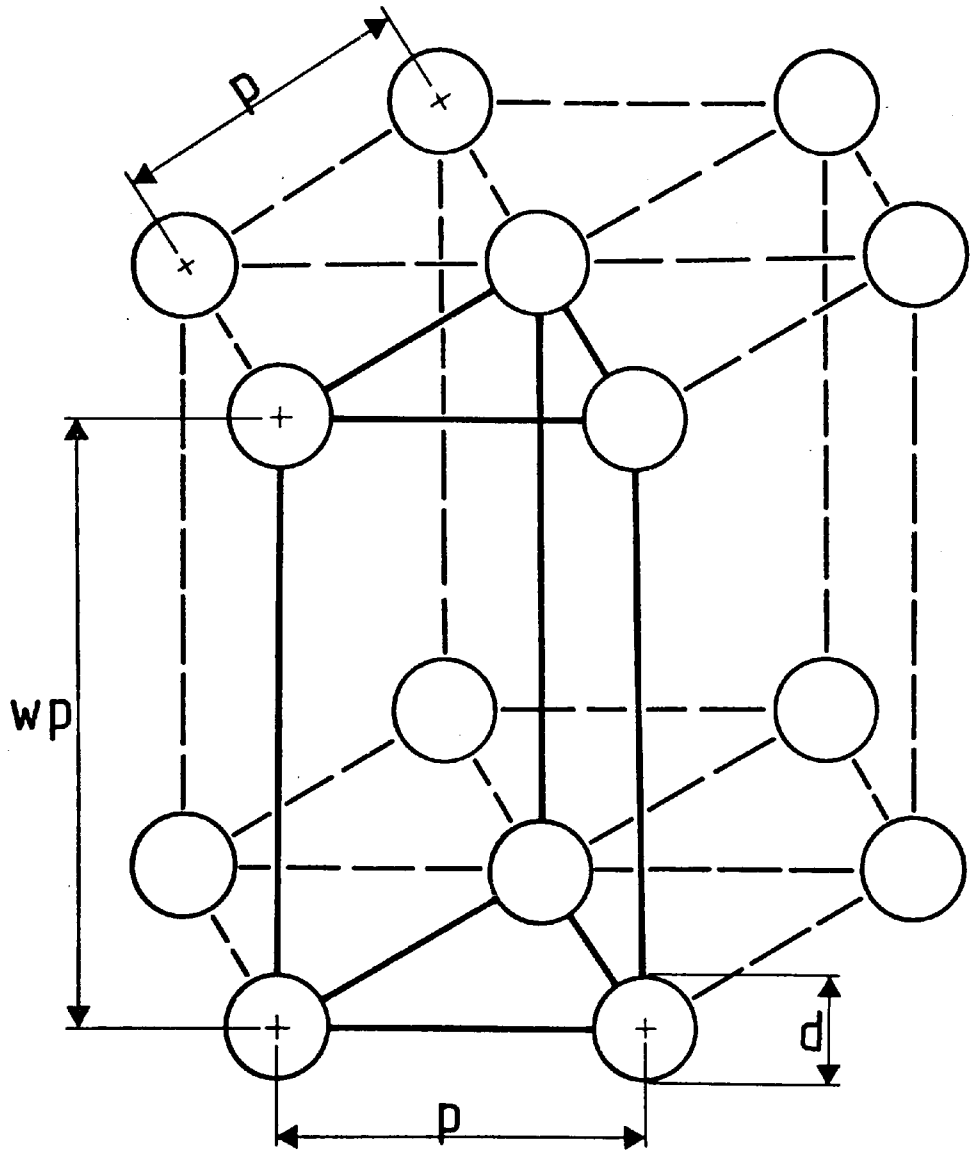

FIG. 7.14 SIMPLE HEXAGONAL CONFIGURATION FOR ISOTROPY, w = 0.866 and k = 1.154

tetrahedra will not form solid tessellations, so that they will not exactly form the icosahedron shown in Fig. 7.11 (ii). Nevertheless, preliminary studies with such a model suggests that values for k can never be less than 0.981, which coincides with the lowest experimental value shown in Table 7.1.

7.8 Models Incorporating the Interaction Effects of Stress Concentrations

Since it has been concluded that the values for "k" as obtained by Ishimaru et al[19], do not only take into account the geometry of the porosity, but, also caters for the interaction effect of the stress concentrations, the new symbol λ will be used to distinguish between this constant, and that used for estimating minimum load bearing areas, only.

Hence, $$\frac{\sigma}{\sigma_o} = 1 - \lambda P^{\frac{2}{3}} = \frac{1 - kP^{\frac{2}{3}}}{K} \qquad \text{----------(11)}$$

where K is the tensile strength reduction factor, which varies with the porosity.

The actual values for K will depend upon the toughness of the matrix material, the separation distances between the cavities, and their corresponding K_t values. The extreme cases arise when dealing with either very ductile or very brittle matrices when $K = 1$ or $K = K_t$ respectively, however, for the ferrous materials referred to in Table 7.1 the following assumptions would seem to be reasonable. $K = 1$ when $P = 0$, whereas in general, $1 < K < K_t$, due to plastic relaxation of the matrix material immediately adjacent to the cavities. However, at the limits of the model, where the theory implies that the cavities are about to become inter-connected, $K = K_t$ due to the absence of sufficient surrounding material to enable the stress concentration factor to be relaxed.

Timoshenko and Goodier[116] provide a complete analytical solution to the local stress distributions set up around a small spherical cavity in a material subjected to a direct tensile stress. For a ferrous based material, this may be summarized as follows:

stress acting at distance $\frac{d}{2}$ from pore centre $\simeq$ average stress x 2

whilst stress acting at distance d from pore centre $\simeq$ average stress.

Hence the stress interaction effect only starts to become apparent (i.e. $K = 1$) when $\rho = 2d$, and is assumed to have the maximum effect (i.e. $K = K_t = 2$) when $\rho = d$. If this is applied to the simple cubic model, which gives the smallest $\frac{A_b}{A_a}$ ratio for an isotropic material, it follows that when $\rho = 2d$, $P = 0.065$.

Furthermore, when $\rho = d$,

$P = 0.5236$ and therefore $\frac{A_b}{A_a} = 0.214$.

However, $\frac{\sigma}{\sigma_o} = \frac{0.214}{K_t} = \frac{0.214}{2} = 0.107$. Substituting these values into eqn. (11)

$0.107 = 1 - \lambda (0.5236)^{\frac{2}{3}}$

hence $\lambda = 1.375$

$$\therefore \frac{\sigma}{\sigma_o} = 1 - 1.375 P^{\frac{2}{3}} \qquad \text{----------(12)}$$

Equation (12) ignores the fact that $K = 1$ for values of porosity ranging from $P = 0 \rightarrow 0.065$. However, it is considered that this small range has little practical significance and the original assumption that $K = 1$ when $P = 0$ is a justifiable approximation. Equation (12) now represents the least possible tensile strengths available from an iron based isotropic material in which all the cavities are assumed to be spherical. Nevertheless, it is still insufficient to explain the reductions in tensile strengths observed by Ishimaru et al, and recourse must therefore be made to a new model

based on combinations of spherical and oblate ellipsoidal cavities, taking into account the interaction effects of the stress concentrations resulting from the latter cavity morphology.

7.9 New Model Based on Variable Morphology

In order that the new model should exhibit uniform density and isotropy, it is necessary to arrange the pores so that a representative cubic array consists of two spheres and six oblate ellipsoidal cavities as shown in Fig. 7.15. It can be seen that the three mutually perpendicular axes passing through any of the spheres, become the axes of revolution of the oblate ellipsoids i.e. coincident with their minor axes. For uniform density, it will be assumed that:

Volume of ellipsoid = volume of sphere

$$\frac{\pi}{6} x^2 y d^3 = \frac{\pi}{6} d^3$$

$$\therefore x^2 y = 1 \text{ and } y = \frac{1}{x^2}$$

$$\therefore \frac{x}{y} = x^3 \qquad \text{---------- (13)}$$

For such an arrangement,

$$\rho_* = 1 - 0.524 \left[\frac{d}{p}\right]^3 \qquad \text{---------- (14)}$$

and from Fig. 7.15 (ii),

$$\frac{A_b}{A_a} = 1 - 0.196 \left[\frac{d}{p}\right]^2 \left(1 + x^2 + \frac{2}{x}\right) \qquad \text{---------- (15)}$$

$$\text{hence } \frac{A_b}{A_a} = 1 - 0.302 \left(1 + x^2 + \frac{2}{x}\right) P^{\frac{2}{3}} \qquad \text{---------- (16)}$$

$$\text{i.e. } k = 0.302 \left(1 + x^2 + \frac{2}{x}\right).$$

Hence, for such a model, if $\frac{x}{y} = 1.5$, then $K_t \sim 2.7$, from Fig. 7.10.

From eqn. (13)

$x^3 = 1.5 \quad \therefore x = 1.145$ subst. in eqn. (16)

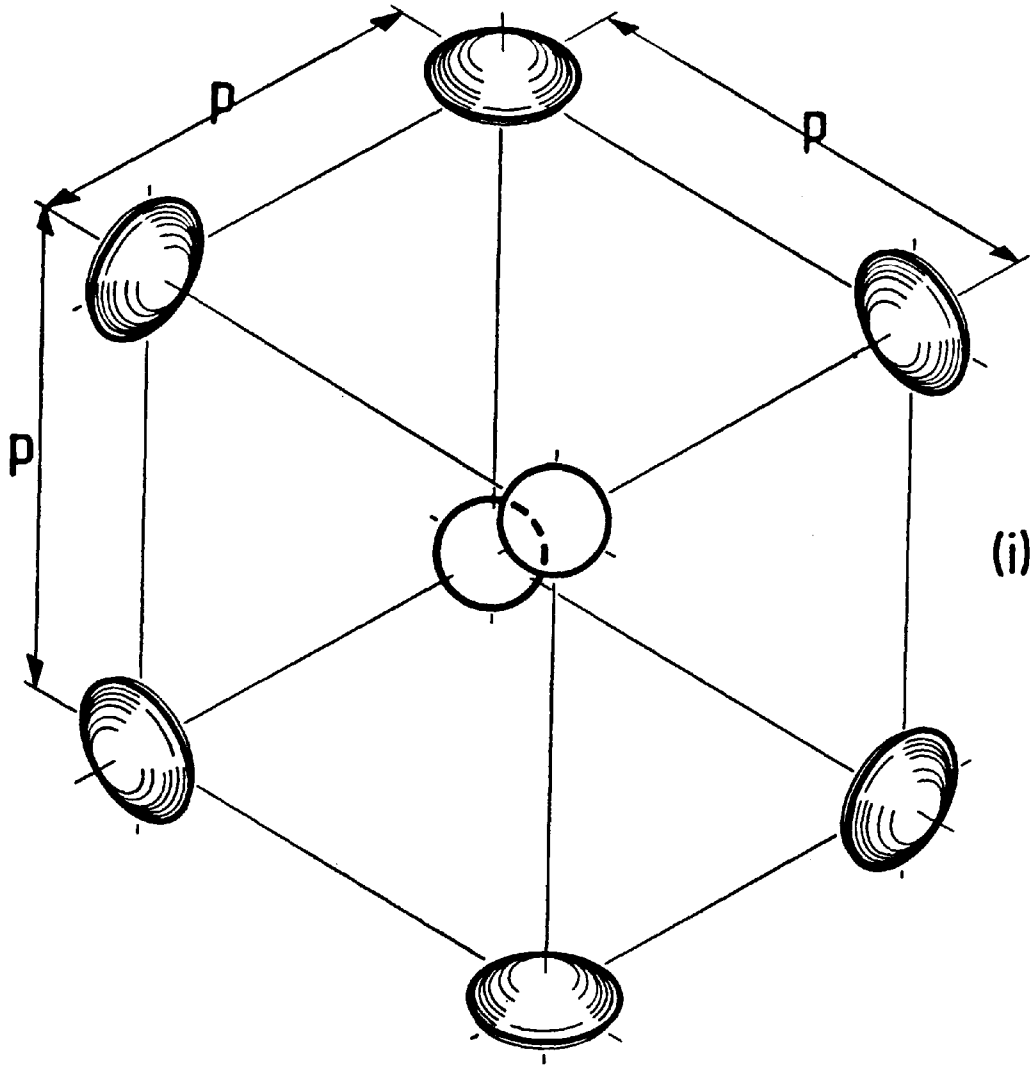

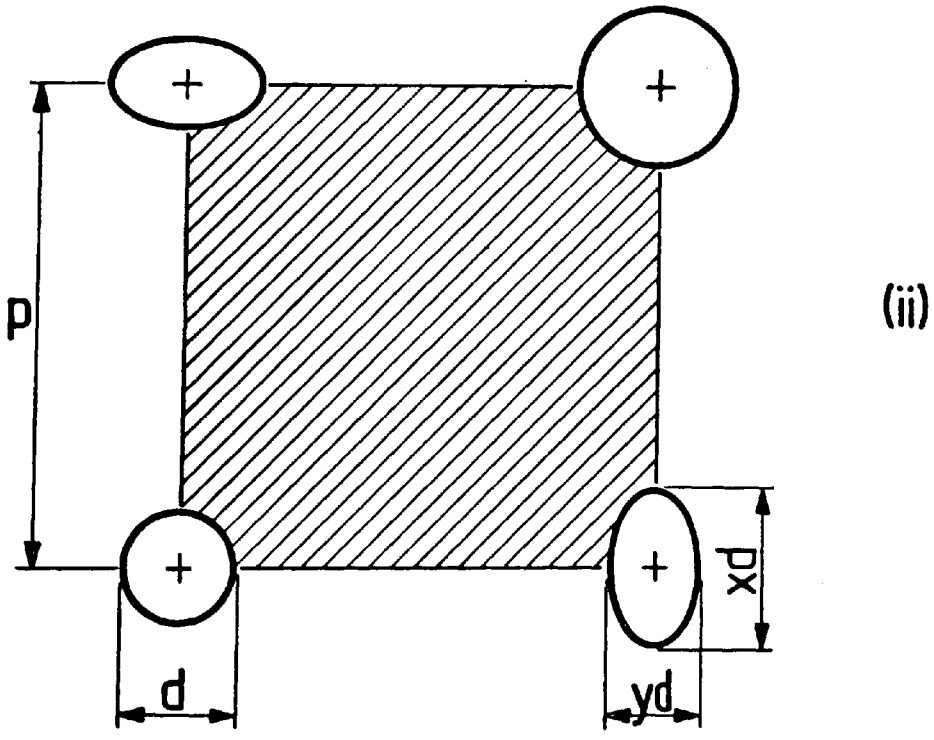

FIG. 7.15 VARIABLE MORPHOLOGY MODEL

hence, $\frac{A_b}{A_a} = 1 - 1.225 P^{\frac{2}{3}}$ ——————————(17)

Limit of model occurs when $p = xd = 1.145\ d$ which when substituted into eqn. (14) gives,

$\rho_* = 0.651$ or $P = 0.349$

$\therefore \frac{A_b}{A_a} = 0.393$

and $\frac{\sigma}{\sigma_o} = \frac{0.393}{K_t} = \frac{0.393}{2.7} = 0.145.$

Substituting these values in eqn. (11)

$0.145 = 1 - \lambda\ (0.349)^{\frac{2}{3}}$

$\therefore \frac{\sigma}{\sigma_o} = 1 - 1.727 P^{\frac{2}{3}}$ ——————————(18)

The above calculations were repeated for $\frac{x}{y}$ ratios ranging up to 2.5, and the corresponding values for k and λ are shown plotted in Fig. 7.16. It can be seen that these adequately cover the range of experimental values shown in Table 7.1. Furthermore, the accompanying values for K_t as obtained from Fig. 7.10 lie within the range 2.7 to 3.8, which corresponds quite well to those referred to by Haynes[117] viz. 2.6 to 3.4 for sintered irons and steels and 2.6 to 3.8 for sintered bronze. This implies that the earlier assumptions made regarding the toughness of the matrix material, were reasonably valid.

7.10 Experimentally Determined Tensile Strengths of Preform Materials

The tensile characteristics of the "as supplied" powder at stresses well below the breaking stress, are shown in Fig. 7.18. These curves were plotted using results obtained from the tests described in Section 7.6. In addition to this general appreciation of the tensile behaviour of the preform material, a series of tensile tests to destruction were carried out at room temperature on specimen manufactured from Hoganas AHC 100.29 iron powder, together with its various fractions. In all cases the powders were admixed with 0.5%

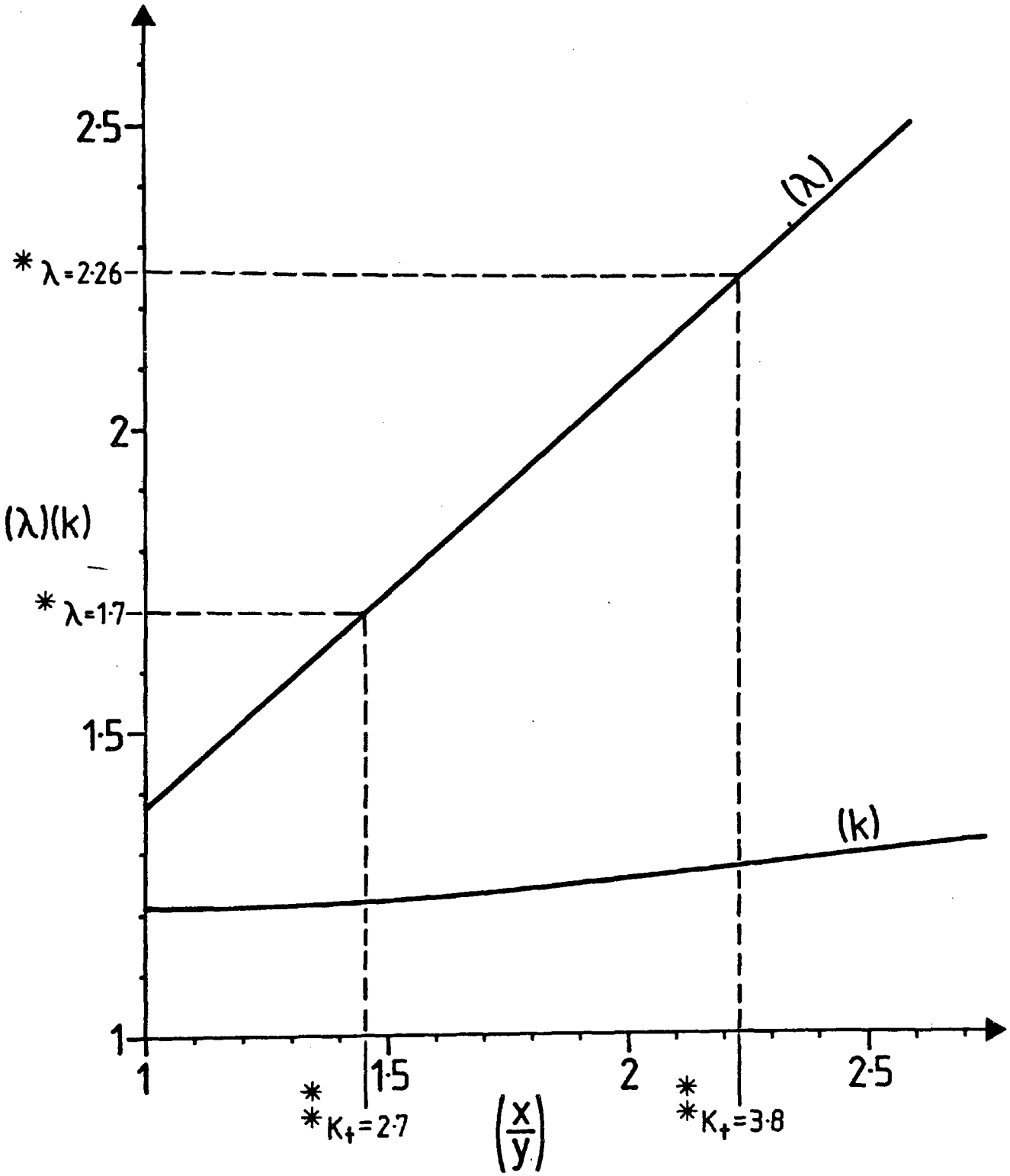

* From Table 7.1

** From Fig. 7.10

FIG. 7.16 CALCULATED VALUES OF k AND λ FOR VARIABLE MORPHOLOGY MODEL

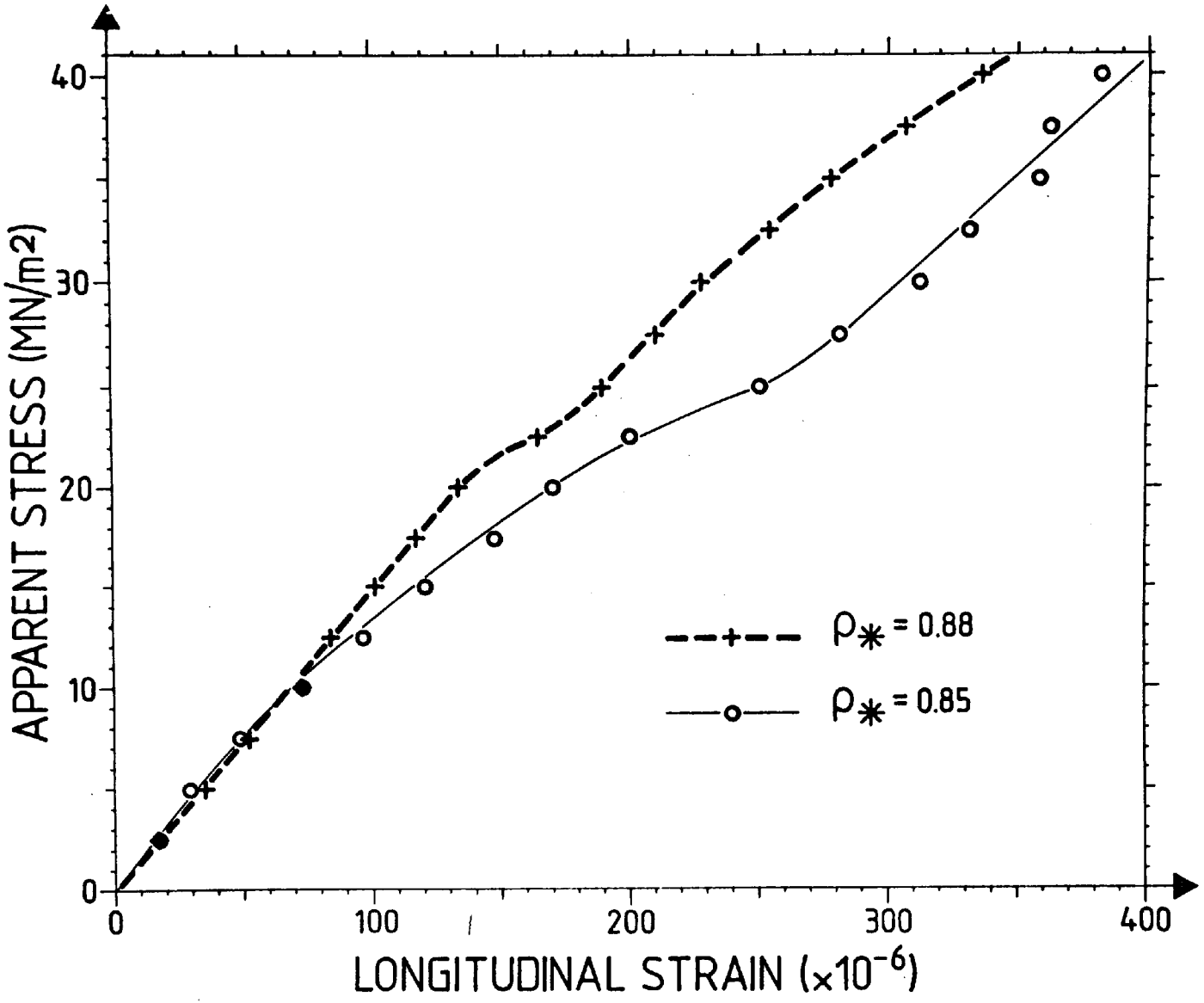

FIG. 7.17 GRAPHS OF APPARENT STRESS VS. LONGITUDINAL STRAIN, PLOTTED USING RESULTS OBTAINED FROM EXPERIMENTS DESCRIBED IN SECTION 7.6

graphite and 1% zinc stearate, whilst the sintering procedure was as outlined in Section 6.1.

The tensile specimen were produced from "wafer" compacts (see Section 5.5), and after sintering they were machined on a MOOG 2 axis N.C. Milling Machine, to the dimensions shown in Fig. 5.10(c). All the tensile tests to destruction were performed on a Dartec M1501 Tensile Testing Machine, and whereas the actual experimental results appear in Appendix I a summary of these results is shown in Table 7.2.

TABLE 7.2.

Summary of the Results of the Direct Tensile Tests *

Powder Fraction (μm)	Number of Pairs of Data Points n	Strength of Pore Free Matrix Material σ_o(MN/m^2)	λ	Correlation Coefficient R
Sub-sieve	5	358	1.86	0.919
(+ 90-125)	22	382.5	1.82	0.939
(+150-180)	14	428.7	1.929	0.942
As supplied	20	351.5	1.952	0.984

The values for σ_o and λ were evaluated on a statistical basis using the "method of least squares[84, 97]", Equation (11) was linearized for this purpose to give

$$\sigma = \sigma_o - (\sigma_o \lambda) P^{\frac{2}{3}} \qquad (19)$$

where σ_o is the "σ- intercept" value corresponding to $P^{\frac{2}{3}} = 0$, and $(\sigma_o \lambda)$ is the slope "m" of the graph of σ Vs $P^{\frac{2}{3}}$, plotted

for "n" pairs of data points.

$$\text{Hence, } \lambda = \frac{\text{slope}}{\text{intercept}} = \frac{m}{\sigma_o} \qquad \text{(20)}$$

$$\text{where } m = \frac{\sum\left(\sigma P^{\frac{2}{3}}\right) - \sum\frac{\sigma P^{\frac{2}{3}}}{n}}{\sum\left(P^{\frac{2}{3}}\right)^2 - \sum\frac{\left(P^{\frac{2}{3}}\right)^2}{n}} \qquad \text{(21)}$$

$$\text{and } \sigma_o = \sum\frac{\sigma}{n} - m\sum\frac{P^{\frac{2}{3}}}{n} \qquad \text{(22)}$$

Since the use of this linear regression technique does not require the actual plotting of a graph, a coefficient of correlation "R" was calculated in order to provide a measure of the accuracy of the fit,

$$\text{where } R = \frac{\sum\left(\sigma P^{\frac{2}{3}}\right) - \sum\left(\frac{\sigma P^{\frac{2}{3}}}{n}\right)}{\left[\sum\left(P^{\frac{2}{3}}\right)^2 - \sum\frac{\left(P^{\frac{2}{3}}\right)^2}{n}\right]\left[\sum\sigma^2\sum\frac{\sigma^2}{n}\right]} \qquad \text{(23)}$$

(For a perfect fit, $R = 1$)

With reference to Table 7.2, it can be seen that the values obtained for R indicate that the experimental data conforms very well to equation (11) in all cases. Furthermore, the experimental values for λ, obtained for the various powder fractions, compare very favourably with the values given in Table 7.1 corresponding to similar powder fractions.

7.11 Discussion and Interpretation of Tensile Results

With reference to Table 7.2 it can be seen that there is only a slight difference between the effects of pore geometry, as indicated by λ for the coarse fraction (+150-180 μ m) as compared to the "as supplied" powder. However there is a marked difference in

their corresponding values for σ_o, despite the fact that the chemical composition of the original powder mixes was the same in both cases. The effect of this is that the mechanical strength of the sintered "coarse fraction" material is superior to that of the sintered "as supplied" material. The reason for this becomes apparent when reference is made to Section 6.4 where it can be seen that for the same powder mix and sintering conditions more pearlite, and hence less free cementite, was formed in the case of the "coarse fraction" powder as compared to the "as supplied" powder. Hence the strengthening of the matrix material is not only due to the presence of a greater amount of pearlite, but also due to the absence of excessive amounts of free cementite.

It would therefore appear that the only advantage of the "as supplied" powder blend, is that of marginally greater compactibility, see Section 5.5. However, this would seem to be more than offset by the disadvantage of the greater inhomogeneity resulting from the use of such a powder blend in accordance with standard industrial practice. It may be that the popularity of such powder blends is the result of the gross over-simplification of always regarding density and mechanical strength as being synonymous.

From Table 7.2 , the average value for λ for the "coarse" and "as supplied" powder is $\sim$ 1.94. The corresponding values obtained from Fig. 7.16 are k = 1.23 and $\frac{x}{y}$ = 1.8 and from Fig. 7.10, K_t = 3.2.

Substituting $\frac{x}{y}$ = 1.8 in eqn. (13)

$x^3 = 1.8$

$\therefore\ x = 1.216$

hence $y = 0.676$

From eqn. (14)

$$\rho_* = 1-0.524\left[\frac{d}{p}\right]^3$$

By transposition

$$p = (0.806P^{-\frac{1}{3}})\ d \qquad \text{---------- (24)}$$

Hence for a given pore diameter d, and porosity P, the preform material may be represented by the model shown in Fig. 7.15 where the values for x, y and p are as given above.

7.12 Use of Apparent Young's Modulus as a Means of Checking Load Bearing Area

If the apparent Young's modulus, of elasticity for a porous material is regarded as the slope of the tangent through the origin of the stress strain curve, then with reference to Fig. 7.17, $E_{ap} \simeq 150\ MN/m^2$ when $\rho_* = 0.88$ or $P = 0.12$. For a given value of strain

$$\frac{\text{apparent stress}}{E_{ap}} = \frac{\text{true stress}}{E}$$

where $E = 210\ MN/m^2$ for steel.

$$\therefore \quad \frac{\text{apparent stress}}{\text{true stress}} = \frac{E_{ap}}{E} \qquad \text{---------- (25)}$$

also over the elastic region of the curve,

$$\frac{\text{apparent stress}}{\text{true stress}} = \frac{A_b}{A_a} = (1-kP^{\frac{2}{3}}) \qquad \text{---------- (10)}$$

Combining equations (25) and (10) gives,

$$k = (1-\frac{E_{ap}}{E})\ P^{-\frac{2}{3}} \qquad \text{---------- (26)}$$

i.e. $k = (1-\frac{150}{210})\ 0.12^{-\frac{2}{3}} = 1.174$

This value for k compares reasonably well with the value of 1.23 obtained in Section 7.11, from the results of the tensile tests to destruction.